SECURITY CLASSIFICATION OF THIS PAGE *(When Data Entered)*

| REPORT DOCUMENTATION PAGE | | READ INSTRUCTIONS BEFORE COMPLETING FORM |
|---|---|---|
| 1. REPORT NUMBER<br>GRL/9501 | 2. GOVT ACCESSION NO. | 3. RECIPIENT'S CATALOG NUMBER |
| 4. TITLE *(and Subtitle)*<br>BASIC STUDY OF THE PUMPING OF A GAMMA-RAY LASER | | 5. TYPE OF REPORT & PERIOD COVERED<br>Annual Report<br>03/15/94 - 03/14/95<br>6. PERFORMING ORG. REPORT NUMBER |
| 7. AUTHOR(s)<br>C. B. COLLINS | | 8. CONTRACT OR GRANT NUMBER(s)<br>N00014-93-K-2005 |
| 9. PERFORMING ORGANIZATION NAME AND ADDRESS<br>University of Texas at Dallas<br>Center for Quantum Electronics<br>P. O. Box 830688<br>Richardson, TX 75083-0688 | | 10. PROGRAM ELEMENT, PROJECT, TASK AREA & WORK UNIT NUMBERS |
| 11. CONTROLLING OFFICE NAME AND ADDRESS<br>Naval Research Laboratory<br>4555 Overlook Avenue, S. W.<br>Washington, D. C. 20375-5000 | | 12. REPORT DATE<br>04/15/95<br>13. NUMBER OF PAGES<br>116 |
| 14. MONITORING AGENCY NAME & ADDRESS *(if different from Controlling Office)*<br>Dr. Paul Kepple<br>Naval Research Laboratory<br>4555 Overlook Avenue, S. W.<br>Washington, D. C. 20375-5000<br>Attn: Code 6721 Bldg. A50 Rm# 148 | | 15. SECURITY CLASS. *(of this report)*<br>Unclassified<br>15a. DECLASSIFICATION/DOWNGRADING SCHEDULE |

16. DISTRIBUTION STATEMENT *(of this Report)*

This document has been approved for public release and sale; its distribution is unlimited.

17. DISTRIBUTION STATEMENT *(of the abstract entered in Block 20, if different from Report)*



18. SUPPLEMENTARY NOTES

19. KEY WORDS *(Continue on reverse side if necessary and identify by block number)*

Gamma-ray laser, Ultrashort wavelength laser

20. ABSTRACT *(Continue on reverse side if necessary and identify by block number)*

The most productive approaches to the problem of the gamma-ray laser have focused upon upconversion techniques in which metastable nuclei are pumped with long wavelength radiation. At the nuclear level the storage of energy can approach tera-Joules ($10^{12}$J) per liter for thousands of years. However, any plan to use such a resource for a gamma-ray laser poses problems of a broad interdisciplinary nature requiring the fusion of concepts taken from relatively unrelated fields of physics. Our research group has described

(continued on next page)





DD FORM 1 JAN 73 1473 EDITION OF 1 NOV 65 IS OBSOLETE
S/N 0102-LF-014-6601

SECURITY CLASSIFICATION OF THIS PAGE *(When Data Entered)*

## TABLE OF CONTENTS

**REPRINTS AND PREPRINTS OF MANUSCRIPTS PUBLISHED OR TO BE PUBLISHED UNDER THIS CONTRACT**



**PREPRINTS OF MANUSCRIPTS TO BE PUBLISHED IN CONFERENCE PROCEEDINGS UNDER THIS CONTRACT**

# PROGRESS IN THE PUMPING OF A GAMMA-RAY LASER

C. B. Collins and J. J. Carroll

University of Texas at Dallas, Center for Quantum Electronics

P. O. Box 830688, Richardson, Texas, USA 75083-0688

## ABSTRACT

A gamma-ray laser would stimulate coherent emission of radiation at wavelengths below 1 Å from excited states of nuclei. However, the difficulties in realizing such a device were considered insurmountable when the first cycle of study ended in 1981. Since then, research on the feasibility of a gamma-ray laser has taken on a completely new character. A nuclear analog of the ruby laser has been proposed and many of the component steps for pumping the nuclei have been demonstrated experimentally. A quantitative model based upon the new data and the concepts of this decade shows the gamma-ray laser to be feasible if some real isotope has its properties sufficiently close to the ideals. The greatest positive impact has come from the discovery of giant resonances for pumping nuclei with photons that greatly reduce the levels of input power needed. Most recently attention has been focused upon efforts to demonstrate prelasing levels of fluorescence from simulation nuclides and actual gamma-ray laser candidates. Problems being addressed are the acquisition of macroscopic samples of the best nuclei for testing and the demonstration of appropriate instrumentation.

CONTENTS

# I. INTRODUCTION

Many advanced technologies would benefit from non-nuclear sources of high energy density. The importance would be greatest if concentrated energies could be stored for long times and then released at controlled rates on time scales of nanoseconds to microseconds. For power released as electromagnetic waves, the archetypical system would probably be the laser, although many applications such as lithography need only the flash of "light" and not its coherence. In any event, gamma rays would represent the ultimate form for such "light."

Gamma rays are subject to the same basic laws governing the absorption and emission of electromagnetic radiation as prevail at longer wavelengths. However, since the energies per photon are so much greater, there seem to be singular advantages in gamma-ray analogs of atomic and molecular sources for the production of intense pulses of "light." Such perceptions have driven the 33 year quest for the ultimate pulsed-power device, ***the gamma-ray laser.*** In fact, the advantages accrue more from the higher densities for the storage of energy than from the shorter wavelengths available upon release. A flash of induced emission at gamma-ray wavelengths would be of great technological importance in its own right, while at the same time demonstrating the means for pumping a gamma-ray laser.

Any grouping of electrically charged particles can radiate electromagnetic waves with the characteristic size of the charge distribution generally determining the type of photons most efficiently emitted. Antennas emit radio waves, waveguide structures emit microwaves, electrons oscillating against the positive nuclei in atoms emit optical light and x rays, and protons and neutrons moving in nuclei emit gamma rays. Once emitted, gamma rays are no different than x rays which often have the same energies. Since the oscillating charges in the nucleus emit their energy as short-wavelength electromagnetic waves ***this process is not a***

***nuclear reaction.*** None of the interior particles are emitted to cause a nuclear reaction and the nucleus finishes as the stable (non-radioactive) ground state of the same isotope of the same element.

The nucleus is the smallest part of an atom which in turn is the smallest structural unit of physical matter. Thus, quantum mechanics teaches that the motions of the charged particles found within the nucleus will represent the highest velocities of circulation possible in a sample of any material. This fundamental precept means that the very highest densities of (non-nuclear) energy storage will be found in the motions of those charges. Just as in the case of atoms, the movement of charges in a nucleus can absorb photons of electromagnetic waves, which in this case are x rays, and make a transition to an excited state of higher energy. Because of the high energy densities and great velocities, the charges usually reradiate such energies in times too short to be measured ($< 10^{-18}$ s.) However, in rare cases selection rules sufficiently inhibit the coupling of the particle motion to the electromagnetic field for the energies to be stored for tens and even thousands of years in those special nuclei. Such long-lived (metastable), high-energy states of excitation are termed isomeric levels and the materials are simply known as isomers. Such isomers are natural sources of high energy densities.

Our research on the gamma-ray laser identified 29 outstanding isomers which store exceptionally high densities of energy. Four examples are cited in Table I; to appreciate the energy densities presented there it should be noted that a $\mu$g of material is comparable to the amount of ink used to print a period at the end of a sentence. It can be seen that the energy storage of the best of the isomers, $^{178}Hf^{m2}$ is more than a gigajoule per gram. Since one of its key transitions for the output of electromagnetic radiation has a lifetime of 70 ns after triggering,

the power density available from that material is ($1.3 \times 10^9$ J $g^{-1}$ / $7 \times 10^{-8}$ s), or about ***0.05 exawatt per gram.***

Since isomers derive their long shelf lives from their poor coupling to electromagnetic waves, it was traditionally thought to be impossible to trigger the release of the stored energy. However, a recent and major breakthrough in research on the feasibility of a gamma-ray laser showed the existence of a giant pumping resonance at an energy near 2.5 MeV in nuclei with masses around 180. In effect, this resonance provided a "gateway" state through which the selection rules making an isomer long-lived could be violated. If an isomeric level initially stored an energy of 2.0 MeV, only 0.5 MeV would be needed to reach a gateway at 2.5 MeV. The absorption of an x-ray photon of that energy would excite the system to such a level which would be very strongly coupled to the electromagnetic fields. The sum of the stored energy and that of the trigger x-ray photon would then be promptly emitted, or dumped, as gamma rays.

The concept for dumping the energy from controlled fractions of isomeric populations has been demonstrated in a series of experiments with the fourth of the materials listed in Table I. This was first accomplished in the Center for Quantum Electronics at the University of Texas at Dallas (UTD) and was subsequently confirmed in separate experiments at the Institut für Kernphysik, Technische Hochschule Darmstadt. The systematics for the occurrence of the giant pumping resonances has been proven in a series of UTD experiments which located them in nuclei in the region of masses between 167 and 195.

The triggered release of stored energy into electromagnetic waves works and works well. The pervasive problem has been that of the 29 promising materials, only two have yet been available for study. The production of this type of ultrahigh energy density materials is still in its infancy, although remarkable progress has already been made. For example, more than $10^{16}$

nuclei of the best of the materials, $^{178}Hf^{m2}$ are already available. Although not yet mass-separated and carrier free, this is an amount from which it should be possible to obtain a target containing more that $10^{15}$ nuclei with essentially 100% inversion for future experiments.

It would be the very best of all possibilities to be able to immediately realize the release of high energy densities into a ***coherent*** radiation field. However, simply the induced emission of gamma rays from an isomeric sample at such powers would be of considerable technological significance. That goal is close at hand. Once attained, the development of increasing levels of coherence can be approached as a next logical objective. The triggering of the gamma radiation has been the object of our research as a first step in the pumping of a gamma-ray laser.

# II. TECHNICAL BACKGROUND

## II.1 History

Research on the development of a gamma-ray laser has followed a cyclical pattern over the past 33 years with a marked abundance of concepts and approaches. Because of the complex branching of approaches it is often difficult to follow the development of a particular idea in order to properly recognize the brilliance of the early work. However, the origins are perfectly clear. The original proposal for a gamma-ray laser was made by the distinguished Russian Professor Lev Rivlin in 1961 [1]. It went largely unnoticed at the time and the first cycle of research on this topic developed a strong momentum two years later as a result of independent early publications from the US [2,3] and Russia [4,5].

In the first cycle of study which lasted from 1963 - 1980, considerable attention was given to the problem of suddenly assembling a critical density of prepumped nuclei to reach the threshold for stimulated emission. At the end of this period it was generally accepted that such

brute force approaches, usually requiring *in situ* pumping and involving only a single (output) photon, were essentially hopeless. In an encyclopedic review, Baldwin and coauthors [6] concluded the general impossibility of a gamma-ray laser based upon all techniques for pumping known in 1980. That review effectively documented the failure of the traditional approaches to a gamma-ray laser, those relying on the use of intense particle fluxes for input energy. However, toward the end of the first cycle of research the precursors of a new interdisciplinary concept began to appear [7-13]. Based upon nuclear analogs of quantum electronics, these "optical" approaches developed rapidly and launched a renaissance in the field. The basic theory [14-16] of upconversion at the nuclear level was in place by 1982 for the two possible variants, coherent and incoherent upconversion. The use of either multiphoton processes or multiple electromagnetic transitions to release the energy stored in isomers avoided many of the difficulties encountered with more traditional pumping schemes.

Since 1980, research on the feasibility of a gamma-ray laser has taken on a completely new character. In the first half decade a series of experiments verified that the concepts of quantum electronics could be applied at the nuclear level [17-21]. By 1986 one blueprint for a gamma-ray laser [16] had been established and a substantial effort was initiated toward the demonstration of its feasibility. This article reviews the major advances of the most recent decade along that line. Those advances have significantly increased the likelihood of the feasibility of a gamma-ray laser while demonstrating the means for the induced emission of gamma radiation. Excellent concepts for the development of coherence in the levels being pumped, together with even more advanced approaches to lasing, are discussed by the proponents of those ideas elsewhere in this issue.

## II.2 Concepts

At first approach it would seem that the prospects for all ultrashort-wavelength lasers would be vitiated by a very fundamental factor [6]. The basic $\nu^3$ dependence of electron transition probabilities upon frequency, $\nu$ so limits the storage of pump energies in atoms and molecules that even now some of the largest pulsed-power machines are able to excite only milliJoules of laser output and then only at soft x-ray energies. In contrast there are four unique advantages of a gamma-ray laser that would accrue from its operation upon electromagnetic transitions of nuclei:

1) The constant linking $\nu^3$ with lifetime is more favorable by orders-of-magnitude because of the accessibility of a variety of transition moments. The effects pumped by an input pulse can be integrated up to larger values for longer times.

2) Nuclear metastables store keV and even MeV for years. With upconversion schemes most of the energy is input *ex situ*, long before the time of use and triggering requirements are small.

3) Nuclear transitions need not experience thermal broadening and natural linewidths are routinely obtained. Without broadening, electromagnetic cross sections are large and values for 1 Å transitions typically exceed the cross section for the stimulation of Nd in YAG.

4) Working metastables can be concentrated to solid densities.

The essential concept driving the renaissance in gamma-ray laser research was the "optical" pumping of nuclei [7-16]. In this context optical meant x rays, but the fundamentals were the same. Useful, resonant absorption of pump power would occur over short distances in a thin low-Z medium to produce high concentrations of excited nuclei while wasted

wavelengths would only be degraded to heat in much larger volumes. This was the basic concept for avoiding the severe material damage which would have destroyed the Mössbauer effect that would have resulted from the particle-pumping schemes of the first cycle of research emphasized before 1980. In the blueprint of 1982 for upconversions [16], one of several possible types of resonant photopumping was envisioned to transfer the stored population of an isomer to a "gateway" state at the head of a cascade leading to the upper laser level. Of the cases considered, this nuclear analog of the ruby laser embodied the simplest concepts for a gamma-ray laser. Not surprisingly, the greatest rate of achievement in the last decade in the pumping of high-energy density media has been realized in that direction.

For ruby, the identification and exploitation of a bandwidth funnel were the critical keys in the development of the first laser. There was a broad absorption band linked through efficient cascading to the narrow laser level. Our theory [16] called for a nuclear analog of this structure which was unknown in 1986 when intensive experiments were started. Now, that theory has been confirmed.

### II.3 Theoretical Model

The sequence for triggering the release of the energy stored in an isomeric state [16,22] is shown in Fig. 1. The population in the initial level is transferred to a broad pump band, or "gateway" state, which bridges the selection rules that would otherwise limit the coupling of the isomer to the electromagnetic fields. The normal decay from the gateway is accompanied by the emission of immediate fluorescence and leads to the principal laser level from which the sustained output of power will be emitted. Population can be accumulated in that level by continuing to run the pump cycle for a time comparable to the lifetime of the output state.

Pumping processes like that of Fig. 1 have been known for over 50 years [23,24] although relatively few results have been published in that time. Practical difficulties with the calibration and availability of sources of irradiation had limited the degree of reproducibility achieved in work prior to about 1987, as discussed in the next section. The processes are classified as inelastic scattering, or $(\gamma,\gamma')$, reactions in the literature of nuclear physics where the $\gamma$ and $\gamma'$ represent the incident and scattered photons, respectively. In terms of the target nucleus, X the notation is $X(\gamma,\gamma')X^*$ in which $X^*$ represents the same nucleus in its final state of excitation. If the final state is an isomer, the * is replaced by m.

For a sample that is optically thin at the pump wavelength, a computation of the number of nuclei pumped by a $(\gamma,\gamma')$ reaction into a given excited state should be straightforward [16,22,25]. Most intense x-ray sources emit continua, either because bremsstrahlung is initially produced or because spectral lines are degraded by Compton scattering in the immediate environment. Then the irradiation of a sample containing $N_i$ target nuclei in the initial state results in a time-integrated yield of final-state nuclei, $N_f$ according to the general relation

$$N_f = N_i \Phi_0 \int_0^{E_0} \sigma(E)\, F(E, E_0)\, dE \quad , \qquad (1)$$

where the photoexcitation reaction is described by the energy-dependent cross section, $\sigma(E)$. The photon continuum is represented by an endpoint, $E_0$ and the time-integrated spectral intensity, $\phi$ which is written as the product of the total x-ray flux incident on the sample, $\Phi_0$ in photons $cm^{-2}$, and a function $F(E,E_0)$ that gives the distribution of intensities within the continuum. The distribution is normalized so that

$$\int_0^{E_0} F(E, E_0)\, dE = 1 \quad . \tag{2}$$

All $(\gamma,\gamma')$ reactions occurring at energies below the threshold for particle evaporation resonantly excite discrete levels [25,26]; for the population of isomers the relevant levels are pump bands like that depicted in Fig. 1. Only one gateway appears there, but there could be more. Each gateway, identified by the index j, would be excited at a different energy, $E_j$ but all would branch to some extent into the same fluorescent final state, f. Although the width of the j-th level is broad on a nuclear scale, it is narrow in comparison to the scale of energies, E over which $F(E,E_0)$ varies. Thus, the final-state yield can be written from Eq. (1) as

$$A_f(E_0) \equiv \frac{N_f}{N_i \Phi_0} = \sum_j (\sigma\Gamma)_{fj}\, F(E_j, E_0) \quad , \tag{3}$$

where the activation, $A_f(E_0)$ has been introduced. This quantity is the fractional yield of the final state, f normalized per unit photon flux in the irradiating continuum. The summation in Eq. (3) extends over all gateways whose excitation energies are less than the endpoint. In this expression $(\sigma\Gamma)_{fj}$ is the integrated cross section for the production of the final-state population, $N_f$ as a result of excitation through the gateway at $E_j$, so that

$$(\sigma\Gamma)_{fj} = \int_{E_j-\Delta}^{E_j+\Delta} \sigma(E)\, dE \quad , \tag{4}$$

where $\Delta$ is an energy small compared to the spacing between gateways but large in comparison to their widths. For each gateway the integration is performed over a Lorentzian line shape which for a purely radiative transition has the natural width, $\Gamma = (\hbar \ln 2)/T_{1/2}$, with $T_{1/2}$ being its halflife. It is straightforward to show that

$$(\sigma\Gamma)_{fj} = (\pi b_a b_o \Gamma \sigma_0/2)_{fj} \quad , \tag{5}$$

in which the branching ratios $b_a$ and $b_o$ specify the probabilities that a population pumped by absorption into the j-th gateway will decay back into the initial state or by cascade to the output level, respectively. The quantity $\sigma_0/2$ is the peak of the Breit-Wigner cross section [25,27] for the absorption transition,

$$\sigma_0 = \frac{\lambda^2}{2\pi} \frac{2I_j+1}{2I_g+1} \frac{1}{\alpha_p+1} \quad . \tag{6}$$

where $\lambda$ is the wavelength of the x ray at the resonant pump energy, $E_j$, the angular momenta of the gateway and ground states are $I_j$ and $I_g$, respectively, and $\alpha_p$ is the total internal conversion coefficient for the pump step shown in Fig. 1.

Whether or not the initial state being pumped is the ground state or a long-lived isomeric level, the principal figure of merit is the integrated cross section. This quantity reflects the efficacy for the transfer of population to a fluorescence level, and therefore available to an output transition. Thus, it is the nuclear equivalent of the fluorescence efficiency so important in the early development of atomic and molecular lasers.

# III. CRITICAL EXPERIMENTS

## III.1 Foundations

### III.1.1 Model Verification

The most tractable $(\gamma,\gamma')$ reactions for study are those for the photoexcitation of stable isotopes from their ground states up to isomeric levels. In many cases the product is sufficiently

long-lived to be readily examined after termination of the input irradiation although lessons can be learned that can be applied to excitation of the shorter-lived levels more useful in a laser. The prototype for basic study has been the reaction $^{111}Cd(\gamma,\gamma')^{111}Cd^{m}$ exciting the 48.6 min level at 396 keV. Three of the classical measurements of integrated cross section were conducted in 1979, 1982, and 1986 as reported in Refs. [28-30], respectively. Probable errors were quoted as varying only from 7 to 14%, and yet no two of the measurements were even within a factor of 2 of each other. This discrepancy led to serious contentions over the way in which the expected fluorescence yields were calculated [29]. Because of the pervasive disagreements in the literature about nuclear photopumping, one of the first priorities in the most recent cycle of research was placed upon quantitative validation of the model.

Many of the early conflicting measurements were performed with the use of radioisotopes for the irradiation of samples. From the perspective of laser physics, those would appear to be the most unreliable sources of energetic photons for $(\gamma,\gamma')$ reaction studies. Although assumed to emit line spectra, in actual usage they produced intensities which were dominated by continua resulting from photons which had sustained multiple Compton scattering by collimators and shielding in the irradiation environment. Such multiple scatterings are difficult to calculate and are still impossible to measure in practical laboratory configurations without further perturbing the spectra. In contrast, the spectral intensities of bremsstrahlung are routinely calculated with high accuracy from measured accelerator currents and target geometries by well-established, modern computer codes [31,32] such as are commonly used in radiological treatment planning [33].

In our experimental work of the last five years the bremsstrahlung from six accelerators in different experimental environments was used to verify the fluorescence model of Eqs. (1)

- (6) and to cross-check the accelerator intensities. The devices involved in this effort were the e-beam machines DNA/PITHON at Physics International and DNA/Aurora at the US Army Research Laboratory, a 4 MeV and a 6 MeV medical linac at the University of Texas Health Sciences Center, the superconducting injector to the storage ring at Darmstadt (S-DALINAC) and our own 4 MeV linac, the Texas-X. Spectral intensities from bremsstrahlung targets irradiated by these accelerators were calculated with the EGS4 coupled electron/photon transport code [31] for the linacs and with the TIGER code [32] for the e-beam devices. The codes were adapted for each individual configuration and closely monitored values of electron currents were used as inputs to the calculations. In this way both $F(E,E_0)$ and $\Phi_0$ were obtained. In some instances $\Phi_0$ was separately verified by in-line dosimetry using thermoluminescent dosimeters (TLD's) or ionization chambers.

Of the many potential nuclides which might be used to confirm the formulations of Eqs. (1) - (6), the early literature [34] supported the calculation of integrated cross sections for very few. Table II includes those which were known with sufficient accuracy to serve as standards. In the convenient units of $10^{-29}$ cm$^2$ keV, values of integrated cross section ranging from the order of unity to a few tens characterize bandwidth funnels that are sufficient for demonstrations of nuclear fluorescence from reasonable amounts of material at readily accessible levels of input.

In the calibration experiments, samples with typical masses of grams were exposed to the bremsstrahlung from the six accelerators for times ranging from seconds to hours for the continuously operating machines and to single flashes from the pulsed devices. The activations, $A_f$ of Eq. (3) were determined by counting the photons spontaneously emitted from the samples after transferring them from an accelerator chamber to a quieter environment. Usual corrections were made for the isotopic abundance, for the loss of activity during irradiation and transit, for

the counting geometry, for the self absorption of the fluorescence, and for the tabulated efficiencies [35] for the emission of signature photons from the populations, $N_f$. The self absorption factor required a calculation of photon transport within the target materials which was verified in some cases by confirming that the same sample masses in different geometries with different correction factors gave the same final populations.

Measured results were in close agreement [36] with the predictions of Eq. (3) using the values of $(\sigma\Gamma)_{fj}$ given in Table II. A typical example for the reaction $^{87}Sr(\gamma,\gamma')^{87}Sr^m$ is shown in Fig. 2b in which the plot of activation against bremsstrahlung endpoint gives its "excitation function" [37]. Particularly valuable were the data [38] obtained with the S-DALINAC because of its ability to continuously vary the endpoint. A change of $E_0$, as well as altering $\Phi_0$, modulates the spectral distribution function, $F(E_j,E_0)$ at all of the important energies for resonant excitation, $E_j$. The largest effect occurs when $E_0$ is increased from a value just below a gateway to one exceeding it so that $F(E_j,E_0)$ varies from zero to some finite value as depicted in Fig. 2a.

Early work [39,40] on $(\gamma,\gamma')$ reactions had shown that excitation functions displayed very pronounced "activation edges" at the resonant excitation energies, $E_j$ of gateways. Such activation edges are clearly seen in the data of Fig. 2b. There is excellent agreement between measurements obtained with the different accelerators, and between the experimental data and the model calculations made using the literature values [38,39] of Table II. It is useful to note that the units of $A_f$ are those of area because they are a type of average cross section quite different from the $\sigma_0$ of Eq. (6) that describes an individual transition. The small ordinate values are due to the normalization of Eq. (3) which effectively averages the large $\sigma_0$ at the resonant energy, $E_j$ over the broad bandwidth of the entire irradiating continuum, within which most $E \neq E_j$.

### III.1.2 Pump Calibration

The high level of agreement between the measurements and the model established a confidence level sufficient to support the use of $(\gamma,\gamma')$ reactions which populate isomers as a means of selectively sampling the spectra of single x-ray pulses like those from e-beam devices. This technique of x-ray activation of nuclei (XAN) directly measures absolute intensities at discrete energies corresponding to the $E_j$ of gateways accessible to the bremsstrahlung [36,41-44]. An example of an XAN calibration is shown in Fig. 3 for the spectrum from a single shot at an endpoint of 1.4 MeV from DNA/PITHON [42]. No scaling was involved and absolute intensities were obtained using Eq. (3), integrated cross sections from Table II, measured masses of the samples, the distances, and the activations produced. Having calibrated the spectral sources used in these experiments, the persisting uncertainties in the optical pumping of $^{115}In^{m}$ and $^{111}Cd^{m}$ were resolved [45,46] as being primarily due to the use of radioisotopes as sources of irradiation [26].

Following the further improvements in the nuclear data base listed in Table II, it has been possible to extend the XAN procedure to span the range to 4 MeV [47,48]. Figure 4 shows an example of direct measurements [47] of the spectral intensity from a 4 MeV linac using the nuclear standards from Table II in comparison with the calculated bremsstrahlung output.

These calibration studies served to confirm both the traditional model of nuclear activation summarized in Eqs. (1) - (6) and to validate the computer codes for calculating bremsstrahlung intensities based on measured accelerator parameters. ***Now, there can be no reasonable doubt of procedures for quantitatively measuring integrated cross sections if an experiment is carefully performed with a bremsstrahlung source of pump radiation.***

### III.1.3 Limits on Spurious Contributions

Sources of possible spurious contaminations of the measurements were carefully considered. Those could have included contributions to the isomeric yield from natural background or excitation of the samples by (e,e'), ($\gamma$,n), (n,$\gamma$) or (n,n') reactions. In the case of natural background, positive identification of the fluorescence signatures and the amounts of yields was accomplished by obtaining both energy (pulse-height) and decay (multichannel scalar) spectra. Typical examples [49] are shown in Figs. 5 and 6 for the isomers of $^{167}Er^{m}$ and $^{123}Te^{m}$. As can be seen in those figures, excellent agreement was obtained between the measured halflives and the literature values [35] of 2.28 s and 123 days, respectively. Fluorescence signatures were clearly identified and were well-separated from any strong background lines when either NaI(Tl) or HPGe detectors were used.

Inelastic electron scattering, or (e,e'), reactions can excite isomeric populations in a manner that at low momentum transfer is quite similar to that of ($\gamma$,$\gamma$') reactions [50]. However, it has been experimentally demonstrated [39] that the cross sections for electro-excitation of isomers are on the order of $10^2$ smaller than for photoexcitation at the same energy. The numbers of electrons available for (e,e') reactions after penetrating the high-Z bremsstrahlung converters are also orders-of-magnitude less than the numbers of x rays produced. An example of a typical converter is the 3-mm thick tantalum target used in irradiations with the Texas-X, within which the range of 4 MeV electrons was only 1.7 mm. Spurious contributions to the measured activations due to (e,e') reactions were therefore negligible. Likewise, contaminations from ($\gamma$,n) reactions could be summarily excluded since photons within the bremsstrahlung had insufficient energy [34] to reach the thresholds for those

processes in the sample materials except in the very highest energy irradiations with DNA/Aurora.

The question of spurious contributions from (n,$\gamma$) or (n,n') reactions received more consideration. All of the accelerators used, other than DNA/PITHON, were capable of evaporating neutrons from some materials in the accelerator environments. Thus, it was important to determine the amount of isomeric yield which could have been attributed to neutrons. This was done in four separate studies [38,47,48,51] published in 1990 - 1993. The largest contribution was found for experiments conducted with the 6 MeV medical linac where neutrons produced from a Be window could have given as much as an additional 6% to the activation yield [49]. In contrast, our 4 MeV Texas-X, built especially to minimize the amounts of Be and cooling water exposed to the irradiation, held neutron contributions [47] to less than 0.001%. Even though the extent of contamination by neutron contributions was negligible in all experiments conducted, the diagnostic procedures used to verify this point are reviewed here for convenience.

In principle, the two types of neutron reactions that had to be considered were inelastic (n,n') reactions which would have required hot neutrons and neutron capture (n,$\gamma$) processes driven by fluxes of thermal or epithermal neutrons. Contributions from the latter were directly determined in accordance with standard procedures [52]. The thermal neutron fluxes were measured by irradiating pairs of thin indium foils, one bare and the other shielded within a cadmium cover. Energy spectra obtained from these foils were examined after exposure for fluorescence from the isomer $^{116}In^{m}$, which is produced by a branch of the reaction $^{115}In(n,\gamma)^{116}In^{m,g}$. The magnitudes of the fluorescence lines observed in both the bare and the shielded samples allowed the determination of the thermal neutron flux which was 12 neutrons

$cm^{-2}$ $s^{-1}$ in the worst case of the 6 MeV linac environment. The contributions to the activations from thermal neutrons are reported in the literature for all nuclides studied [49] and in all cases were small.

In reduced-Be accelerators like the Texas-X, fast neutrons primarily arise from the photodissociation of the deuterium fraction in the cooling water, the humidity of the air, and the concrete used in construction. It is useful to recall that the production of significant fluxes of fast neutrons is unlikely, *a priori*, because the dissociation energy of deuterium is 2.22 MeV. For a bremsstrahlung endpoint of 4 MeV, this leaves only a maximum of 0.89 MeV kinetic energy for each of the resulting proton and neutron. Those must recede at right angles from the path of the incident photon in order to conserve momentum. Nevertheless, one might assume there to be a large mass of deuterium geometrically placed at right angles to the line-of-sight between the bremsstrahlung target and the sample being illuminated. This would enable the primary neutrons carrying the full 0.89 MeV to irradiate the material under study and they might contribute to the excitation. However, cross sections [53] for inelastic excitation by 1-MeV neutrons rarely exceed 1b so the probable impact parameter can be readily bounded and it can be concluded that only s-wave, p-wave, and perhaps d-wave scattering are probable. In the cases of most isomers, the angular momentum and its projections between initial and final states differ by more than two units so excitation by fast neutrons must confront the same difficulties encountered by photoexcitation. Moreover, only levels lying below 0.89 MeV can be accessed where there is a paucity of gateway states. Photoexcitation with 4 MeV bremsstrahlung can access pump levels up to 4 MeV, *so photoneutrons present no natural advantages in exciting high-multipolarity transitions, even assuming the unlikely geometry needed to produce large numbers of those particles.*

Notwithstanding the lack of a credible rationale for concern about the possible contamination of yields by (n,n') reactions, measurements were made of the fast neutron flux at the position of the irradiated targets using standard techniques [54]. Samples were covered with foils containing $^{46}$Ti, $^{47}$Ti, and $^{58}$Ni, nuclides having large cross sections for (n,p) reactions at energies in the relevant range. No fluorescence was detected to indicate product nuclei and measurements were completely negative in all photoexcitation experiments [53]. Calculations of the expected flux of fast neutrons from the environment were consistent with this negative, predicting effects orders-of-magnitude below the threshold of detection. The possibility of fast-neutron contributions was further examined by covering samples used in the ($\gamma$,$\gamma$') studies with a planchette containing heavy water, $D_2O$ to enhance the prevalence of photodissociation neutrons. Still no increase was observed in isomeric yields, in complete agreement with computations. Photoneutron production from other potential sources such as photodissociation of $O_2$ in the air was also found to be unimportant [53].

All of these negatives for (n,n') contributions were consistent with the successes in reproducing the absolute measurements of the calibration ($\gamma$,$\gamma$') reactions known from the literature [34] with so many different accelerators having such a variety of windows, cooling geometries, and physical enclosures. The contamination of ($\gamma$,$\gamma$') reaction yields by (n,n') reactions was assuredly undetectable in comparison to possible contributions from (n,$\gamma$) reactions which could have been as large as 0.1% in typical cases and 6% in the worst case [47,49,51] given the measured values of neutron flux and neutron cross sections. Overall, spurious contributions to the measured activations due to natural background and incidental (e,e'), ($\gamma$,n), (n,$\gamma$) and (n,n') reactions were found to be negligible.

## III.2 Giant Pumping Resonances

### III.2.1 Discovery

Expressed as partial widths, $b_a b_o \Gamma$, the integrated cross sections for the excitation of $^{77}Se^m$, $^{79}Br^m$, and $^{115}In^m$ seen in Table II correspond to 39, 5, and 94 $\mu$eV, respectively. While among the largest values reported prior to our studies, these results still left an aura of credibility to the traditional impressions that partial widths for exciting isomers would be limited to about 1 $\mu$eV.

Tempering expectations that integrated cross sections of even the magnitudes of Table II might be expected for the dumping of actual isomeric candidates for a gamma-ray laser was a concern for the conservation of various projections of the angular momenta of the nuclei. Many of the interesting candidate isomers belong to the class of nuclei deformed from the normally spherical shape. For those nuclides there is an additional quantum number of dominant importance, K which is the projection of individual nucleonic angular momenta upon the axis of elongation. To this is added the collective rotation of the nucleus to obtain the total angular momentum, J. The resulting system of energy levels resembles that of a diatomic molecule for which

$$E_n(K,J) = E_n(K) + B_n J(J+1) \quad , \qquad (7)$$

where $J \geq K \geq 0$ and J takes the values $|K|$, $|K| + 1$, $|K| + 2$,.... In this expression $B_n$ is a rotational constant that is inversely proportional to the nuclear moment of inertia, and $E_n(K)$ is the lowest value for any level in the resulting "band" of energies identified by other quantum numbers, n. That level is termed the "bandhead." The selection rules for electromagnetic transitions then require both $|\Delta J| \leq M$ and $|\Delta K| \leq M$, where M is the multipolarity of the

transition. In most cases an isomeric state has a large lifetime because it lies in a band whose value of K differs considerably from those of lower levels to which it would otherwise be radiatively connected. As a consequence, bandwidth funneling processes such as shown in Fig. 1 that start from isomeric levels must span substantial changes in K and component transitions have been expected to have large, and hence unlikely, multipolarities.

From this perspective the candidate isomer, $^{180}Ta^{m}$ was the most initially unattractive as it had the largest difference in K between isomer and ground state, 8ħ. However, because a macroscopic sample was readily available, $^{180}Ta^{m}$ became the first isomeric material to be optically pumped to a fluorescent level. This particular nuclide carries a dual distinction. It is the rarest stable isotope occurring in nature [35] and it is the only naturally occurring isomer. The ground state of $^{180}Ta$ is $1^{+}$ with a halflife of 8.1 hours while the tantalum nucleus of mass 180 occurring with 0.012% natural abundance is actually the $9^{-}$ isomer, $^{180}Ta^{m}$. It has an adopted excitation energy of 75.3 keV and a halflife in excess of $1.2 \times 10^{15}$ years.

In an experiment conducted in 1987, 1.2 mg of $^{180}Ta^{m}$ was exposed to bremsstrahlung and a large fluorescence yield was obtained [55]. This was the first time a $(\gamma,\gamma')$ reaction had been excited from an isomeric target as needed for a gamma-ray laser and was the first evidence of the existence of giant pumping resonances. Simply the observation of fluorescence from a milligram-sized target proved that an unexpectedly large reaction channel had opened. Usually grams of material had been required in this type of experiment [49].

The energy-level diagram of $^{180}Ta$ and its daughters [34] is shown in Fig. 7, together with a schematic representation of the individual steps in the excitation and detection of the $^{180}Ta^{m}(\gamma,\gamma')^{180}Ta$ reaction. As can be seen in the figure, the principal means for the detection of the $^{180}Ta$ ground state lies in observing the $K_{\alpha}$ lines of its daughter $^{180}Hf$, produced by electron

capture decay. The efficiency for the emission of $K_\alpha$ photons relative to the number of $^{180}$Ta decays is about 57% [35]. The target used in these experiments was enriched to contain 1.2 mg of $^{180}$Ta diluted in 24.7 mg of $^{181}$Ta. Deposited as a dusting of oxide near the center of the surface of a 5-cm disk of Al and overcoated with a 0.25 mm layer of Kapton, this sample was believed to be free from self absorption of the x rays from the daughter Hf. Such a construction minimized corrections to the raw data and since self absorption was neglected, the final results could only underestimate the activation had there been some unexpected absorption.

The sample was exposed to bremsstrahlung from the 6 MeV medical linac whose output dose rate had been calibrated with an accuracy of $\pm$ 3%. This was the machine that presented the worst-case neutron flux which could have contributed another 6% error. However, as described below, the measurements were subsequently confirmed in absolute comparisons with data taken at the S-DALINAC. After the irradiation, the sample was counted with an n-type, HPGe spectrometer. Conventional techniques were used to calibrate the counting system with isotopic standards. Figure 8 shows the spectra from the enriched target before and after a 4-h, 6-MeV irradiation, while Fig. 9 shows the dependence upon time of the counting rate observed in the Hf($K_\alpha$) peaks after the exposure. Data points are plotted at the particular times at which the instantaneous counting rate equals the average counting rate measured over the finite time intervals shown. The figure shows the close agreement between the measured decay and the literature value for the ground-state halflife of 8.1 h. Analyses [38,55] of the data indicated that the partial width for the dumping of $^{180}$Ta$^m$ was around 0.5 eV.

To determine the transition energy, $E_j$ from the $^{180}$Ta$^m$ isomer to the gateway level, a series of irradiations [38] was made at the S-DALINAC facility using fourteen different endpoints in the range from 2.0 to 6.0 MeV. The existence of an activation edge was clearly

seen in the data shown in Fig. 10b. The fitting of such data to the expression of Eq. (3) by adjusting trial values of $(\sigma\Gamma)_{fj}$ provided the integrated cross sections for the dumping of $^{180}Ta^{m}$ isomeric populations into freely radiating states. Reported values [38] are summarized in Table III and shown schematically in Fig. 10a. The lowest-lying giant pumping resonance was found at an excitation energy near 2.8 MeV.

The integrated cross sections in Table III are enormous values exceeding anything previously reported for transfer through a bandwidth funnel by two orders-of-magnitude. In fact they are 10,000 times larger than the values usually measured for $(\gamma,\gamma')$ reactions in nuclei.

### III.2.2 Systematics

A survey of 19 isotopes [49] conducted with the four U.S. accelerators over a fairly coarse mesh of bremsstrahlung endpoints confirmed the existence of giant resonances for the photoexcitation of isomers in the region of masses near 180. A summary of the results is shown in Fig. 11. Activation edges observed in excitation functions measured [56] using the S-DALINAC continued to support the identifications of integrated cross sections for pumping and dumping of isomers in the mass-180 region that were on the order of 10,000 times greater than usual values. Another study [51] with the S-DALINAC showed that the giant pumping resonances reappeared at lower masses near 120. The close similarity seen in Fig. 11 for integrated cross sections and excitation energies for gateways between nuclei with such dissimilar single-particle structures seems to support the identification of the giant pumping resonances with some type of property of the nuclear core. Whatever the mechanisms, the experimental fact remains that interband transfer processes connecting isomers to freely-radiating levels can almost commonly be pumped through enormous partial widths reaching 0.5 eV, even when the transfer

of angular momentum must be as great as $\Delta K = 8$. It seems this is the nuclear analog of the giant resonance for pumping ruby at the atomic level.

### III.2.3 Structure

As encouraging as were the studies showing the frequency with which giant pumping resonances occurred throughout the table of nuclides, a major concern remained. To lower pump requirements for a laser it is necessary that the $(\sigma\Gamma)$ be large, but this alone is not sufficient. In the ideal case [57] the integrated cross section would be elevated by a strong width multiplying a cross section for absorption having the maximum value possible from Eq. (6). In that case the ratio of pump power per unit volume absorbed resonantly to excite nuclei to the fraction absorbed nonresonantly and degraded to heat would be the largest possible. This is an important factor in thermal survival.

The density of excited states is very high in the nuclei favored in Fig. 11, and is especially so in $^{180}$Ta because it is one of the few stable odd-odd nuclei. It could have been the case that the remarkable magnitude found for $(\sigma\Gamma)$ in the dumping of the population of $^{180}Ta^{m}$ was the result of a great number of adjacent gateways with $(\sigma\Gamma)_{fj}$ of unremarkable size, but adding in Eq. (3) to give a surprising total yield. While such a result would have still been exciting, it would have been much less helpful in rejecting the waste pump power degraded to heat. To show that this was not the case required that scattering measurements be performed.

From Fig. 1 it can be seen that photoexcitation events which do not lead to the population of the state f should be detected by the reemission, or elastic scattering, of the incident photon initially absorbed by the gateway. In analogy with the $(\sigma\Gamma)_{fj}$ of Eq. (5), the integrated cross section for scattering can be written,

$$(\sigma\Gamma)_{0j} = (\pi b_a^2 \Gamma\sigma_0/2)_{0j} \quad . \tag{8}$$

A large value of $(\sigma\Gamma)_{0j}$ would insure that enough photons could be scattered for spectroscopic analysis to determine at what energies the corresponding transitions were excited. In the event $b_a < 1$, some fraction of the gateway-state population would also decay to the isomer to contribute to $(\sigma\Gamma)_{fj}$ and the energies for excitation of some of the giant pumping resonances could be accurately determined.

The design of an experiment to compliment activation measurements by identifying scattering from the pumping resonances requires a nuclide with several favorable properties. It must have an isomer with a reasonable lifetime of seconds to hours and be available in gram quantities with isotopic purity. Beyond such practical concerns would be the desire to have the nuclear structure well-characterized for energies below those at which giant pumping resonances would be expected. With these constraints it was relatively straightforward to identify $^{115}$In as an optimal vehicle for a first test.

A modern experimental arrangement especially designed for nuclear resonance fluorescence (NRF) experiments has been recently described [58]. The spectrum of the intense bremsstrahlung produced by the S-DALINAC accelerator was calibrated in real time from readily-resolved reference transitions observed in the scattered radiation from Al and B wafers which sandwiched the In target. In order to cover an energy range $E_j \simeq 1.5$ - 4.5 MeV, measurements were performed at endpoints of 3.1, 4.6 and 5.2 MeV. The variation of $E_0$ also provided the means to distinguish ground-state (elastic) transitions from decays to excited states. Detailed scattering spectra are shown in the literature [59].

The integrated cross sections obtained from the excitation of the final state, $^{115}In^{m}$ and the photon scattering are shown in Fig. 12a. The excitation energies corresponding to the large $(\sigma\Gamma)_{fj}$ values of gateways are shown in the upper part of Fig. 12a. The widths of the histograms represent the experimental uncertainty in those energies. The striking result is that except for a few moderate levels around 3.0 and 3.7 MeV, all strongly scattering $(\gamma,\gamma')$ transitions were found within the energy regions corresponding to the gateways. Thus, those transitions (or a subset thereof) must have been responsible for the isomer population. No other $(\gamma,\gamma')$ states were resolved in the lower part of Fig. 12a up to $E_j$ = 5 MeV. This confirmed that all important pump bands in this range had been identified.

Further insight was attained from a theoretical analysis within the unified-model [58] which is well-suited to nuclei like $^{115}In$ near shell closure. The configuration space was built by proton 1h-states (relative to the semi-magic $^{116}Sn$ nucleus) and 1p-2h states across the major shell (relative to $^{114}Cd$) coupled to collective phonons (up to three quadrupole and two octupole) in the underlying cores. A residual interaction was then used to mix the two subspaces. The comparison to experiment was accomplished by first computing all possible upward E1, M1, or E2 transitions in such a system. Then for states with a large partial width for transitions to the ground state, the full decay cascade was taken into account to determine model values for $(\sigma\Gamma)_{0j}$ and $(\sigma\Gamma)_{fj}$. In accordance with the experimental results, strong gateways were found only in a limited energy region above $E_j$ = 2.5 MeV; typical $(\sigma\Gamma)_{fj}$ values at lower energies were reduced by a factor of about 10 - 100. The total number of important states was small, in agreement with the measurements.

Figure 12b presents the theoretical results which show a rough division of transition strengths into two groups which might be related to the experimental $(\sigma\Gamma)_{fj}$ data. Although a

one-to-one correspondence seemed beyond the limits of the approach, simply summing the model $(\sigma\Gamma)_{fj}$ within each group compared favorably to the experimental values. The overall agreement seemed quite encouraging and indicated that no major part of the relevant configuration space was missed. A detailed analysis of the main decay branches revealed a clear picture of the important amplitudes in the gateway wavefunctions. All theoretical pump bands had $J^\pi = 7/2^+$ and the coupling to the ground state was dominated in all cases by single-particle $1g_{9/2} \rightarrow 1g_{7/2}$ spin-flip transitions. The first steps in the decays to the isomer in the model calculations proceeded mainly via E1 or E2 transitions.

The critical point to be made from this study, and supported by similar results [60] for the reaction $^{89}Y(\gamma,\gamma')^{89}Y^m$, is that nuclear structure theory, scattering measurements and photoactivation experiments all confirmed that giant pumping resonances corresponded to a small number of discrete gateways. Absorption cross sections approached those ideals of Eq. (6) needed to separate the wasted deposition of heat from the useful excitation of nuclei in a sample pumped with intense x rays.

### III.2.4 Significance

The significance of these favorable developments to laser feasibility may be appreciated with the help of analogs from the atomic scale. In atoms there is a familiar increase in the density of levels available for excitation as transition energies approach the limit for photoionization. The number of such Rydberg states is generally on the order of $n^3$, where n is the principal quantum. Thus it is difficult to pump significant energy into a selected level with a continuum source of modest spectral width. The general difficulty in scaling x-ray lasers is a clear illustration of this problem and it seems that only the rigor imposed by selection rules allows the few cases demonstrated to work at all.

In nuclei the situation could have been even worse because the likelihood is much greater for there to be levels that from the atomic perspective would be considered analogous to multiply excited states. The nuclear level density is more difficult to specify quantitatively, but an approximation of exp ($\sqrt{n}$) is reasonably indicative as excitation energies approach that needed to remove the first particle in a photonuclear reaction. Since selection rules were shown to be bridged by the striking efficiency with which $\Delta K = 8$ could be lost in $^{180}$Ta, there was a clear hazard that highly-excited nuclear levels could not be selectively excited as needed for a gamma-ray laser. Sum rules limit the strength per unit bandwidth available at a particular transition energy and there was the possibility that the sum would be smoothly distributed over the great number of levels in any interval of high excitation. Then the deposition of pump energy into nuclear excitation would have been diluted into a much larger volume by the small cross sections available to any component transition. Such a distribution of gateway strength was not found, constituting a second breakthrough of comparable importance to that achieved by dumping the population of $^{180}$Ta$^{m}$.

The giant pumping resonances found in $^{115}$In show the transition strength is concentrated into relatively few discrete lines. The nuclear structure model identified this particular case as an example of fragmented spin-flip transition strength, but the point critical to laser feasibility is the limited degree of the fragmentation. Relatively few transitions to gateway states collected all of that type of transition strength available over the range of energies from 2 - 5 MeV. The mechanism for this fragmentation was less clear, having arisen from detailed unified-model calculations.

An interesting speculation is currently being investigated [61,62] which may explain the existence of strong, low-multipolarity transitions similar to the giant pumping resonances in

nuclei near mass 180. At certain energies of excitation, collective oscillations of the core nucleons may break the symmetry upon which rests the identification of angular-momentum projections of the pure single-particle states. Within this energy range single-particle states of differing K would be strongly mixed and the possibility for transferring larger amounts of $\Delta K$ with greater partial widths might be enhanced. Some support for this speculation has been found in unexpected enhancements to transitions which hinted at K mixing [61,62]. However, the most striking result was recently measured [63] for the spontaneous deexcitation of the 3.7-$\mu$s isomer $^{174}Hf^{m}$. There the decay of the isomer was found to occur primarily by a transition through a state at 2685 keV in which sufficient K mixing occurred for $\Delta K = 14$ to be lost between the isomer and the ground-state bands. As shown in Fig. 13, this energy is remarkably close to that of the giant pumping resonance at 2800 $\pm$ 100 keV for $^{180}$Ta, and other large gateways (Fig. 11) for neighboring nuclei in the mass-180 island. The energetics for giant pumping resonances for nuclei with quite dissimilar single-particle structures supports the identification of those gateways with K-mixing levels arising from a core property. In such a case, the integrated cross sections and excitation energies would be expected to vary slowly among neighboring nuclei. This behavior [56] is seen in Fig. 14 that plots the quantity S which is proportional to ($\sigma\Gamma$) against nuclear deformation, a core property.

## IV. THERMAL ECONOMY OF A GAMMA-RAY LASER

Our model of a gamma-ray laser for the 1990's is not fundamentally different from the nuclear analog of the ruby laser described [16] in 1982, envisioned as a thin film of diluent doped with isomeric nuclei and pumped with a flash of x rays in a slab geometry. The question of feasibility still rests on the degree to which the properties of some real nuclide approach those

of the ideals being modeled. What has changed over the past half decade is that the discovery of giant pumping resonances has enabled some of the original constraints to be relaxed. The result is that the feasibility of a gamma-ray laser has been enhanced by orders-of-magnitude over that originally estimated in 1982. Thus, as summarized here it has been useful [57] to recompute the model in terms of the new data obtained during the past five years.

Since the better candidate isomers for a gamma-ray laser have never been fabricated in macroscopic amounts, precise knowledge of the properties of the best nuclide is not available. Moreover, since feasibility is such a complex function of the nuclear parameters, the assumptions introduced into any model will critically affect the estimates of feasibility in strongly nonlinear ways. For the computation reported here the following parameters were assumed:

1) A single pump band exists which is a giant pumping resonance with a partial width of $b_a b_0 \Gamma = 1$ eV.

2) The pump transition is centered on an energy $E_j = 30$ keV.

3) The initial state is assumed to be isomeric with an excitation energy so high that 2) is possible.

4) The output transition is around 100 keV.

5) The active nuclei are diluted in a thin film of diamond or Be.

6) The Borrmann effect contributes a factor of 10 enhancement to the ratio of cross sections for resonant to nonresonant absorption.

The most sensitive assumptions are those of statements 2) and 3) about the width and excitation energy of the giant pumping resonance. The range of excitation energies over which isomers can be found is very large and it has already been shown experimentally that isomers can be dumped into freely-radiating states, even through $\Delta K = 8$ or $\Delta K = 14$. The only doubt

here is a statistical one; whether or not a giant pump resonance can be found within 30 keV of an isomer.

Following our development [16] of 1982, under small signal conditions the midrange requirement of $10^{-4}$ is obtained for the pumped fraction,

$$\frac{N_f}{N_i} \geq \frac{\sigma_{NR}}{\sigma_R} \approx 10^{-4} \quad , \tag{9}$$

where $\sigma_R$ and $\sigma_{NR}$ are the cross sections for useful, resonant nuclear absorption and nonresonant photoelectric absorption, respectively. The value of $10^{-4}$ includes a Borrmann enhancement to a value of $\sigma_{NR}/\sigma_R \approx 10^{-3}$ from Ref. [6]. Equation (9) sets the pump intensity needed for threshold, and with it the amount of waste heat to dissipate.

The essential concept in the management of the thermal economy is that the mean free path (MFP) for a photon resonant with the nuclear pump transition is much shorter than the MFP for nonresonant, photoelectric absorption to produce heat. Also, the MFP for a photoelectron produced in the nonresonant channel is greater in the diluent than the MFP for the photons pumping the nuclear resonance. This means that a thin film of diamond can be doped or implanted with active nuclei to provide useful absorption of incident photons in the bandwidth of the giant pumping resonance while the majority of the nonresonant photons will pass through the film into a substrate which can be cooled by ablation or cryogenics. Moreover, primary photoelectrons produced by the small fraction of nonresonant events occurring in the film can escape before their energy is degraded to heat.

The quantitative expression of this strategy is obtained by substituting Eq. (3) into Eq. (9) and assuming a single giant resonance dominates so that the sum is unnecessary. Solving

for the spectral intensity, $\phi_j = \Phi_0 F(E_j,E_0)$ for 30 keV pump photons, the spectral fluence, $F_j \equiv E_j\phi_j$ at threshold is found to be

$$F_j = 177\ mJ\ cm^{-2}\ eV^{-1} \quad . \tag{10}$$

This gives the energy flux per unit bandwidth within the gateway resonance which must be incident upon the film.

For the likely cases of rare earth or platinide elements, the 30 keV pump energy lies below the K edge and about 15 keV above the L edge. As a result, primary photoelectrons produced by nonresonant absorption in the active medium should have energies on the order of 15 keV and ranges of 6.0 and 3.0 $\mu$m in Be and C, respectively [64]. Thus, only about 10% and 20% of the primaries, respectively, should be stopped in a 0.67 $\mu$m thick host film of Be or diamond. This thickness corresponds to the MFP for resonant absorption at a concentration of 10% doping. The fraction of the incident pump energy degraded into heat in the laser film because of nonresonant absorption becomes

$$f\ (Be) = 4.8 \times 10^{-4} \quad , \text{ or} \tag{11a}$$

$$f\ (C) = 2.4 \times 10^{-4} \quad . \tag{11b}$$

Considering that edge filters or ablation layers could reduce the bandwidth of the pump radiation to 3 keV before reaching the doped layer of active medium, the incident fluence lying outside the bandwidth for resonant absorption would be 3000 times greater than the value of Eq. (10). However, only the fractions of Eqs. (11a) and (11b) are capable of being degraded into heat in the sensitive layer. The resulting energy balance can be summarized at threshold by the first two lines of Table IV.

Dividing those fluences by the 0.67 $\mu$m thickness gives the energy loading of the laser film shown in Table IV. These values are quite significantly below the levels of heating required to degrade the recoil-free fractions in the case of Be or diamond lattices. Baldwin has summarized [6] the involved dependence of the recoil-free fraction of gamma transitions upon recoil energy, lattice parameters, and temperature. He showed that even at a temperature, T equal to the Debye temperature, $\Theta_D$, the recoil-free fraction is not significantly degraded (by more than a factor of 2) for a transition even so energetic as to give a classical recoil energy of 0.14 $\Theta_D$. Since diamond is characterized by $\Theta_D$ = 2230 K, this means a transition of 100 keV is little affected by a temperature increase up to T = $\Theta_D$. It is a textbook computation [65] to estimate that the energy content of the phonons for a material with $\Theta_D$ = 2230 K at a temperature of T = $\Theta_D$ is about 11 kJ cm$^{-3}$. Comparing this with the estimated thermal loading of 3.8 kJ cm$^{-3}$ gives a "safety factor" of almost three. A comparable margin is obtained for a Be lattice.

To summarize, it is convenient to recast the threshold fluence of Eq. (10) into more tangible terms. The spectral fluence of 177 mJ cm$^{-2}$ eV$^{-1}$ corresponds to 530 J cm$^{-2}$ if the bandwidth of the pump x rays is arranged to be 3 keV, a practical separation which might be filtered between K edges. Even if pumped instantaneously so that no waste heat were transported away, the thermal loading would reach only 1/3 of the limit for retaining the Mössbauer effect in a diamond lattice. If derived from an x-ray line of 30 eV width, the threshold fluence would be only 5.3 J cm$^{-2}$. In that case the thermal loading would reach only 1/300 of the critical limit.

Even beyond this point much can be done to reduce heating further. All calculations so far considered the generation of the waste heat to be instantaneous. The time for the transit of

a phonon across the 0.67-$\mu$m thickness of the inverting layer is on the order of only 100 ps so that the transport of significant amounts of heat into a diamond heat sink is possible on a nanosecond time scale. Yet most of the fluorescent levels of interest for inversion [16] have lifetimes of tens of nanoseconds to tens of microseconds. This is many times the period for the transport of phonons out of the film so that orders-of-magnitude can be realized in reducing the thermal loading further below the limits specified so far. However, all these techniques require precise knowledge about the energy levels and absorption edges of the materials involved. Until the properties of the best candidate for a gamma-ray laser are known, the exact specifications of the solution to the disposal of the waste heat cannot be generally articulated. The examples summarized here show that there are many orders-of-magnitude in the safety margin between likely amounts of heating and the much larger amounts which can be tolerated in stiff lattices such as Be and diamond.

# V. CANDIDATE ISOMER FOR A GAMMA-RAY LASER

## V.1 Candidates and Simulations

An exact ranking of the 29 candidate isomers for a gamma-ray laser depends upon a complex weighting of combinations of nuclear parameters, many of which are poorly known. However, the potential importance of several nuclides is magnified by some very pragmatic considerations. These issues are typified by comparisons of the four examples presented in Table I.

From the perspective of shelf life and availability, $^{180}Ta^{m}$ is far superior. It is a naturally occurring material composing 0.012 % of all tantalum and can be prepared simply by separating natural Ta by atomic mass. Samples of milligram weight exist and one such specimen was used

in the breakthrough experiment that proved x rays can dump the energy stored in isomeric populations. In contrast, the entire world inventory of $^{178}Hf^{m2}$ was reported in 1992 to be about $10^{15}$ nuclei [66] although recently this amount has been increased to about $5 \times 10^{16}$.

However, from the perspective of triggering $^{180}Ta^{m}$ appears to be much less practical. Although the energy storage is still impressively high, the isomeric level lies quite low in energy when compared to the value for the excitation of the K-breaking gateway at 2.8 MeV. For $^{178}Hf^{m2}$ the energy of the isomer at 2.45 MeV is the highest known that still lies below the likely gateway energy between 2.5 - 3.0 MeV [67]. The isomer $^{174}Hf^{m}$ is even higher at 3.312 MeV, but the availability [63] of a spontaneous transition down to the K-mixing level at 2.685 MeV reduces its shelf halflife to only 3.7 $\mu$s. Ideally for ease of triggering, an isomer would store as much energy as possible without exceeding that of the K-breaking level for that nuclide. As long as the transition energy needed for triggering is positive, the isomer cannot dump spontaneously as happens with $^{174}Hf^{m}$. The lifetime of the initial population will then be long and problems of storage will be minimized. Guided to $^{178}Hf^{m2}$ by energetics, a reasonable next concern from the pragmatic viewpoint is for the duration of the trigger pulse.

Even in the best scenarios the requirement for the energy in a trigger pulse is large. The problem is compounded if the fluorescence lifetime of the level into which the isomeric population is to be dumped is too short. Large pulsed-power devices typically deliver their outputs over durations of nanoseconds to a few microseconds, so it would be desirable to utilize a laser candidate with strong fluorescence lines of comparable lifetimes. In this case as well, the $^{178}Hf^{m2}$ is favorable since it has transitions with lifetimes of both tens of ns and tens of $\mu$s, as will be seen in the following section.

The experiments needed to confirm our pragmatic scoring of the better of the 29 candidates for a gamma-ray laser have been postponed by the difficulties in obtaining samples. Thus, it has seemed fruitful to identify simulation nuclei which could serve as vehicles with which to develop systems and instrumentations for future triggering studies. To be useful a simulation nuclide needs to have a strong output fluorescence transition that can be reached by cascade from a K-breaking resonance pumped from the ground state by intense x-ray pulses. Moreover the levels radiating such transitions should have lifetimes of tens of ns to tens of $\mu$s. Meeting these criteria were the four convenient simulation nuclides listed in Table V whose excitation we have recently studied [68].

Excitation of those nuclides was provided by our 4 MeV Texas-X linac which produces 150-mA pulses of electrons of 4-$\mu$s duration at a repetition rate of 250 Hz. These are routinely converted to bremsstrahlung with a cooled Pt converter. The difficulty in this type of experiment which must be performed *in situ* lies in Compton scattering of the bremsstrahlung from the samples and a milligram-sized target support which produces background noise that tends to obscure gamma fluorescence. Our present system has used electronic gating to reduce the sensitivity of the detector during the pump pulses. A combination of issues limits the recovery of the data acquisition system by a minimum product of fluorescence energy and delay time which currently is 150 keV x 2 $\mu$s. Shown in Fig. 15 are data [68] from delayed fluorescence at 482 keV from the 18-$\mu$s level of $^{181}$Ta after a recovery time of 7.22 $\mu$s from the end of the x-ray pulse. The literature value of the fluorescence-state lifetime agrees well with the measured decay. The energetics of the process are summarized in the diagram of Fig. 16. Similar results are shown in Fig. 17 for the nuclide $^{176}$Hf for which the relevant energy levels are summarized in Fig. 18. Analyses of the fluorescence data using Eqs. (1) - (4) yielded new

values for the integrated cross sections for pumping of short-lived $\mu$s fluorescence. Figure 19 shows these results included in the summary plot of Fig. 11. It is encouraging to observe that the systematics for the pumping of these simulated laser levels closely follows the trends already established for the excitation of longer-lived levels which were easier to study. As yet the complementary data on the excitation energies needed to reach the pumping gateways have not been measured in these simulations, but they might reasonably be expected to also continue the established systematics.

### V.2 First-Ranked Candidate

The first priority candidate for a gamma-ray laser is the 31-year isomer of $^{178}$Hf, superior to the next possibilities by orders-of-magnitude. The energy-level diagram [69-71] for $^{178}$Hf is shown in Fig. 20 with prominent fluorescent transitions indicated. The fundamental question is whether the giant pumping resonance will be found at the level shown in the figure that is predicted by systematics. In case of a weak success in which K-breaking is tending to fail we would expect pumping to preferentially populate the band to the right of the figure. This would lead to fluorescence at 437 keV with 35% efficiency from the bandhead having a 68-$\mu$s lifetime, well within current experimental capabilities demonstrated by the simulations.

In the event of a strong success in which K-breaking is complete, we would expect to preferentially populate the left-side band which leads to fluorescence at 922 keV with 65% efficiency and 1247 keV with 30% efficiency from the bandhead having a 78-ns lifetime. Demonstrations of dumping the stored energy from the isomer would then require the use of an accelerator with shorter pulses such as the APEX-I device in our facility. This e-beam machine produces 30 kA of electrons in pulses of 30-ns duration at energies variable from 0.7 - 1.2 MeV. Although a single-shot device, it served well in our first investigations of gamma

fluorescence [36,42]. Moreover, there is a great advantage in the use of this type of device since it can be configured to use bremsstrahlung having 0.7 - 0.8 MeV endpoints to pump the left-side band that will give signal fluorescence at 1.25 MeV. It should be straightforward to set discrimination levels in the detection electronics to reject the scattered pump radiation which consists of photons at much lower energies.

The expected number of fluorescent photons can be calculated with two assumptions about the overall integrated cross section for pumping to fluorescence,

$$(\sigma\Gamma)_{sys} = 5 \times 10^{-25}\ cm^2\ keV \quad \text{, and} \tag{12a}$$

$$(\sigma\Gamma)_{best} = 2.5 \times 10^{-23}\ cm^2\ keV \quad , \tag{12b}$$

where the first value is consistent with the measurements of Fig. 19 and the second is scaled for the dependence on pump energy given by Eq. (6). The range of excitation energies spanned by the measurements of Figs. 11 and 19 is insufficient to determine any further correlation between ($\sigma\Gamma$) and the energy needed for triggering. For a target of $10^{15}$ nuclei, the Texas-X linac would produce $8 \times 10^5$ or $4 \times 10^7$ fluorescence photons per hour for the cross sections of Eqs. (12a) and (12b), respectively. In that case there is an ample safety margin for the arrangement of realistic geometries for the collection and detection of the fluorescence.

## VI. Conclusions

The current cycle of research into the feasibility of a gamma-ray laser started in 1982 with the emergence of a strongly interdisciplinary approach. Generally characterized by the study of nuclear analogs of concepts of quantum electronics already proven at the atomic and molecular levels, major advances have been realized in this period. Documented throughout this

volume, they provide a richness of options for developing output coherence once excited nuclear states can be coupled to the radiation field.

Reviewed here have been our own works concerned with pumping (or triggering) enough nuclei into states which can be coupled when desired. Supported by strong collaborations with colleagues at the Technische Hochschule Darmstadt, the Flerov Laboratory for Nuclear Reactions at Dubna, and the CSNSM and IPN Laboratories at the Orsay Campus, major breakthroughs have been achieved that drastically improve the prospects for success. Primary has been the discovery of K-breaking levels in some nuclei at reasonably accessible energies. Unknown before 1988 [55], such levels have significance also in astrophysics [72], and were independently found in the decay of exotic nuclei [63] in 1990.

Transitions to the K-breaking levels provide giant pumping resonances which are analogous to the bandwidth funnels that made the ruby laser possible. Since they can be accessed either from ground states or from isomeric levels, K-breaking levels make *ex-situ* pumping of a gamma-ray laser a reasonable proposition. Precursive nuclides can be pumped into isomeric states either by reactors or by accelerators outside of the more fragile structures in which they would be used. Studies of systematics have shown the pervasive occurrence of K-breaking levels across islands of mass that contain the 29 candidate isomers originally preferred for a gamma-ray laser. In principle, many of these isomers could be produced *ex-situ* so that the requirements for triggering the conversion to freely-radiating states would represent relatively modest demands for the remainder of the *in-situ* pumping to the K-breaking level. While computations of the thermal economy of the *in-situ* step depend upon high exponents of the unknown properties of the particular isomer and its host medium, reasonable targets are not necessarily destroyed by the waste pump power. Safety margins of orders-of-magnitude built

into the estimates of thermal loading anticipate the emergence of parameter values less favorable than those modeled.

Most recently, an extension of the systematics studies has shown that the favorable occurrence of giant resonances for pumping nuclear fluorescence extends to the excitation of laser-like transitions having lifetimes on the order of $\mu$s. Also, the basic structural concept of doping the working nuclides into a thin diamond film at a target concentration of 10% has been demonstrated [73] and examples of Mössbauer nuclei implanted into diamond are already commercially available.

From the larger perspective it seems reasonable to conclude that the first breakthrough in determining the feasibility of a gamma-ray laser has been followed by a second. The proof that isomeric populations can be dumped by pumping them with intense pulses of x rays has been followed by the demonstration that the strengths for doing so are fragmented into relatively few discrete transitions of great intensity. These are precisely the necessary conditions for the concentration of useful pump power into the selective excitation of nuclear populations while dissipating power degraded to heat in much larger volumes. In the test case of $^{115}$In, most amenable to computation, the pump step was found to be a spin-flip transition whose strength was only slightly fragmented into weaker components despite the higher state densities between 2 - 5 MeV. Complete agreement was demonstrated between our pumping measurements, independent scattering studies and theory in 1991 [59]. The particular structure of the K-breaking levels in the higher mass range of most importance has been proposed for the case of $^{174}$Hf [63]. We have tried to develop algorithms for rationalizing transition strengths in neighboring nuclides from scaling studies like that of Ref. [56], but the matter of accurate interpolation among the measurements remains a complex question.

While the paucity of actual samples has inhibited the final demonstration of feasibility, estimates of likely yields from such experiments have shown that strong levels of fluorescence from laser-like levels of the 31-year isomer $^{178}Hf^{m2}$ should be observable when the material becomes available. On the basis of shelflife and energy storage it seems a clear choice for the best candidate isomer for induced gamma-ray emission [67], a key triggering step in a gamma-ray laser. These conclusions would seem to provide a strong motivation for the production of this first ranked candidate for use in a gamma-ray laser. If two steps of *ex-situ* pumping can be considered, it also serves as a vehicle for an interesting proposal [74]. The estimates of the likely yields from a microweight sample with the Texas-X suggest that a macroscopic sample could be converted by $^{178}Hf^{m2}(\gamma,n)^{177}Hf^{m2}$ with a more robust source to produce a significant amount of the 51-minute $^{177}Hf^{m2}$. As described in a companion article in this issue [67], systematics indicate that the transition energy from that latter isomer to the K-mixing level is too small to estimate. It might serve very well for one of the many attractive schemes for a gamma-ray laser in which very low-energy photons are used to mix properties of an isomeric level with those of some member of a freely-radiating yrast band which is nearly resonant in energy.

The strongest conclusion to communicate here is that the persistent tenets of theoretical dogma which have historically [6] inhibited the development of a gamma-ray laser have been eliminated by experimental studies of the past five years. There is no need to melt the host lattice in order to pump a nuclear system to the laser threshold. There are no *a priori* obstacles to the realization of a gamma-ray laser. A gamma-ray laser seems feasible if the right combination of energy levels occurs in some real material. The overriding question to resolve is whether or not one of the better of the candidate nuclides has its isomeric level within a few

tens or even hundreds of keV of one of the giant resonances for dumping angular momenta as seems to be the case with the priority candidate for a gamma-ray laser, $^{178}Hf^{m2}$.

## REFERENCES


1. Rivlin, L. A., *USSR Patent #621265*, Appl. January 10, 1961.
2. Baldwin, G. C., Neissel, J. P., Terhune, J. P., and Tonks, L., 1963, *Proc. IEEE*, **51**, 1247.
3. Vali, V. and Vali, W., 1963, *Proc. IEEE*, **51**, 182.
4. Rivlin, L. A., 1963, *Vopr. Radioelectron.*, **6**, 43.
5. Chirikov, B. V., 1963, *Sov. Phys. JETP*, **17**, 1355.
6. Baldwin, G. C., Solem, J. C., and Goldanskii, V. I., 1981, *Rev. Mod. Phys.* **53**, 678.
7. Letokhov, V. S., 1974, *Sov. J. Quant. Electron.*, **3**, 360.
8. Arad, B., Eliezer, S., and Paiss, Y., 1979, *Phys. Lett.* **74A**, 395.
9. Collins, C. B., Olariu, S., Petrascu, M., and Popescu, I., 1979, *Phys. Rev. Lett.*, **42**, 1397.
10. Collins, C. B., Olariu, S., Petrascu, M., and Popescu, I., 1979, *Phys. Rev. C*, **20**, 1942.
11. Olariu, S., Popescu, I., and Collins, C. B., 1981, *Phys. Rev. C*, **23**, 50.
12. Olariu, S., Popescu, I., and Collins, C. B., 1981, *Phys. Rev. C*, **23**, 1007.
13. Collins, C. B., in *Proceedings of the International Conference on Lasers '80*, ed. Collins, C. B., 1981 (STS Press, McLean, VA) p. 524-531.
14. Collins, C. B., in *Laser Technique for Extreme Ultraviolet Spectroscopy*, ed. McIlrath, T. J. and Freeman, R. R., 1982 (AIP Conf. Proc. No. 90, New York) p. 454-464.
15. Collins, C. B., in *Proceedings of the International Conference on Lasers '81*, ed. Collins, C. B., 1982 (STS Press, McLean, VA) p. 291-295.

16. Collins, C. B., Lee, F. W., Shemwell, D. M., DePaola, B. D., Olariu, S., and Popescu, I., 1982, *J. Appl. Phys.*, **53**, 4645.

17. DePaola, B. D. and Collins, C. B., 1984, *J. Opt. Soc. Am.*, **1**, 812.

18. Collins, C. B. and DePaola, B. D., in *Laser Techniques in the Extreme Ultraviolet*, eds. Harris, S. E., and Lucatorto, T. B., 1984 (AIP Conf. Proc. No. 119, New York) p. 45-53.

19. Collins, C. B. and DePaola B. D., 1985, *Optics Lett.*, **10**, 25.

20. DePaola, B. D., Wagal, S. S., and Collins, C. B., 1985, *J. Opt. Soc. Am. B*, **2**, 541.

21. DePaola, B. D. and Collins, C. B., 1984, *J. Opt. Soc. Am. B*, **1**, 812.

22. Collins, C. B., in *Handbook of Laser Science and Technology*, 1991 (CRC Press, Boca Raton) p. 561-567.

23. Pontecorvo, B. and Lazard, A., 1939, *C. R. Acad. Sci.*, ***208, 99.***

24. Collins, G. B., Waldman, B., Stubblefield, E. M., and Goldhaber, M., 1939, *Phys. Rev.*, **55**, 507.

25. Metzger, F. R., 1959, *Prog. Nucl. Phys.*, **7**, 54.

26. von Neumann-Cosel, P., Richter, A., Carroll, J. J., and Collins, C. B., 1991, *Phys. Rev. C*, **44**, 554.

27. Breit, G., and Wigner, E., 1936, *Phys. Rev.*, **49**, 519.

28. Watanabe, Y. and Mukoyama, T., 1979, *Bull. Inst. Chem. Res., Kyoto Univ.*, **57**, 72,

29. Krcmar, M. Ljubicic, A., Pisk, K., Logan, B., and Vrtar, M., 1982, *Phys. Rev. C*, **25**, 2097.

30. Bikit, I., Slivka, J., Anicin, I. V., Marinkov, L., Ruydic, A., and Hamilton, W. D., 1987, *Phys. Rev. C*, **35**, 1943.

31. Nelson, W. R., Hirayama, H., and Rogers, D. W. O., 1985, *Stanford Linear Accelerator Center Report No. SLAC 265* (unpublished).

32. Halbleib, J. A., and Mehlhorn, T. A., 1984, *ITS: The Integrated TIGER Series of Coupled Electron/Photon Monte Carlo Transport Codes, Sandia National Laboratories Report SAND84-0573* (unpublished).

33. Mohan, R., Chui, C., and Lidofsky, L., 1985, *Med. Phys.*, **12**, 595.

34. *Evaluated Nuclear Structure Data File*, 1986 (Brookhaven National Laboratory, Upton, New York).

35. Browne, E. and Firestone, R. B., 1986, *Table of Radioactive Isotopes*, (Wiley, New York) p. 180.

36. Anderson, J. A. and Collins, C. B., 1987, *Rev. Sci. Instrum.*, **58**, 2157.

37. Carroll, J. J., and Collins, C. B., 1994, in *Proc. Int. Conf. Lasers and Appl. (LASERS '93)* p. 171-178.

38. Collins, C. B., Carroll, J. J., Sinor, T. W., Byrd, M. J., Richmond, D. G., Taylor, K. N., Huber, M., Huxel, N., von Neumann-Cosel, P., Richter, A., Spieler, C., and Ziegler, W., 1990, *Phys. Rev. C*, **42**, R1813.

39. Booth, E. C. and Brownson, 1967, *Nucl. Phys.* **A98**, 529.

40. Guth, E., 1941, *Phys. Rev.*, **59**, 325.

41. Paiss, Y., Eberhard, C. D., and Collins, C. B., 1987, *J. de Phys.*, **48**, 131.

42. Anderson, J. A. and Collins, C. B., 1988, *Rev. Sci. Instrum.* **59**, 414.

43. Anderson, J. A., Carroll, J. M., Taylor, K. N., Carroll, J. J., Byrd, M. J., Sinor, T. W., Collins, C. B., Agee, F. J., Davis, D., Huttlin, G. A., Kerris, K. G., Litz, M. S., Whittaker, D. A., Pereira, N. R., and Gorbics, S. G., 1989, *Nucl. Instrum. Meth.*, **B40/41**, 1189.

44. Anderson, J. A., Eberhard, C. D., Taylor, K. N., Carroll, J. M., Carroll, J. J., Byrd, M. J., and Collins, C. B., 1989, *IEEE Trans. Nucl. Sci.*, **36**, 241.

45. Collins, C. B. , Anderson, J. A., Paiss, Y., Eberhard, C. D., Peterson, R. J., and Hodge, W. L., 1988, *Phys. Rev. C*, **38**, 1852.

46. Anderson, J. A., Byrd, M. J., and Collins, C. B., 1988, *Phys. Rev. C*, **38**, 2833.

47. Carroll, J. J., Richmond, D. G., Sinor, T. W., Taylor, K. N., Hong, C., Standifird, J. D., and Collins, C. B., 1993, *Rev. Sci. Instrum.*, **64**, 2298.

48. von Neumann-Cosel, P., Huxel, N., Richter, A., Spieler, C., Carroll, J. J., and Collins, C., B., 1994, *Nucl. Instrum. Meth.*, **A338**, 425.

49. Carroll, J. J., Byrd, M. J., Richmond, D. G., Sinor, T. W., Taylor, K. N., Hodge, W. L., Paiss, Y., Eberhard, C. D., Anderson, J. A., Collins, C. B., Scarbrough, E. C., Antich, P. P., Agee, F. J., Davis, D., Huttlin, G. A., Kerris, K. G., Litz, M. S., and Whittaker, D. A., 1991, *Phys. Rev. C*, **43**, 1238.

50. *Nuclear Theory, Vol. 2: Excitation Mechanisms of the Nucleus, Electromagnetic and Weak Interactions*, Eisenberg, J. M., and Greiner, W., 1970 (North Holland, Amsterdam) Parts I and II.

51. Carroll, J. J., Sinor, T. W., Richmond, D. G., Taylor, K. N., Collins, C. B., Huber, M. Huxel, N., von Neumann-Cosel, P., Richter, A., Spieler, C., and Ziegler, W., 1991, *Phys. Rev. C*, **43**, 879.

52. *ASTM Standard Method for Determining Thermal Neutron Reaction and Fluence Rates by Radioactivation Techniques, Publication E 262-86*, 1987 (American Society for Testing and Materials, Philadelphia) and references cited there.

53. Anderson, J. A., Eberhard, C. D., Carroll, J. J., Byrd, M. J., and Collins, C. B., in *Center for Quantum Electronics Annual Report FY-1988*, 1988 (unpublished) p.147-176.

54. *ASTM Standard Method for Determining Neutron Flux, Fluence, and Spectra by Radioactivation Techniques, Publication E 261-77*, 1987 (American Society for Testing and Materials, Philadelphia) and references cited there.

55. Collins, C. B., Eberhard, C. D., Glesener, J. W., and Anderson, J. A., 1988, *Phys. Rev. C*, **37**, 2267.

56. Collins, C. B., Carroll, J. J., Taylor, K. N., Richmond, D. G., Sinor, T. W., Huber, M., von Neumann-Cosel, P., Richter, A., and Ziegler, W., 1992, *Phys. Rev. C*, **46**, 952.

57. Collins, C. B., Carroll, J. J., Taylor, K. N., Sinor, T. W., Hong, C., Standifird, J. D., and Richmond, D. G., 1992, *Laser Interaction and Related Plasma Phenomenon*, eds. Miley, G. H., and Hora, H. (Plenum, NY) **10**, 151.

58. Ziegler, W., Rangacharyulu, C., Richter, A., and Spieler, C., 1990, *Phys. Rev. Lett.*, **65**, 2515.

59. von Neumann-Cosel, P., Richter, A., Spieler, C., Ziegler, W., Carroll, J. J., Sinor, T. W., Richmond, D. G., Taylor, K. N., Collins, C. B., and Heyde, K., 1991, *Phys. Lett. B*, **266**, 9.

60. Huber, M., von Neumann-Cosel, P., Richter, A., Schlegel, C., Schulz, R., Carroll, J. J., Taylor, K. N., Richmond, D. G., Sinor, T. W., Collins, C. B., and Ponomarev, V., Yu., 1993, *Nucl. Phys.*, **A559**, 253.

61. Friedrichs, H., Lindenstruth, S., Schlitt, B., Wesselborg, C., Bauske, I., Heil, R. D., Kneissl, U., Margraf, J., Pitz, H. H., Häger, D., Müller, G., Schumacher, M., von Brentano, P., Herzberg, R. D., and Zilges, A., 1993, *Nucl. Phys.*, **A553**, 553.

62. Xie, H., Ender, Ch., Gerl, J., Härtlein, Th., Köck, F., Kröll, Th., Reiter, P., Schwalm, D., Thirolf, P., Vetter, K., Wieswesser, A., and Wollersheim, H. J., 1993, *Phys. Rev. C*, **48**, 2517.

63. Walker, P. M., Sletten, F., Gjørup, N. L., Bentley, M. A., Borggreen, J., Fabricius, B., Holm, A., Howe, D., Pedersen, J., Roberts, J. W., and Sharpey-Schafer, J. F., 1990, *Phys. Rev. Lett.*, **65**, 416.

64. Knopf, G., and Paul, W., in *Alpha, Beta and Gamma-Ray Spectroscopy*, ed. Siegbahn, K., 1965 (North Holland, Amsterdam) p. 1 - 25.

65. *Introduction to Solid State Physics, 6th Edition*, Kittel, C., 1986 (Wiley, New York) p. 106.

66. Oganessian, Yu. Ts., Karamian, S. A., Gangrski, Y. P., Gorski, B., Markov, B. N., Szeglowski, Z., Briançon, Ch., Ledu, D., Meunier, R., Hussonnois, M., Constantinescu, O., and Subbotin, M. I., 1992, *J. Phys. G: Nucl. Part. Phys.*, **18**, 393.

67. Collins, C. B., Carroll, J. J., Oganessian, Yu. Ts., and Karamian, S. A., 1994, *Laser Physics* (This issue).

68. Hong, C., Taylor, K. N., Carroll, J. J., Sinor, T. W., and Collins, C. B. (in preparation).

69. Khoo, T. L., and Løvhøiden, G., 1977, *Phys. Lett.*, **67B**, 271.

70. Sheline, R. K., Burke, D. G., Minor, M. M., and Sood, P. C., 1993, *Phys. Rev. C*, **48**, 911.

71. *National Nuclear Data Center Online Evaluated Nuclear Structure Data File (ENSDF)*, 1994, Brookhaven National Laboratory.

72. Carroll, J. J., Anderson, J. A., Glesener, J. W., Eberhard, C. D., and Collins, C. B., 1989, *Astrop. J.*, **344**, 454.

73. Sinor, T. W., Standifird, J. D., Davanloo, F., Taylor, K. N., Hong, C., Carroll, J. J., and Collins, C. B., 1994, *Appl. Phys. Lett.*, **64**, 1221.

74. Oganessian, Yu. Ts., Karamian, S. A., Collins, C. B., and Carroll, J. J., 1994 (in preparation).

75. Carroll, J. J., Collins, C. B., Heyde, K., Huber, M., von Neumann-Cosel, P., Ponomarev, V. Yu., Richmond, D. G., Richter, A., Schlegel, C., Sinor, T. W., and Taylor, K. N., 1993, *Phys. Rev. C*, **48**, 2238.

## TABLE I

Summary of important properties [35] of four of the 29 most promising candidate isomers for a gamma-ray laser.

| Isomer | Energy Density [J/$\mu$g] | Shelf Halflife, $T_{1/2}$ | Trigger Photon [MeV] |
|---|---|---|---|
| $^{177}Hf^{m}$ | 1,500 | 51 min | ~ 0 |
| $^{178}Hf^{m2}$ | 1,300 | 31 yr | < 0.5 |
| $^{179}Hf^{m}$ | 600 | 25 d | ~ 1.5 |
| $^{180}Ta^{m}$ | 40 | > $10^{15}$ yr | ~ 2.8 |

# TABLE II

Summary of nuclides, and excitation energies, $E_j$ and integrated cross sections for their gateway states, that are sufficiently well-known from the literature to permit their use as calibration standards. Some integrated cross sections were calculated by Eqs. (5) and (6) using constituent parameters found in the literature [34,35], while other values were directly obtained in the referenced experiments.

| Isomer | $T_{1/2}$ | $E_{fluor}$ [keV] | $E_j$ [MeV] | $(\sigma\Gamma)_{fj}$ [$10^{-29}$ $cm^2$ keV] |
|---|---|---|---|---|
| *Levels useful below 1.4 MeV* [36,39,42] | | | | |
| $^{77}Se^m$ | 17.45 s | 162 | 0.250 | 0.20 |
| | | | 0.480 | 0.87 |
| | | | 0.818 | 0.7 |
| | | | 1.005 | 30 |
| $^{79}Br^m$ | 4.9 s | 207 | 0.761 | 5.9 |
| $^{87}Sr^m$ | 2.8 h | 388 | 1.2 | 8.5 |
| $^{115}In^m$ | 4.5 h | 336 | 1.078 | 18.7 |
| *Levels useful below 4 MeV* [39,47,48,75] | | | | |
| $^{79}Br^m$ | 4.9 s | 207 | 1.8 | 65 |
| $^{87}Sr^m$ | 2.8 h | 388 | 1.9 | 16 |
| | | | 2.7 | 430 |
| $^{115}In^m$ | 4.5 h | 336 | 1.4 | 64 |
| | | | 1.6 | 10.1 |
| | | | 2.8 | 540 |
| | | | 3.3 | 760 |
| $^{137}Ba^m$ | 2.6 min | 662 | 3.2 | 220 |

## TABLE III

Recently measured values [38] of integrated cross sections and excitation energies for gateways in the reaction $^{180}Ta^{m}(\gamma,\gamma')^{180}Ta$.

| $E_j$ [MeV] | $(\sigma\Gamma)_{fj}$ [$10^{-29}$ cm$^2$ keV] |
|---|---|
| 2.8 $\pm$ 0.1 | 12,000 $\pm$ 2,000 |
| 3.6 $\pm$ 0.1 | 35,000 $\pm$ 5,000 |

## TABLE IV

Summary of the thermal economy at threshold for a gamma-ray laser nuclide doped into a film of 0.67-$\mu$m thickness of the low-Z materials shown.

| Quantity | Material | |
|---|---|---|
| | Be | C (Diamond) |
| Resonant input fluence | 177 mJ $cm^{-2}$ | 177 mJ $cm^{-2}$ |
| Fluence degraded to heat | 127 mJ $cm^{-2}$ | 255 mJ $cm^{-2}$ |
| Resonant energy density | 2.6 kJ $cm^{-3}$ | 2.6 kJ $cm^{-3}$ |
| Thermal loading | 1.9 kJ $cm^{-3}$ | 3.8 kJ $cm^{-3}$ |

## TABLE V

Summary of properties [35,71] of nuclides useful in simulating the pumping of the better of the 29 candidates for a gamma-ray laser.

| Nuclide | Abundance [%] | Output transitions [keV] | Fluorescence lifetime [$\mu$s] |
|---|---|---|---|
| $^{81}$Br | 49.31 | 260<br>276 | 37.6 |
| $^{176}$Hf | 5.206 | 736<br>1043 | 9.6, 9.9 |
| $^{181}$Ta | 99.998 | 346<br>482 | 18 |
| $^{201}$Hg | 13.1 | 521 | 92 |

## CAPTIONS

Figure 1: Schematic representation of the pumping of a fluorescence level through a pump band, or gateway state, of natural width $\Gamma$. The initial level from which population is excited with an absorption cross section $\sigma_0$ can be either a ground state or an isomer. The branching ratios $b_a$ and $b_o$ give the probabilities that the gateway will decay directly back to the initial state, and directly or by cascade to the fluorescence level, respectively. Only a single gateway is shown but there could be more; the index j is used to identify individual pump bands.

Figure 2: (a) Calculated spectral distribution function, $F(E,E_0)$ for a typical bremsstrahlung continuum (dashed line) with an endpoint of $E_0$ = 3.5 MeV plotted with the left-hand axis. Gateway excitation energies and integrated cross sections available from the earlier literature [39] are shown by the thin vertical bars and are plotted with the right-hand axis. The thick vertical bar indicates a gateway found in the recent experiments of Ref. [38]. All gateway parameters are listed in Table II. (b) Measured activations, $A_f(E_0)$ obtained using five different accelerators [37,38,49] for the reaction $^{87}Sr(\gamma,\gamma')^{87}Sr^m$ plotted with symbols as functions of bremsstrahlung endpoint. The solid curve plots the expected excitation function computed with the model of Eqs. (1) - (6).

Figure 3: Spectral intensity expressed in units of total photon energy per unit bandwidth for 1.4-MeV bremsstrahlung from DNA/PITHON measured [42] using the XAN technique (symbols) with the gateway parameters of Table II, compared with a spectrum computed (curve) with the TIGER code [32]. Uncertainties of the measured points are comparable to the size of the symbols except where otherwise indicated.

Figure 4: Instantaneous spectral intensity, $\phi$ for 4-MeV bremsstrahlung from the Texas-X measured [47] using the XAN technique (symbols) with the gateway parameters of Table II, compared with a spectrum computed (lines) with the EGS4 code [31]. Statistical errors associated with the calculations are indicated by the bars on the histograms. Uncertainties of the measured points are comparable to the size of the symbols except where otherwise indicated.

Figure 5: Fluorescence data [49] from the decay of $^{167}Er^{m}$ following its excitation with 6-MeV bremsstrahlung from a medical linac for an irradiation of 25 s. The pulse-height (energy) spectrum of (a) and the multichannel-scalar (decay) spectrum of (b) were obtained using a NaI(Tl) spectrometer. The measurements of fluorescence energy and lifetime were in excellent agreement with the literature values [35].

Figure 6: Fluorescence data [49] from the decay of $^{123}Te^{m}$ following its excitation with 6-MeV bremsstrahlung from a medical linac for an irradiation of 2 h. The pulse-height (energy) spectrum of (a) and the counting-rate (decay) spectrum of (b) were obtained using a HPGe spectrometer. Counting periods used to obtain the measurements of (b) were 10 h. The measurements of fluorescence energy and lifetime were in excellent agreement with the literature values [35].

Figure 7: Schematic energy-level diagram [34,55] of $^{180}Ta$ and its daughters. Energies are given in keV and the halflives of the tantalum ground state and the isomer are shown. The upward arrow indicates the pump transition to the gateway represented by the hatched level. The cascade from the gateway is unknown but leads to the ground state which transmutes to the

two daughters by electron capture and beta decay. The primary signatures of the decay of the ground state are K lines from $^{180}$Hf characterized by the lifetime of the parent, $^{180}$Ta$^{g}$.

Figure 8: Pulse-height spectra [55] showing fluorescence counting rates from an enriched sample of $^{180}$Ta$^{m}$ before (dotted) and after (solid) irradiation with the 6-MeV medical linac. The measurements were made with a HPGe spectrometer. The prominent K lines from daughter $^{180}$Hf nuclei produced by decay of $^{180}$Ta ground states indicate the dumping of significant numbers of $^{180}$Ta isomers in this mg-sized sample.

Figure 9: Decay spectrum [55] plotting counting rates measured for the Hf $K_{\alpha}$ lines seen in Fig. 8 as a function of time elapsed from the end of the irradiation. The measurements were made over the intervals shown and uncertainties in the observations were comparable to the size of the plotted symbols. The measured decay rate was in excellent agreement with the literature value [35].

Figure 10: (a) Calculated spectral distribution function, $F(E,E_0)$ for a typical bremsstrahlung continuum (dashed line) with an endpoint of $E_0$ = 3.5 MeV plotted with the left-hand axis. Gateway excitation energies and integrated cross sections measured in the experiments of Ref. [38] are shown by the thick vertical bars and are plotted with the right-hand axis. (b) Measured activations, $A_f(E_0)$ obtained with the S-DALINAC [38] for the reaction $^{87}$Sr$(\gamma,\gamma')^{87}$Sr$^{m}$ plotted with symbols as functions of bremsstrahlung endpoint. The activation edge at 2.8 $\pm$ 0.1 MeV indicated the excitation energy of the lowest gateway; its magnitude was sufficient to characterize it as a giant pumping resonance.

Figure 11: Integrated cross sections and excitation energies, plotted with the left-hand and right-hand axes, respectively, for gateways measured in the experiments of Refs. [38,49,56] which pump or dump populations of isomers. The groupings of pumping strengths seen in the figure correspond to mass islands between magic numbers for neutrons and protons. The best candidates for a gamma-ray laser lie within the mass-180 island which contains the largest values of integrated cross section corresponding to giant pumping resonances. Within each island, the integrated cross sections and gateway excitation energies vary only slowly with changing mass number, A, despite differing single-particle structures among neighboring nuclides.

Figure 12: Comparison of integrated cross sections [59] for $^{115}$In plotted as functions of gateway excitation energy, $E_j$, obtained from (a) experimental measurements and (b) unified-model calculations. The upper panels show values of $(\sigma\Gamma)_{fj}$ of Eq. (5) for the photoexcitation reaction $^{115}In(\gamma,\gamma')^{115}In^m$, while the lower panels show values of $(\sigma\Gamma)_{0j}$ of Eq. (8) for elastic photon scattering, $^{115}In(\gamma,\gamma)^{115}In$.

Figure 13: Energetics for the spontaneous decay of the 3.7-$\mu$s isomer $^{174}Hf^m$ through a K-mixing level at 2.6 MeV which provided $\Delta K = 14$, compared with that for the dumping of populations of $^{180}Ta^m$ through a giant pumping resonance at $2.8 \pm 0.1$ MeV which provided $\Delta K = 8$. Both intermediate levels are expected to be admixtures of single-particle states having differing values of the K quantum number.

Figure 14: Isomer excitation probabilities, S plotted as a function of ground-state deformation, $\delta$ showing a slow variation consistent with a core property for the giant pumping resonances

[56]. The quantity $S \equiv (\sigma\Gamma)_{fj}/E_j$, defined assuming a dipole character for the absorption step, is summed over the energy region 2 - 4.5 MeV and is proportional to the reduced transition probability.

Figure 15: Fluorescence detected at 482 keV from the decay of the 615 keV isomer of $^{181}$Ta. The data were obtained [68] using a gated detector system and corresponded to nearly $10^6$ acquisition cycles taken over 45 min. The solid line shows a fit to the data which agrees well with the literature value [34] for the lifetime of the 615-keV level.

Figure 16: Schematic diagram showing the energy levels [71] important for the excitation of the 615-keV, 18-$\mu$s state in $^{181}$Ta. The large upward arrow indicates the absorption transition to a gateway located [68] near 2.8 MeV which populates that laser-like level by a branch of its decay cascade (shown by the dashed arrow). Transitions providing photons used to detect the fluorescence are indicated with their energies.

Figure 17: Fluorescence detected from the decay of the 1333 keV isomer of $^{176}$Hf. The data were obtained [68] using a gated detector system and corresponded to nearly $10^5$ acquisition cycles taken over 5 min. The solid line shows a fit to the data which agrees well with the literature value [34] for the lifetime of the 1333-keV level.

Figure 18: Schematic diagram showing the energy levels [71] important for the excitation of the 1333-keV, 9.6-$\mu$s state in $^{176}$Hf. The large upward arrow indicates the absorption transition to a gateway located [68] near 2.8 MeV which populates that laser-like level by a branch of its

decay cascade (shown by the dashed arrow). Transitions providing photons used to detect the fluorescence are indicated with their energies.

Figure 19: Integrated cross sections for populating laser-like levels in the simulation nuclei superimposed on those of Fig. 11 for the pumping and dumping of long-lived isomers. Again, the groupings correspond to mass islands between magic numbers and the best candidates are identified as neighbors of $^{180}$Ta.

Figure 20: Schematic energy-level diagram [69-71] of $^{178}$Hf. The spontaneous decay of the 31-year isomer proceeds through an yrast band which does not excite transitions in the left-hand K = 6 band or the K = 14 band. The 68-$\mu$s bandhead decays by cascade through the right-hand K = 8 band. The position of the K-mixing giant pumping resonance inferred from systematics is shown by the wide shaded band near 2.8 MeV and the large upward arrow indicates the pump transition from the 31-year isomer. Transitions providing fluorescence photons useful for the detection of the pumping reaction are identified along with their energies.

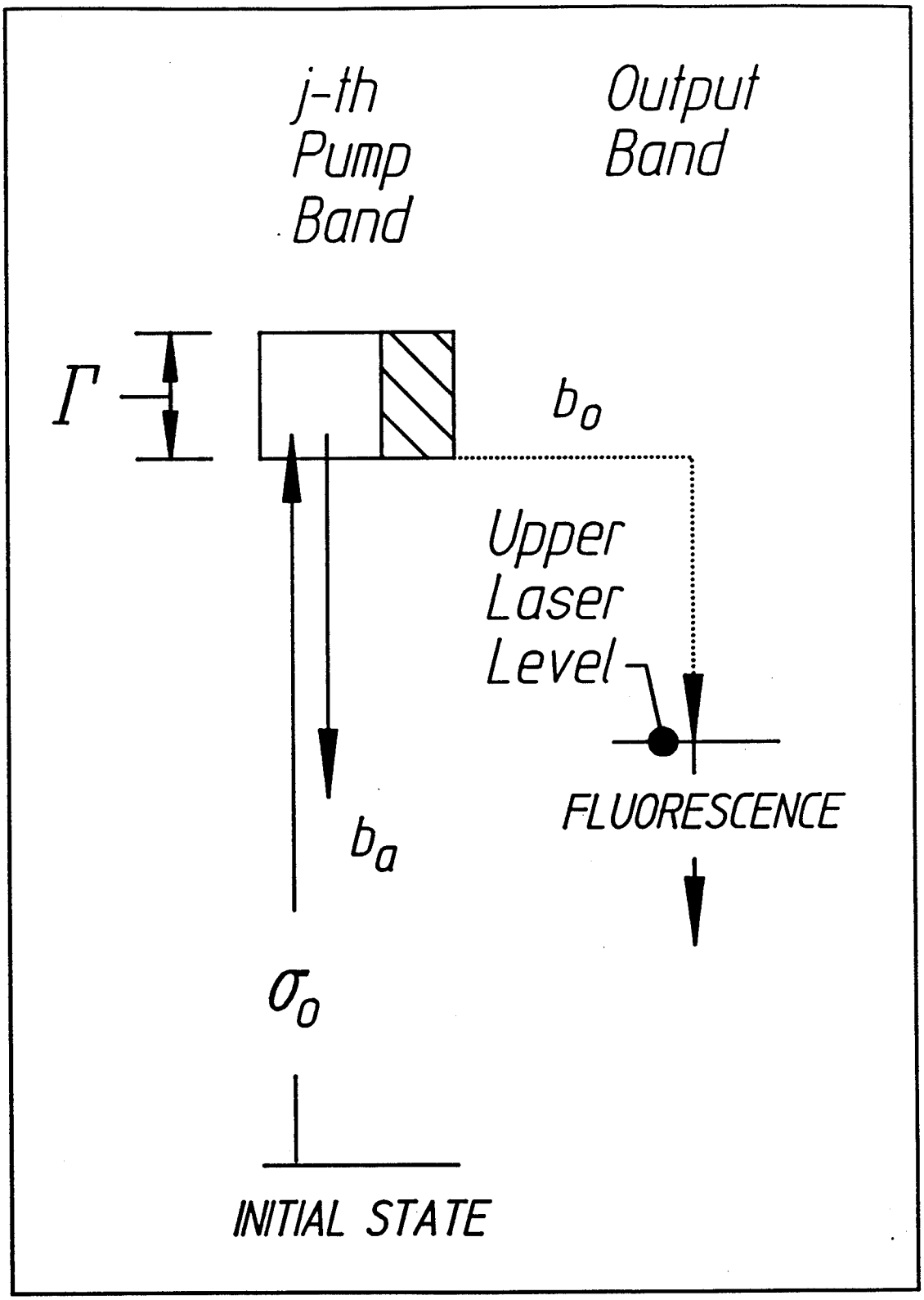
j-th
Pump
Band
Output
Band
Γ
$b_o$
Upper
Laser
Level
FLUORESCENCE
$b_a$
$\sigma_o$
INITIAL STATE

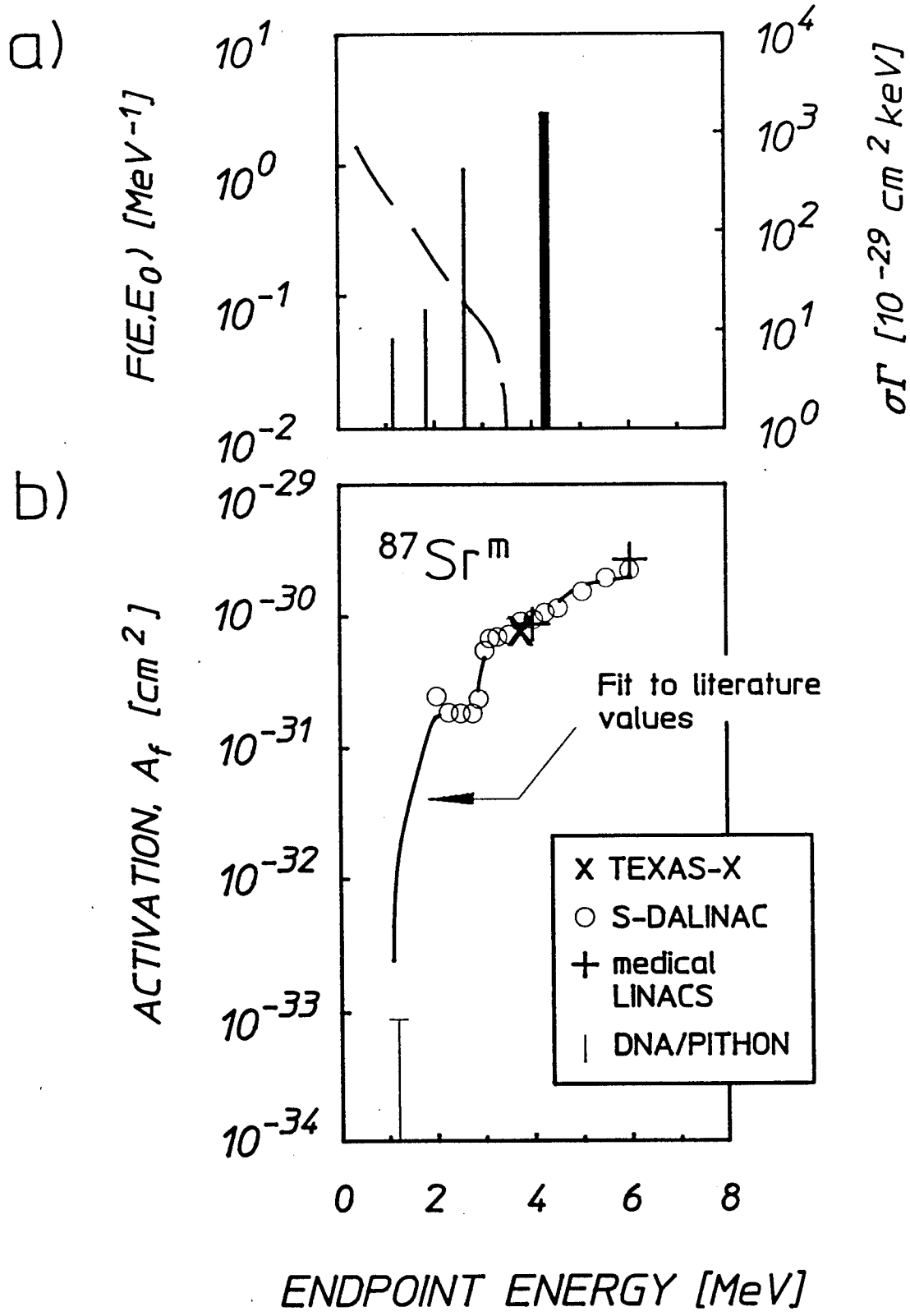
a)
b)
$10^{1}$
$10^{0}$
$10^{-1}$
$10^{-2}$
$F(E,E_0)$ [MeV$^{-1}$]
$10^{4}$
$10^{3}$
$10^{2}$
$10^{1}$
$10^{0}$
$\sigma\Gamma$ [$10^{-29}$ cm$^2$ keV]
$10^{-29}$
$10^{-30}$
$10^{-31}$
$10^{-32}$
$10^{-33}$
$10^{-34}$
ACTIVATION, $A_f$ [cm$^2$]
$^{87}Sr^{m}$
Fit to literature values
X TEXAS-X
○ S-DALINAC
+ medical LINACS
| DNA/PITHON
0
2
4
6
8
ENDPOINT ENERGY [MeV]

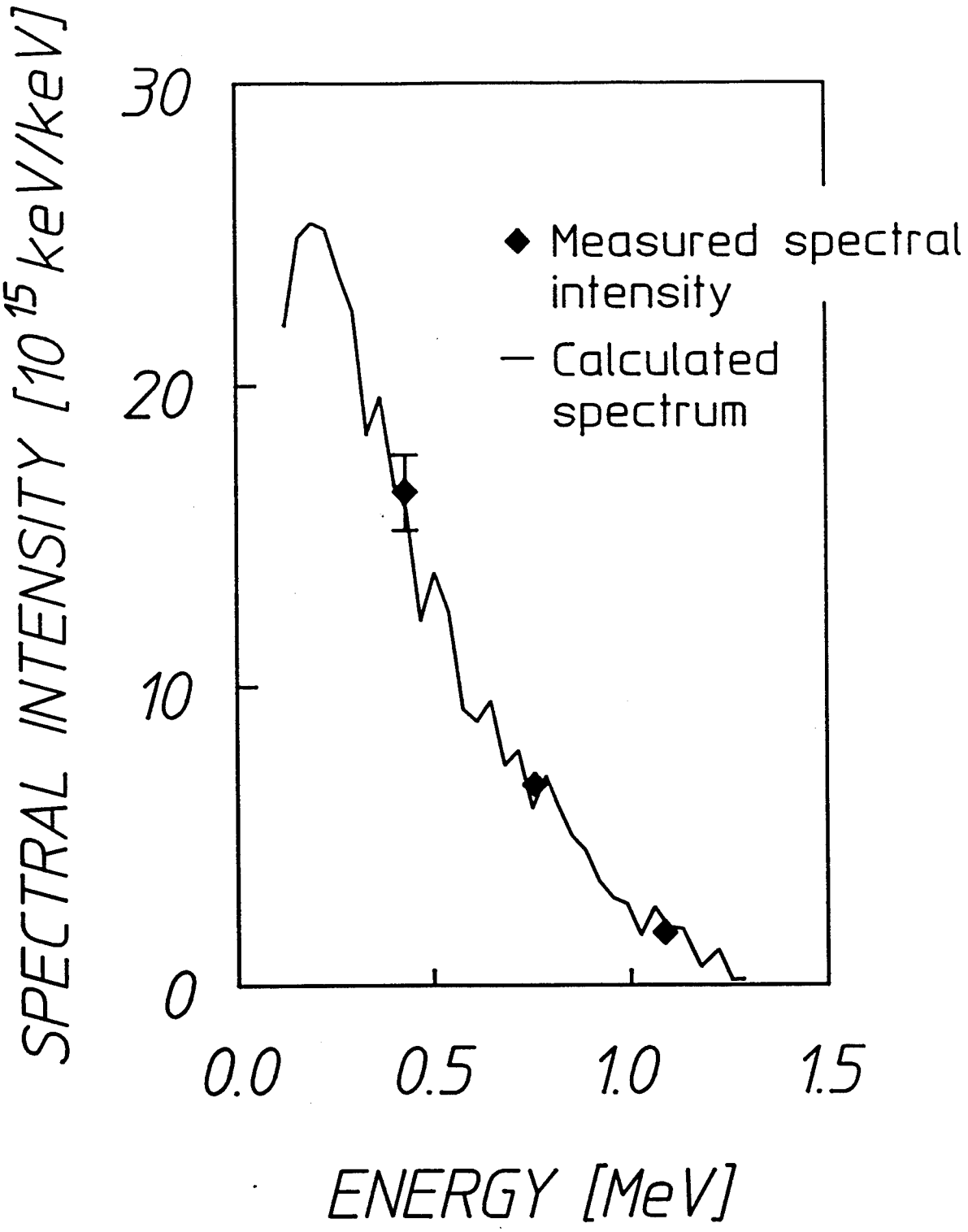
SPECTRAL INTENSITY [10^15 keV/keV]
30
20
10
0
0.0
0.5
1.0
1.5
ENERGY [MeV]
Measured spectral intensity
Calculated spectrum

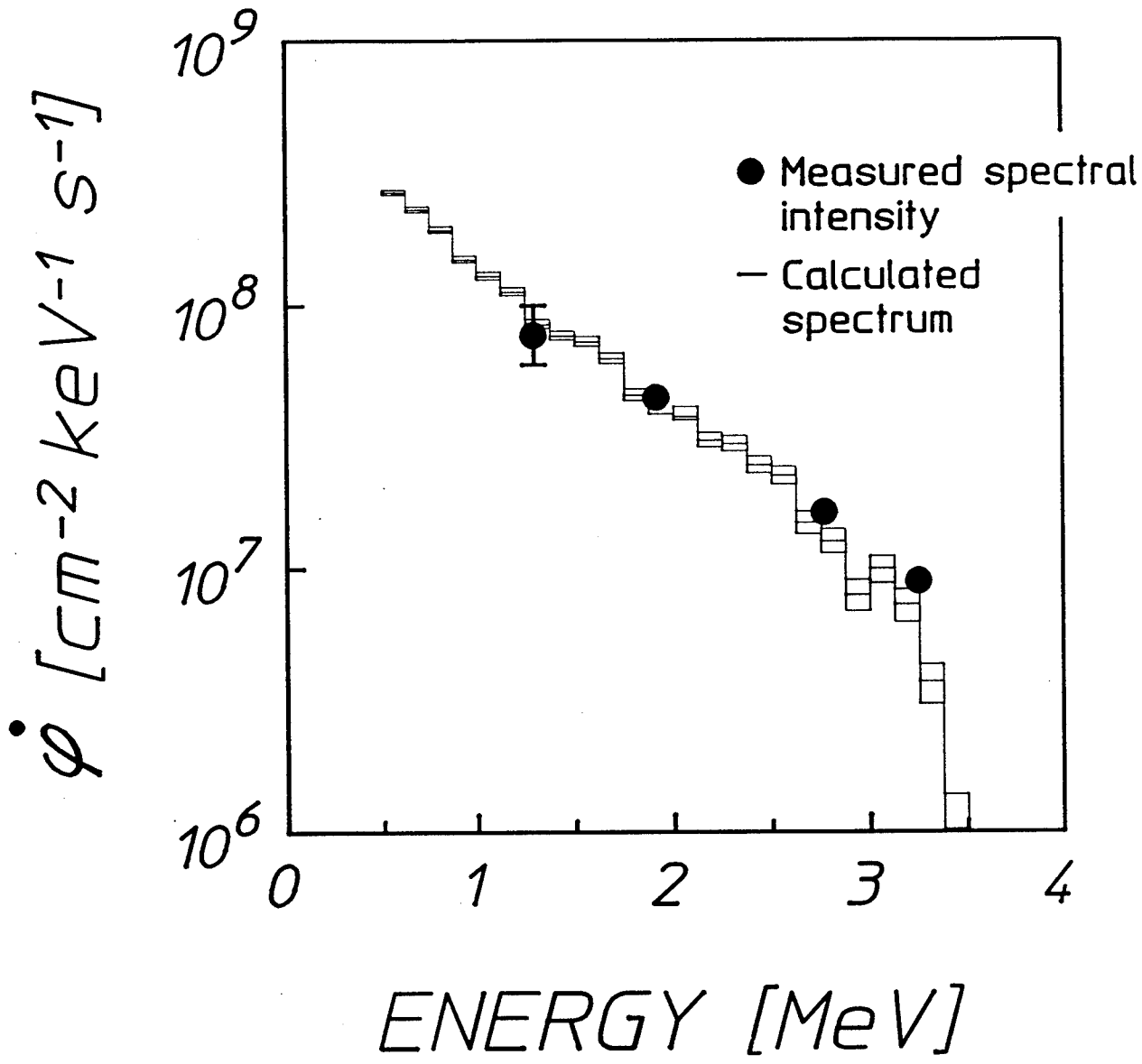
$10^9$
$10^8$
$10^7$
$10^6$
$\dot{\varphi}$ [cm-2 keV-1 s-1]
0
1
2
3
4
ENERGY [MeV]
Measured spectral intensity
Calculated spectrum

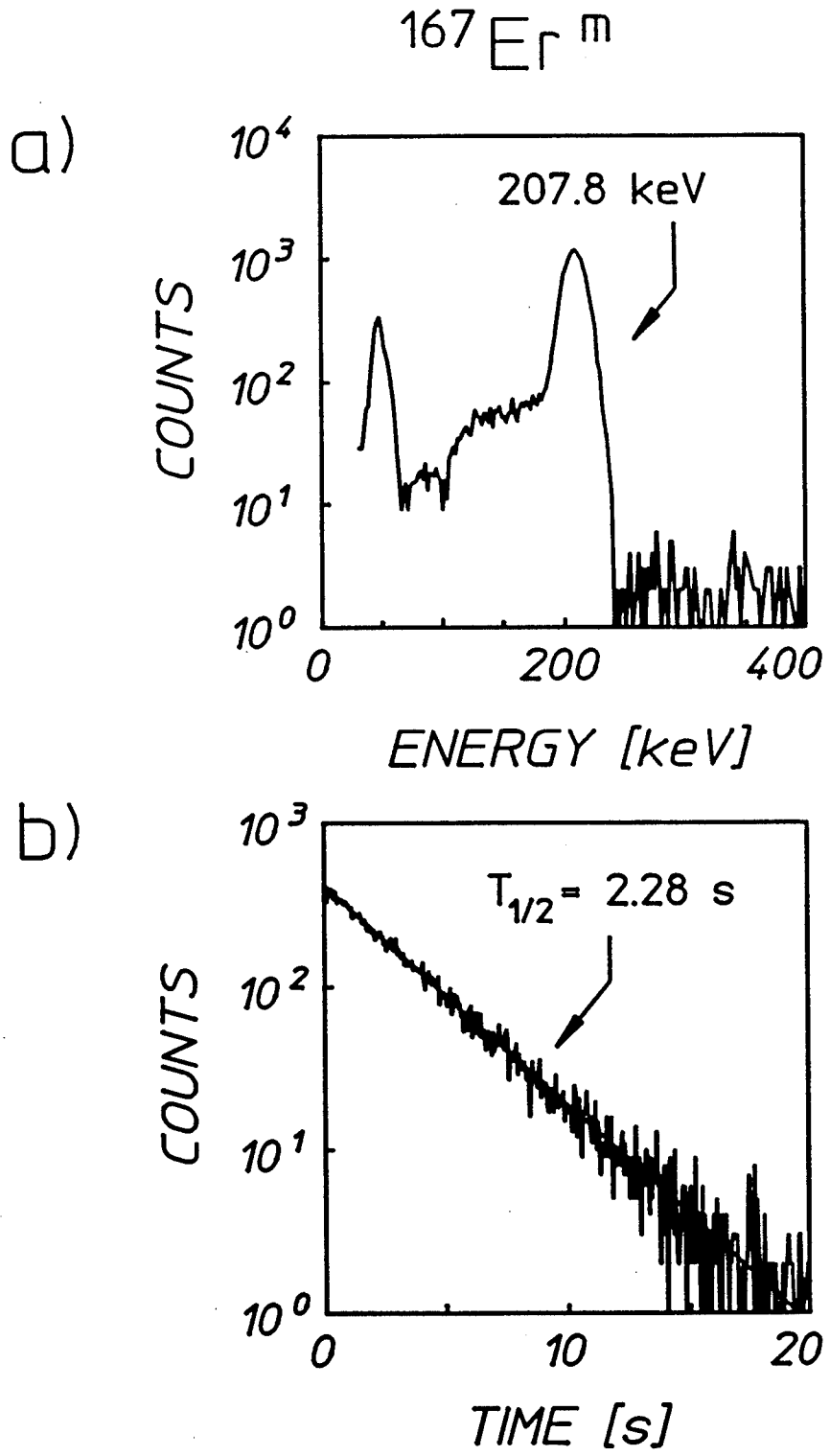
167 Er m
a)
207.8 keV
COUNTS
10^4
10^3
10^2
10^1
10^0
0
200
400
ENERGY [keV]
b)
T1/2 = 2.28 s
COUNTS
10^3
10^2
10^1
10^0
0
10
20
TIME [s]

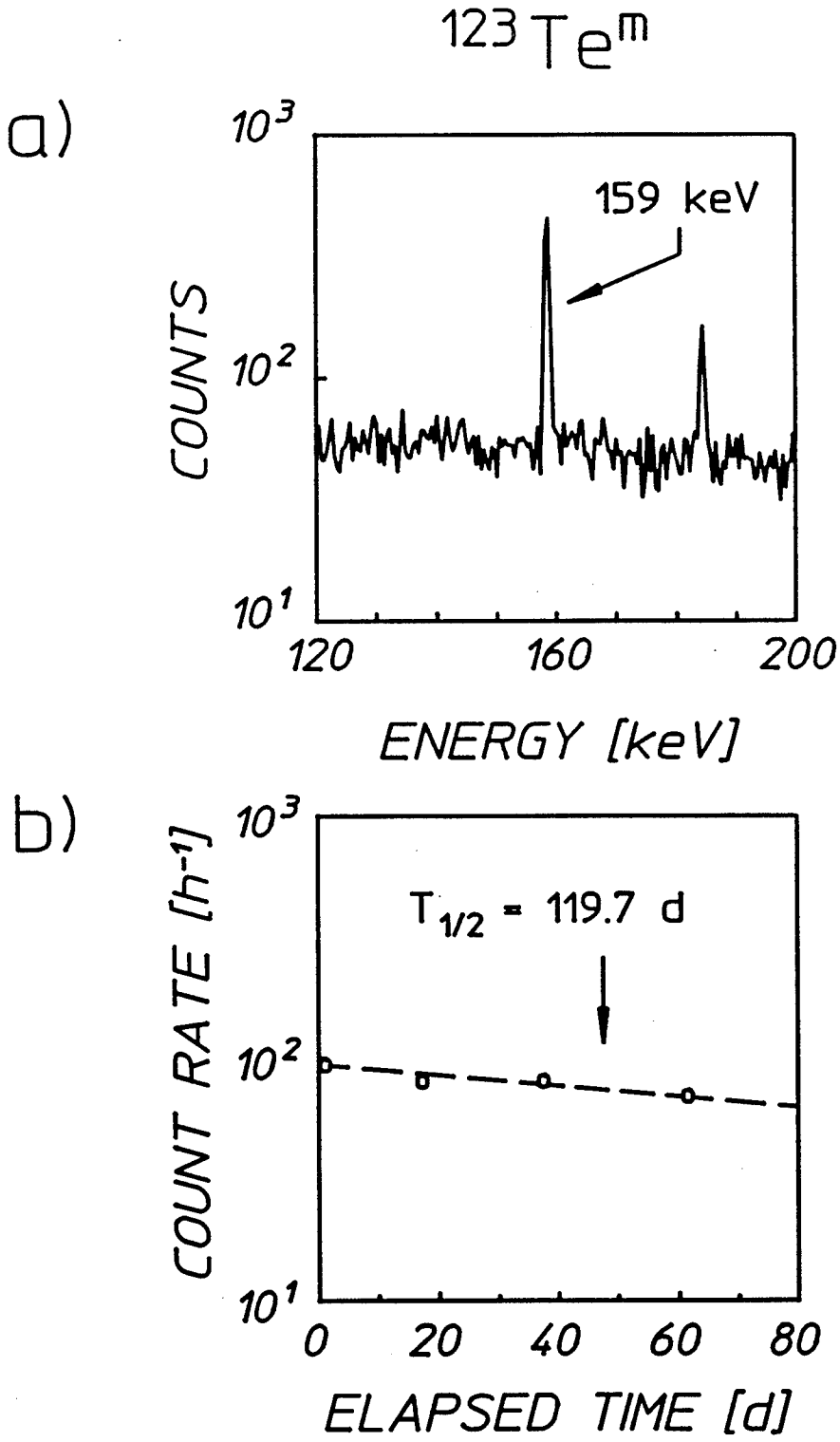
123Tem
a)
10³
10²
10¹
COUNTS
159 keV
120
160
200
ENERGY [keV]
b)
10³
10²
10¹
COUNT RATE [h⁻¹]
T1/2 = 119.7 d
0
20
40
60
80
ELAPSED TIME [d]

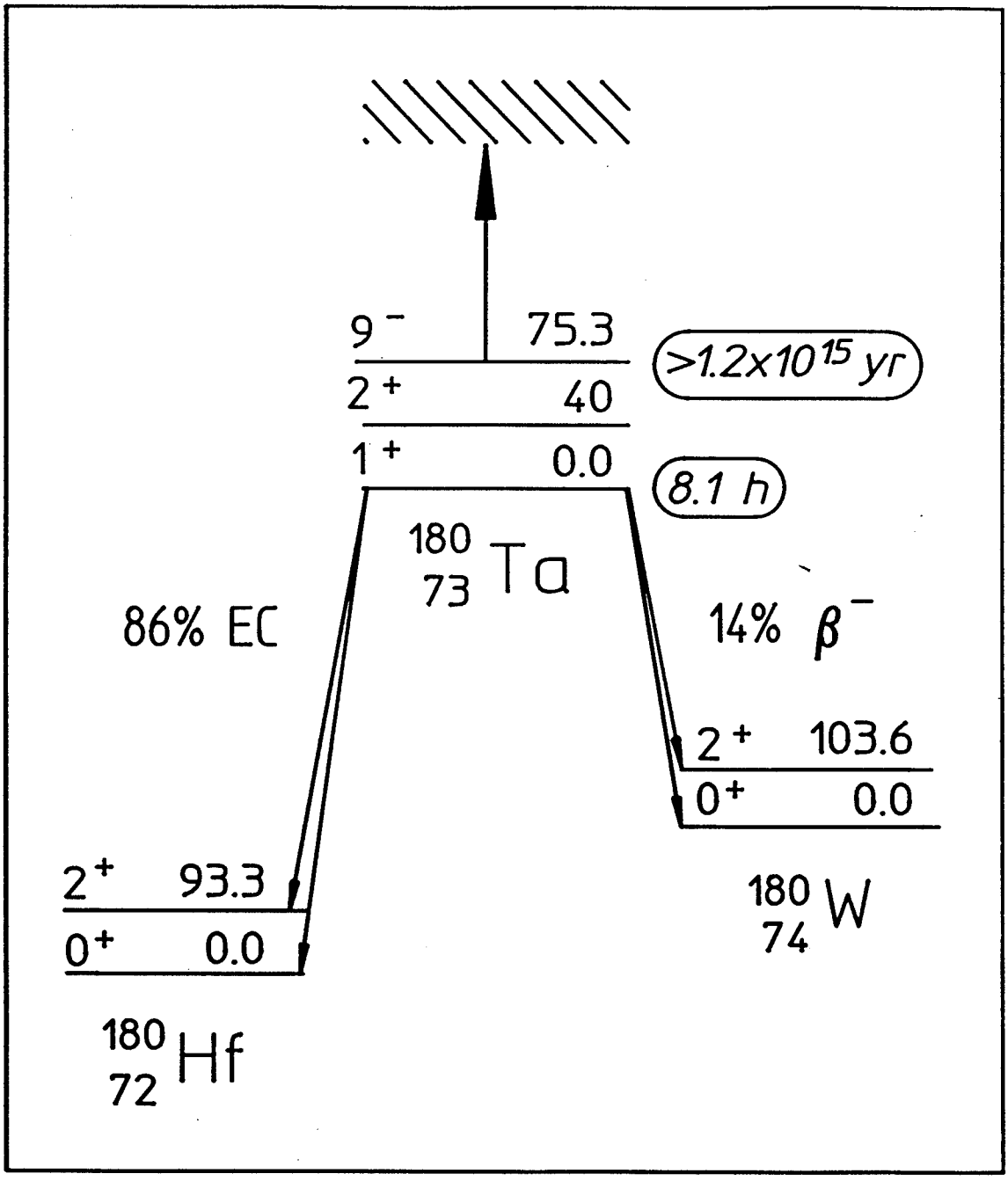
9⁻ 75.3
>1.2x10¹⁵ yr
2⁺ 40
1⁺ 0.0
8.1 h
180 73 Ta
86% EC
14% β⁻
2⁺ 103.6
0⁺ 0.0
2⁺ 93.3
0⁺ 0.0
180 74 W
180 72 Hf

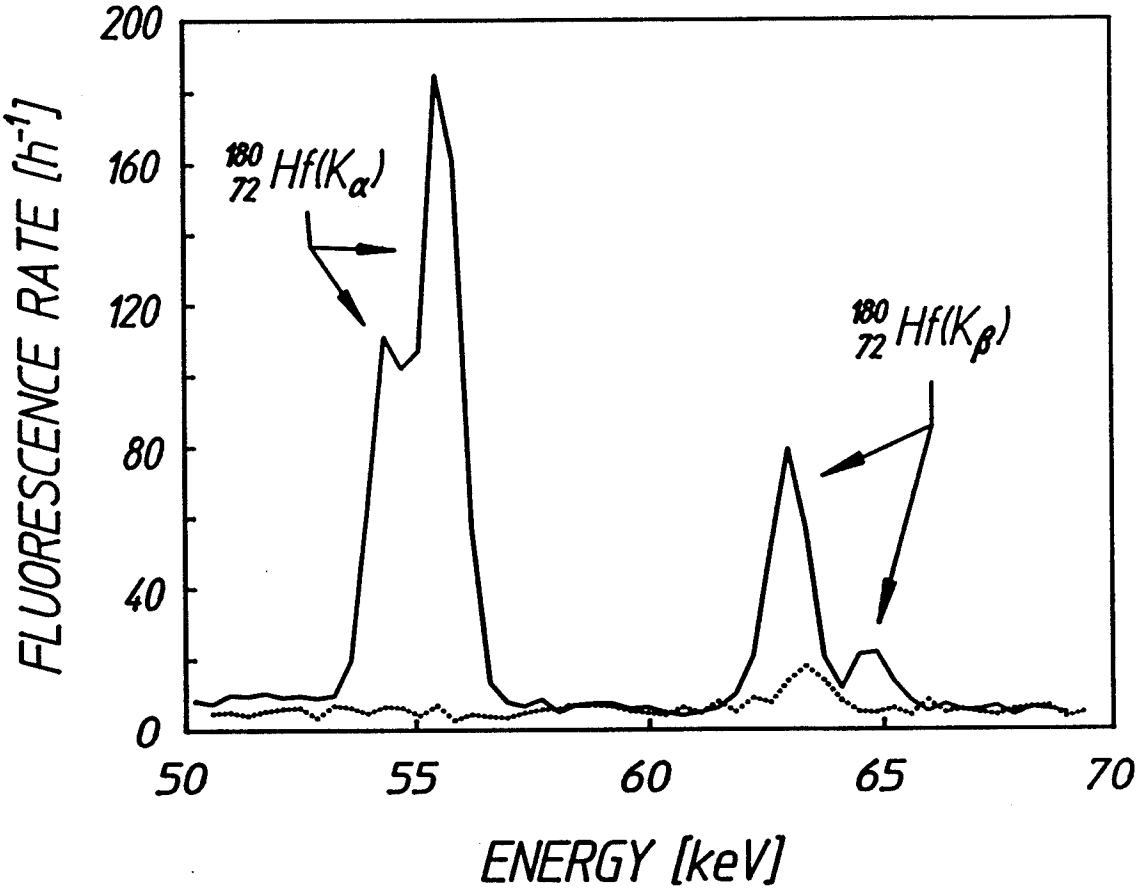
200
160
120
80
40
0
FLUORESCENCE RATE [h⁻¹]
$^{180}_{72}Hf(K_\alpha)$
$^{180}_{72}Hf(K_\beta)$
50
55
60
65
70
ENERGY [keV]

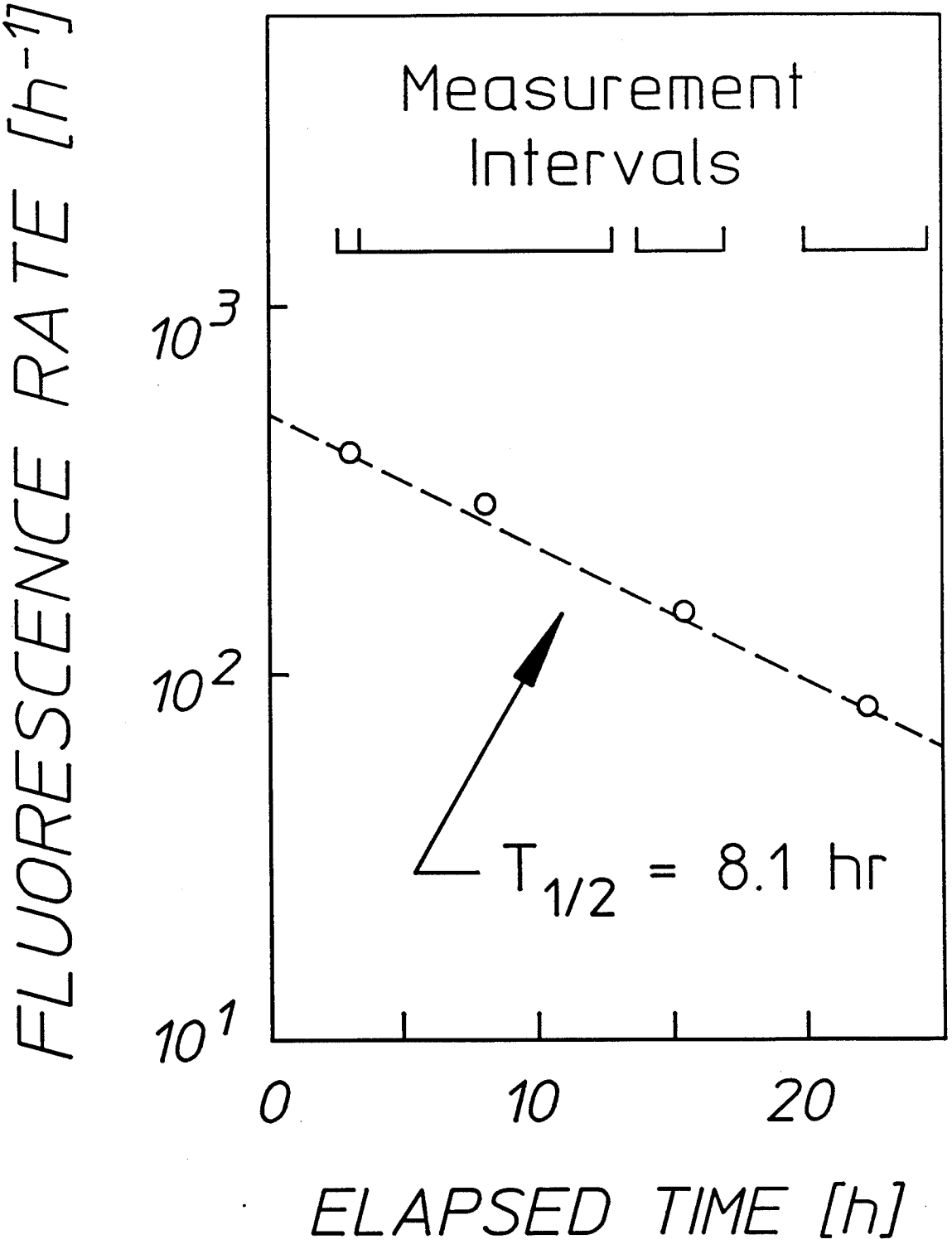
Measurement
Intervals
FLUORESCENCE RATE [h-1]
10^3
10^2
10^1
T1/2 = 8.1 hr
0
10
20
ELAPSED TIME [h]

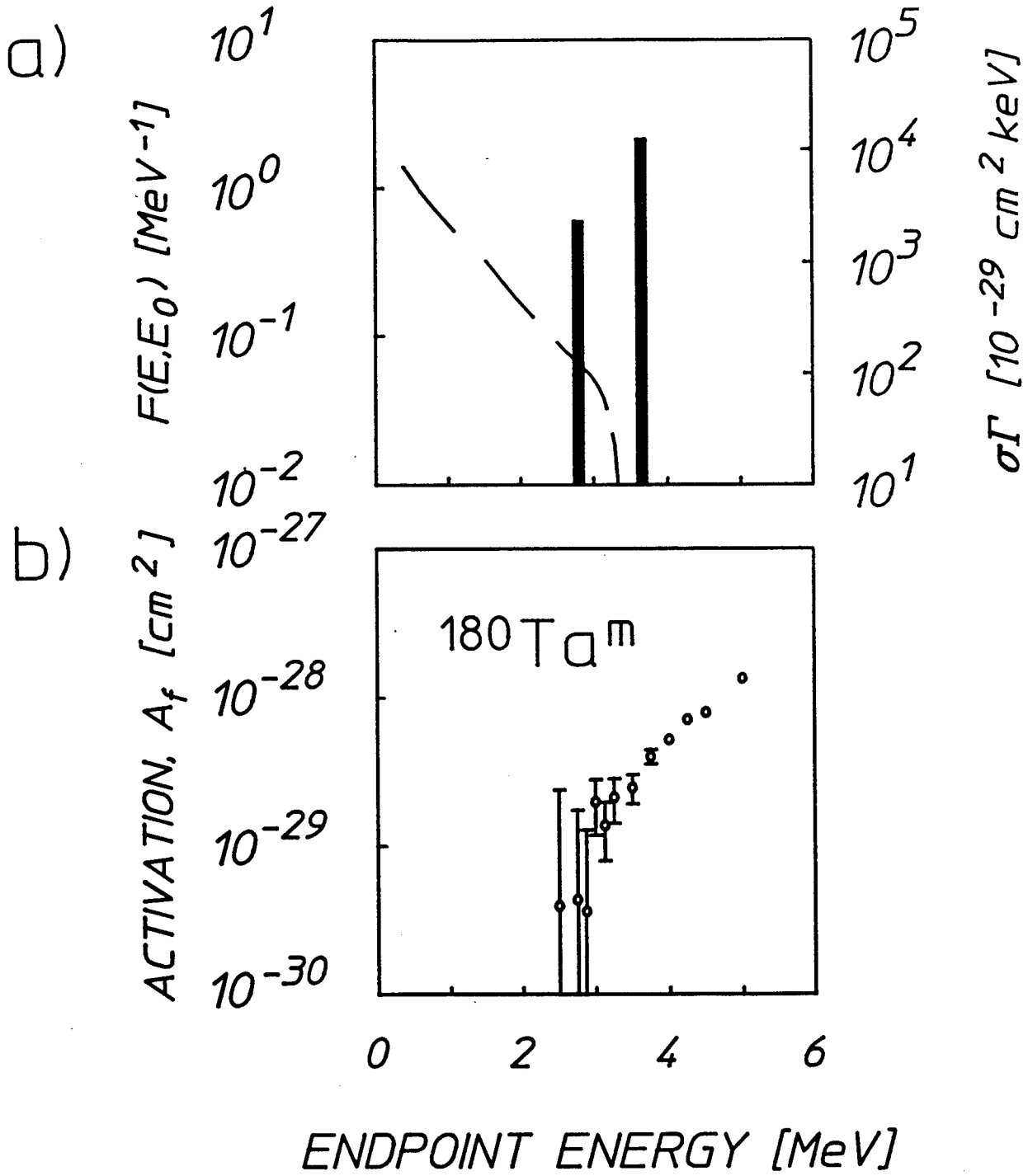
a)
b)
$10^{1}$
$10^{0}$
$10^{-1}$
$10^{-2}$
$F(E,E_0)$ [MeV$^{-1}$]
$10^{5}$
$10^{4}$
$10^{3}$
$10^{2}$
$10^{1}$
$\sigma\Gamma$ [$10^{-29}$ cm$^2$ keV]
$10^{-27}$
$10^{-28}$
$10^{-29}$
$10^{-30}$
ACTIVATION, $A_f$ [cm$^2$]
180Tam
0
2
4
6
ENDPOINT ENERGY [MeV]

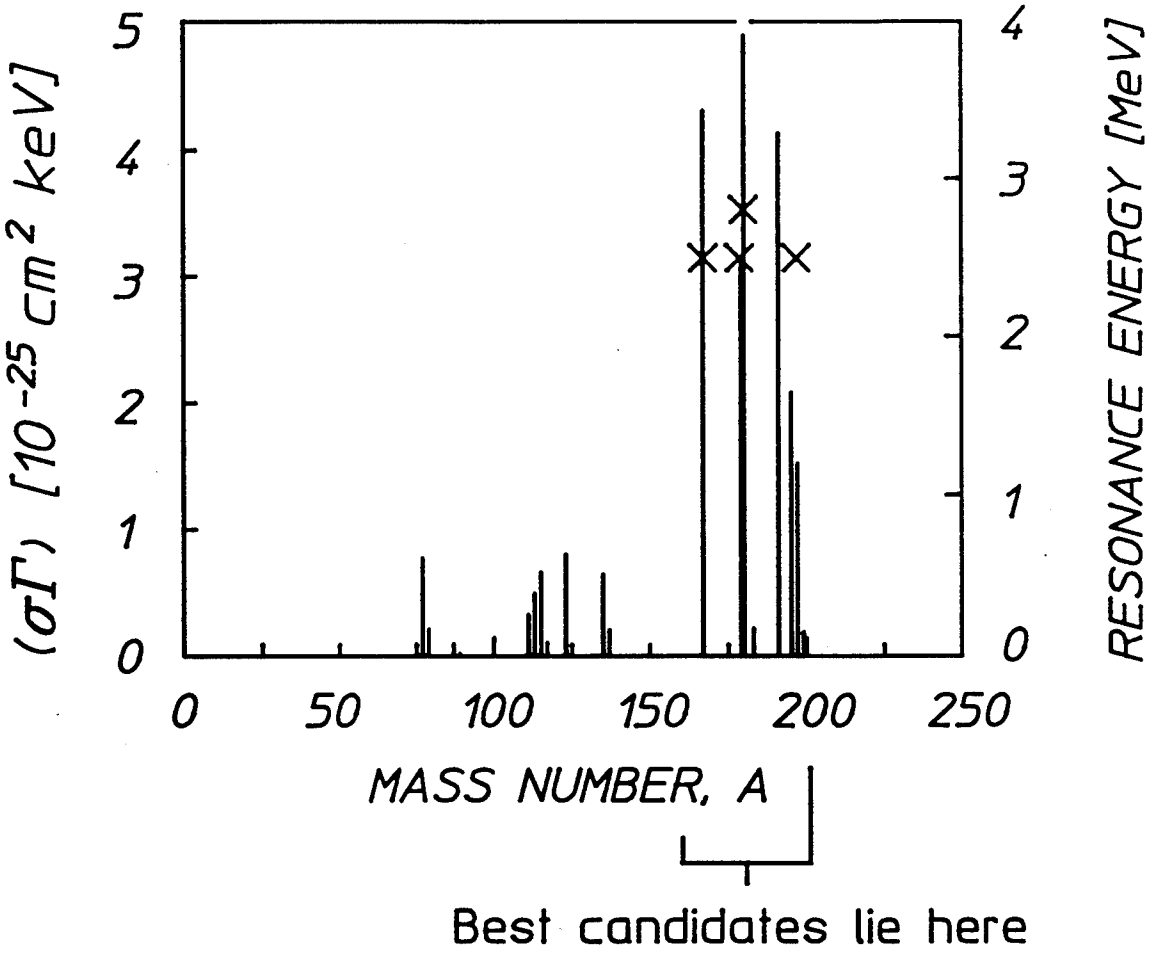
(σΓ) [10⁻²⁵ cm² keV]
RESONANCE ENERGY [MeV]
MASS NUMBER, A
0
50
100
150
200
250
1
2
3
4
5
Best candidates lie here

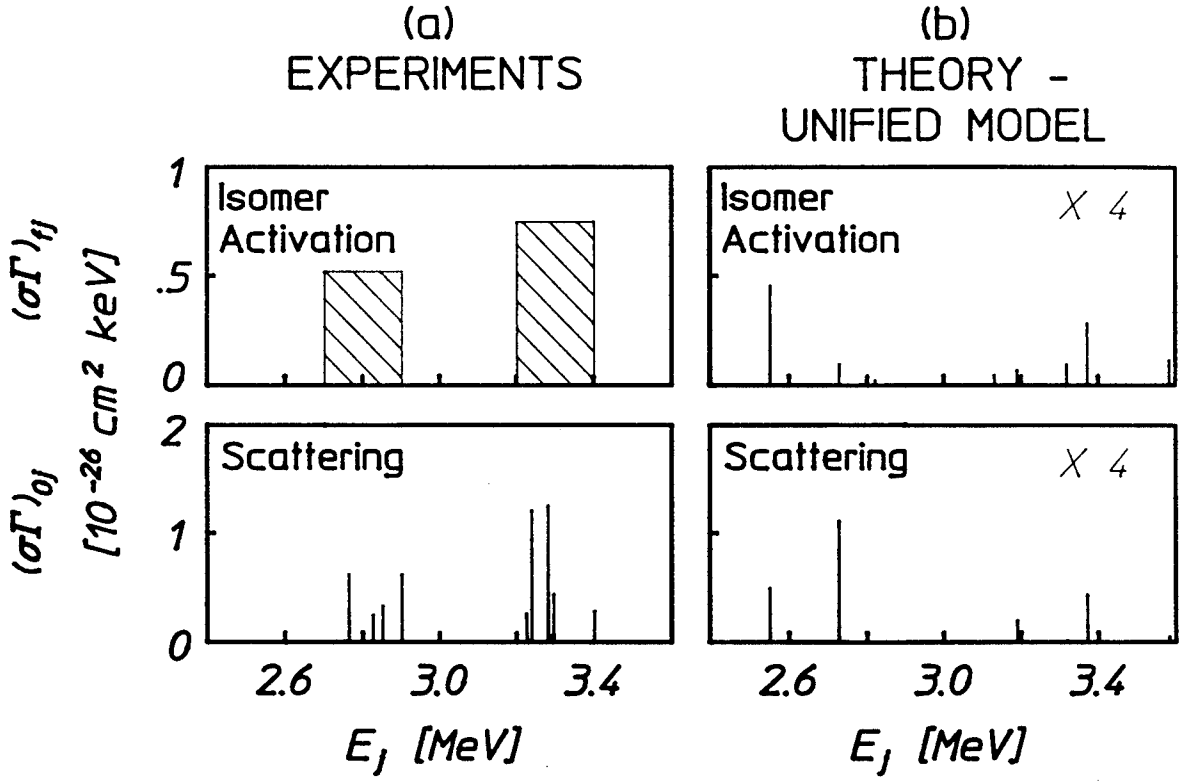
(a)
EXPERIMENTS
(b)
THEORY -
UNIFIED MODEL
Isomer
Activation
Isomer
Activation
X 4
Scattering
Scattering
X 4
1
.5
0
2
1
0
2.6
3.0
3.4
2.6
3.0
3.4
$E_j$ [MeV]
$E_j$ [MeV]
$(\sigma\Gamma)_{ij}$
$(\sigma\Gamma)_{0j}$
[$10^{-26}$ cm$^2$ keV]

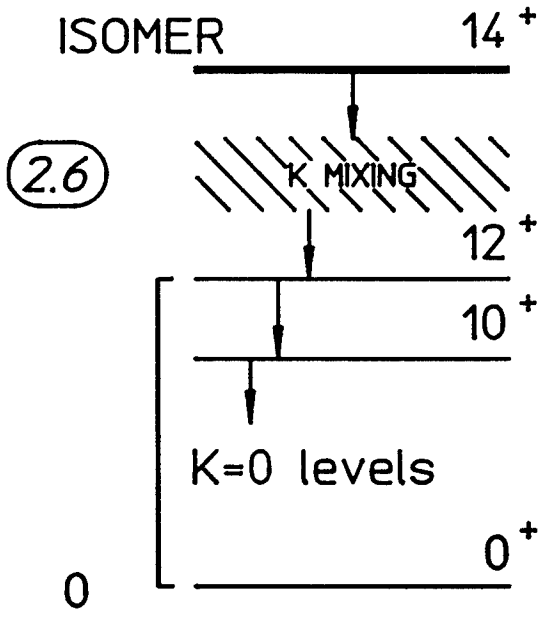


$^{174}Hf^{m}$

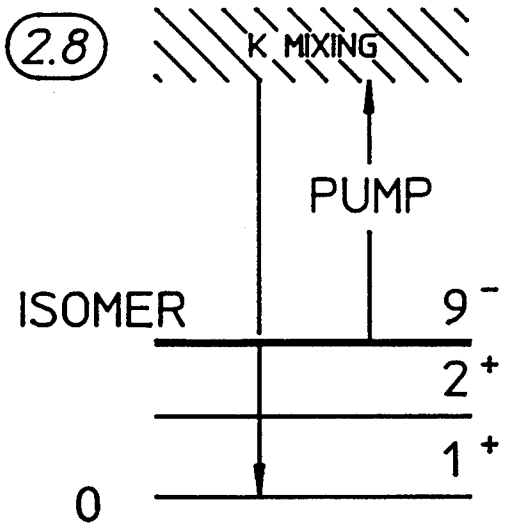


$^{180}Ta^{m}$

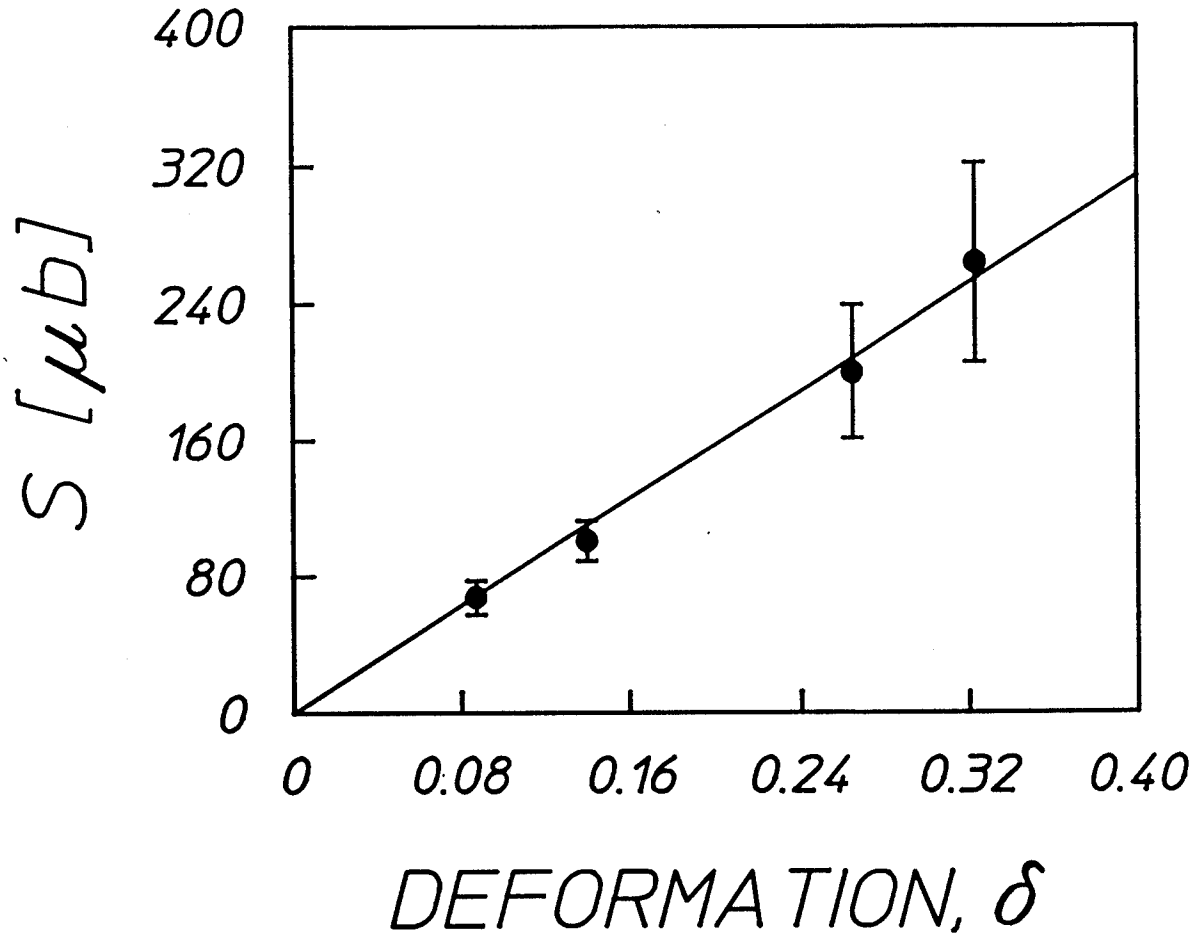
400
320
240
160
80
0
S [μb]
0
0.08
0.16
0.24
0.32
0.40
DEFORMATION, δ

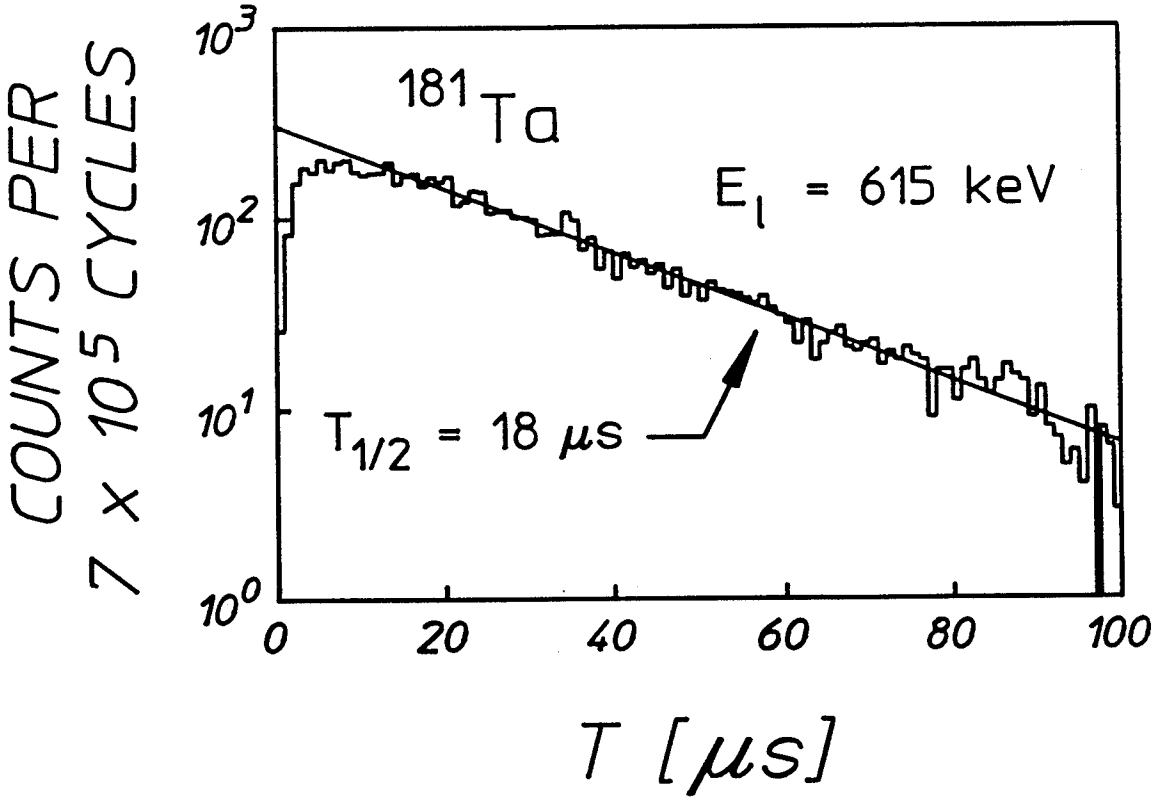
COUNTS PER
7 X 10⁵ CYCLES
10³
10²
10¹
10⁰
181 Ta
E_l = 615 keV
T_1/2 = 18 μs
0
20
40
60
80
100
T [μs]

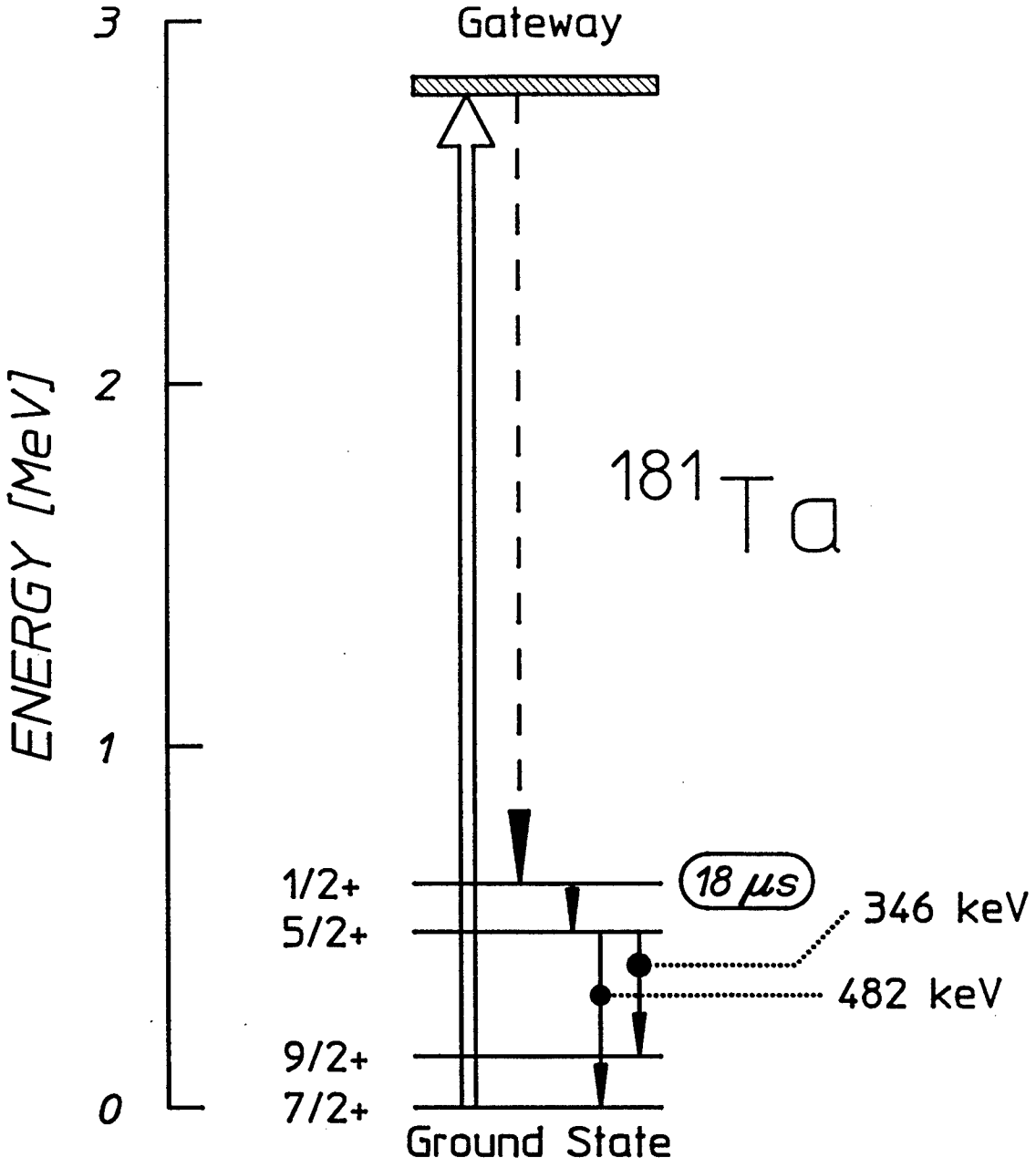
3
2
1
0
ENERGY [MeV]
Gateway
181Ta
1/2+
5/2+
9/2+
7/2+
Ground State
18 μs
346 keV
482 keV

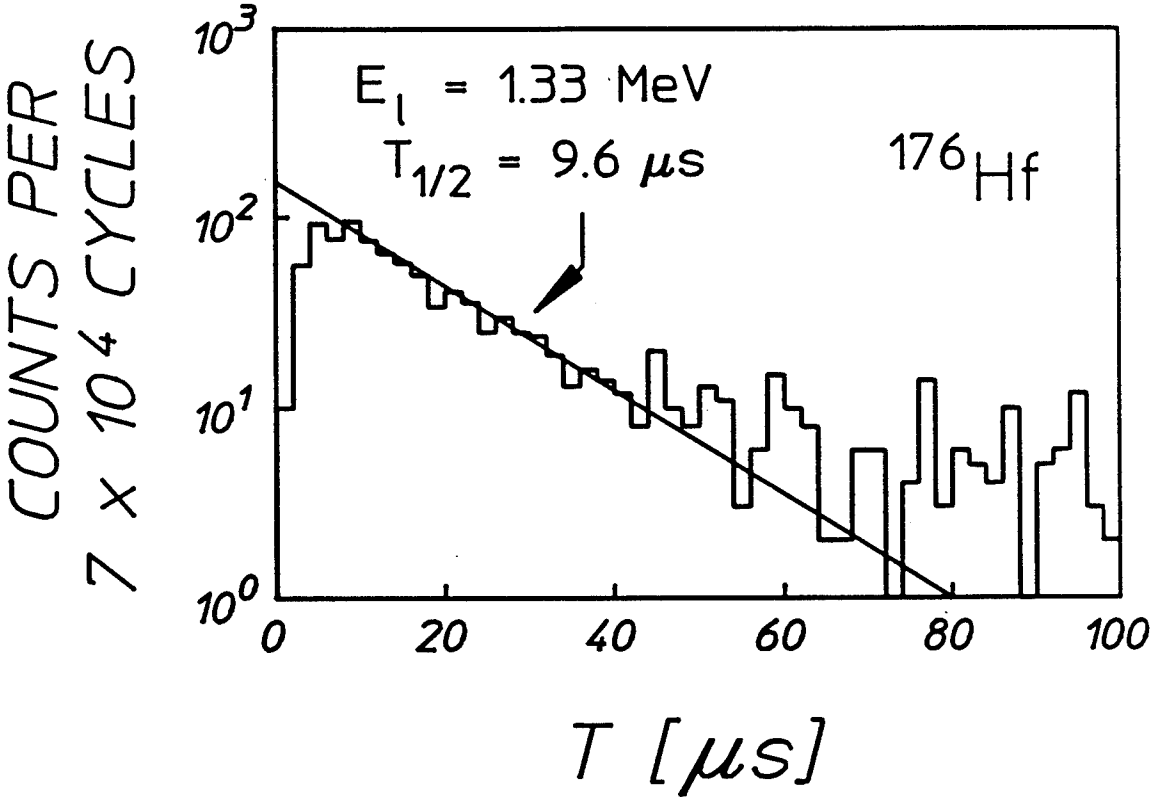
COUNTS PER
7 X 10⁴ CYCLES
10³
10²
10¹
10⁰
E_l = 1.33 MeV
T_1/2 = 9.6 μs
176Hf
0
20
40
60
80
100
T [μs]

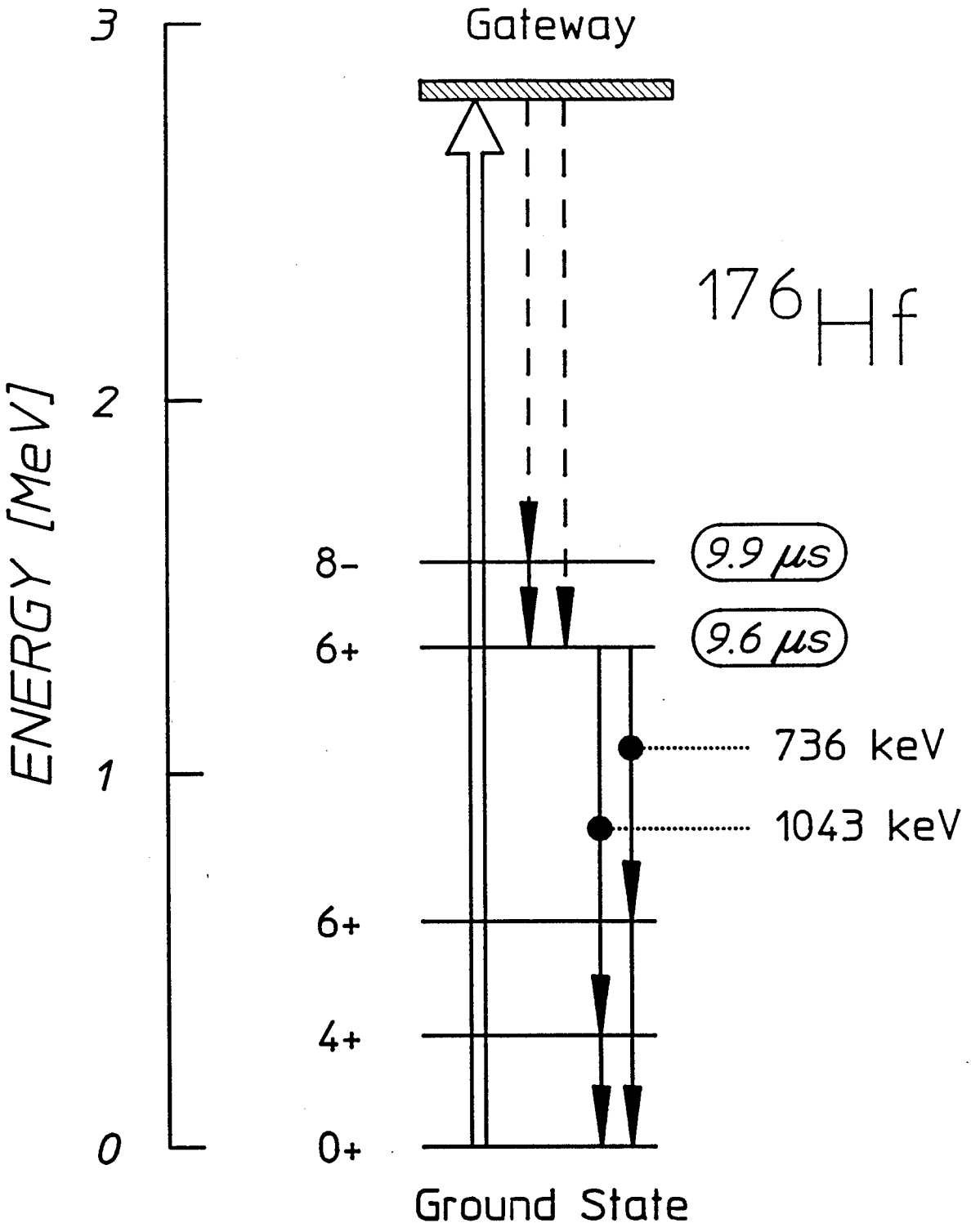
Gateway
3
2
1
0
ENERGY [MeV]
176Hf
8-
9.9 μs
6+
9.6 μs
736 keV
1043 keV
6+
4+
0+
Ground State

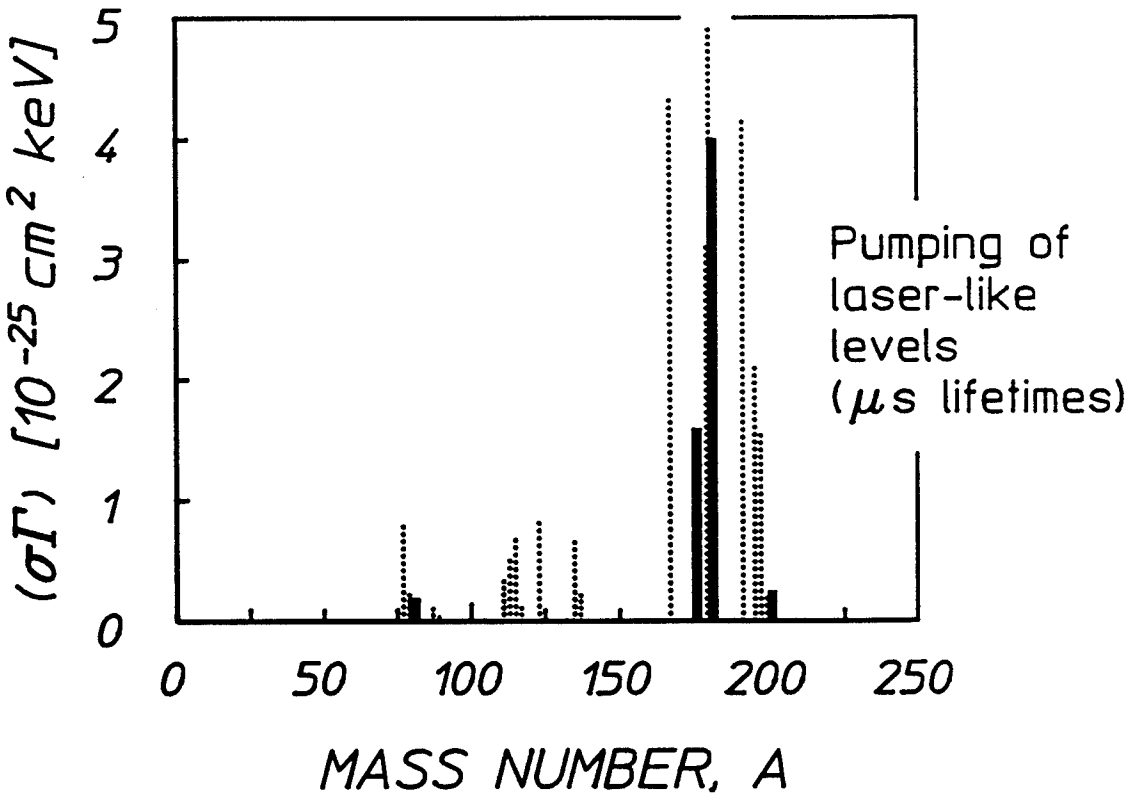
$(\sigma\Gamma)$ $[10^{-25}\ cm^2\ keV]$
0
1
2
3
4
5
0
50
100
150
200
250
MASS NUMBER, A
Pumping of laser-like levels ($\mu$s lifetimes)

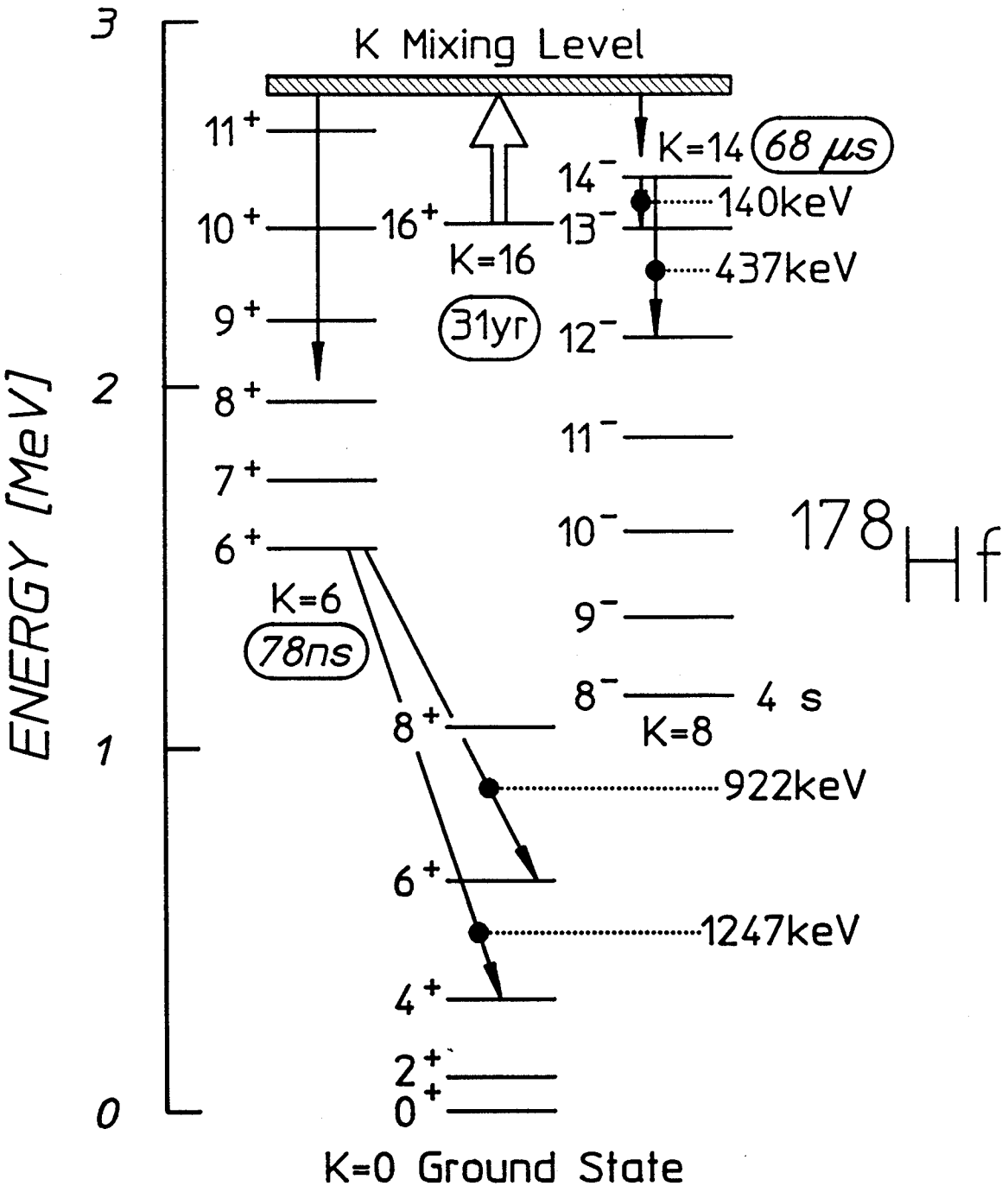
ENERGY [MeV]
3
2
1
0
K Mixing Level
11+
10+
9+
8+
7+
6+
K=6
78ns
16+
K=16
31yr
K=14
68 μs
14−
13−
12−
140keV
437keV
11−
10−
9−
8−
4 s
K=8
178Hf
8+
922keV
6+
1247keV
4+
2+
0+
K=0 Ground State

# K MIXING IN $^{178}$Hf

**C. B. Collins and J. J. Carroll**

**The University of Texas at Dallas, Center for Quantum Electronics**

**P. O. Box 830688, Richardson, Texas 75083-0688**

**and**

**Yu. Ts. Oganessian and S. A. Karamian**

**Joint Institute for Nuclear Research, Flerov Laboratory of Nuclear Reactions**

**Dubna, P. O. Box 79, 101000 Moscow, Russia**

## ABSTRACT

Systematics for the appearance of K-mixing levels for the pumping or spontaneous decay of multi-quasiparticle isomers in Hf isotopes are detailed in this letter. The possible location of such a level in the nuclide $^{178}$Hf is discussed and an experiment is proposed to investigate its existence.

Multi-quasiparticle states in the isotopes of Hf appear as high-spin isomers that are distinguished by the combination of MeV excitation energies and long lifetimes [1]. As is typical for mid-shell isotopes, Hf nuclei have marked prolate deformations that provide a body axis upon which the total angular momentum, J can be quantized in units of K$\hbar$. Thus multi-quasiparticle states serve as the heads of rotational bands corresponding to large values of projection quantum number, K.

The Hf isomers also have angular momenta which are quite different from those of other intrinsic nuclear states. Since strong electromagnetic transitions are generally characterized by low orders of multipolarity, L and selection rules require $|\Delta J| \leq L$, the apparent necessity for large changes in angular momentum would seem to be the cause of the long isomeric lifetimes. However, large $\Delta J$ transitions need not be required. The excitation energies of multi-quasiparticle states are so great that levels with similar angular momenta can be found, built upon the low-spin ground state from as many as 10 - 15 quanta of rotation, while still remaining below the energy of the isomers. Thus the selection rule upon $\Delta J$ alone cannot be the cause of the isomerism.

The long lifetimes of multi-quasiparticle states of Hf result from the analogous selection rule upon K, generally accepted to be $|\Delta K| \leq L$ for transitions between states in different rotational bands. This is the restriction which severely hinders electromagnetic decay of the isomers to yrast levels of similar J, but dissimilar K. While providing storage of great energy densities, the selection rule on K would also seem to vitiate otherwise attractive proposals to use concentrations of high-spin isomers for superelastic particle beam applications, $(\gamma,\gamma')$ frequency upconversion, and the nuclear analog to the ruby laser. It is very difficult *a priori* to conceive of a trigger process or reaction which would transfer so much $\Delta K$ as would be needed to

deexcite populations of high-spin isomers to freely-radiating states in an efficient, controlled manner.

The key to transitions between high-spin isomers of Hf and yrast states may lie in the existence of mediating levels having mixed values of K. Those "K-mixing" levels would be described by superpositions of eigenfunctions for several different projection quanta corresponding to comparable values of J and could be reached by transitions of low multipolarity both from isomers and from members of bands built upon much lower values of K. A discussion of what type of perturbation could provide the interaction energy necessary for such a fortunate K mixing is left for later.

The first evidence for the deexcitation, or "dumping," of a multi-quasiparticle isomer through a K-mixing level seems to have been reported in 1987 and published [2] in 1988. Populations of the $10^{15}$-year, two-quasiparticle isomer $^{180}Ta^{m}$ were dumped to the ground state in the reaction $^{180}Ta^{m}(\gamma,\gamma')^{180}Ta$, despite a total change of $\Delta K = 8$. Identified [3] in 1990 as proceeding directly through a previously unobserved state at 2.8 MeV, the reaction was found to be excited with a surprisingly large integrated cross section of $1.2 \times 10^{-25}$ cm$^2$ keV. Independently, the same year the deexcitation of the 3.7-$\mu$s, four-quasiparticle isomer $^{174}Hf^{m}$ was reported [4] to occur as a result of *spontaneous emission* through a K-mixing level lying below the metastable state at 2.685 MeV and providing $\Delta K = 14$. The similarity of the excitation energies of the mediating levels in $^{180}Ta$ and $^{174}Hf$, on the order of a pairing interaction, suggested an examination of the systematics of other $(\gamma,\gamma')$ reactions that spanned large $\Delta K$. While those reactions might have proceeded through complex cascades, they could have also benefitted from more direct transitions through K-mixing states.

Figure 1 summarizes the results reported earlier for a systematic investigation [5,6] of integrated cross sections and excitation energies measured for $(\gamma,\gamma')$ processes mediating large

changes of $\Delta K$. The only known reactions starting on multi-quasiparticle levels seem to be those of $^{174}Hf^{m}$ and $^{180}Ta^{m}$, so the others shown are for the excitation of one- or two-quasiparticle isomers from ground-state targets. Nevertheless, the trend is compelling and suggests the pervasive existence of a K-mixing level between 2.5 - 2.8 MeV in many mid-shell nuclides below p = 82. Moreover, the values of integrated cross section for $(\gamma,\gamma')$ reactions occurring through such levels seem to peak in this region, notwithstanding the large $\Delta K$ between initial and final states. Such magnitudes would suggest strong transitions of low multipolarity, requiring the change in K to occur in the mediating state.

The persuasive nature of the data plotted in Fig. 1 encourages the tentative conclusion that a similar K-mixing level can be expected in the $^{178}Hf$ system. This would be particularly important for the 31-year, four-quasiparticle isomer $^{178}Hf^{m2}$ since such an intermediate state could connect it to yrast states, providing the means for realizing an induced release of the stored energies. Unfortunately, few studies have been conducted for reactions involving $^{178}Hf^{m2}$ due to great difficulties in obtaining appropriate targets. The present objective is to attempt to estimate the parameters that would describe such a reaction, $^{178}Hf^{m2}(\gamma,\gamma')^{178}Hf$ from the data which has recently become available [7].

Figure 2 shows an expanded view of the data of Fig. 1 for the mass island immediately below p = 82. Measured excitation energies of apparent K-mixing levels mediating those reactions are plotted as X and + symbols by the right-hand ordinate and fall between 2.5 - 2.8 MeV, defining an interval $\Delta E_K$ within which such levels may be reasonably expected. The circles give the energies of the four- and five-quasiparticle isomers $^{174}Hf^{m}$, $^{175}Hf^{m}$, $^{176}Hf^{m3}$, $^{177}Hf^{m2}$ and $^{178}Hf^{m2}$, which trend to lower values with increasing mass numbers. Relevant parameters for those isomers are shown in Table I. The important detail in Fig. 2 is the position of those isomers relative to the possible excitation energies of K-mixing levels. At present no direct

observations of $(\gamma,\gamma')$ reactions are available for those isotopes and thus the discussion is based on $\Delta E_K$ which bounds the likely energies of mediating states.

For $^{174}Hf^{m}$ and $^{175}Hf^{m}$ the isomers lie well above the upper bound of $\Delta E_K$ and it can be reasonably expected from Fig. 2 that those multi-quasiparticle states would be relatively short-lived due to the availability of K-mixing states which could mediate spontaneous decay. As mentioned before this is indeed the case for $^{174}Hf^{m}$ with a halflife of 3.7 $\mu$s. Similarly, $^{175}Hf^{m}$ has a 1.21-$\mu$s halflife. In the case of $^{176}Hf^{m3}$, the isomer lies at 2.866 MeV, slightly above the upper bound of $\Delta E_K$. Thus, it could be expected to have a short lifetime somewhat lengthened by a small transition energy to a K-mixing level. This is supported by a measured halflife of 401 $\mu$s. The isomer $^{177}Hf^{m2}$ lies just below the upper bound of $\Delta E_K$, possibly at a lower energy than any mediating state. In that event a long lifetime would be suggested since spontaneous decay could not occur, but this could also be the result if a K-mixing level were located little below the isomer. The measured halflife of 51 min agrees well with either possibility. Of most importance to the present discussion, the isomer $^{178}Hf^{m2}$ appears to lie below the likely position of a mediating state. This points to a long lifetime and indeed the measured value is 31 years. Clearly the known halflives of these multi-quasiparticle Hf isomers agree well with the speculation that K-mixing levels are prevalent and lie between 2.5 - 2.8 MeV.

The strong dependence of isomer lifetime on the possible excitation energy of a mediating state is shown directly in Fig. 3. Again, $\Delta E_K$ indicates the interval within which all measured values for possible K-mixing levels lie. This interval can be further constrained by comparing the data to lifetimes derived from single-particle widths. Since low-multipolarities would be indicated for transitions between the isomers and states of mixed K, dipole radiation is considered here. Derived using the typical $1/(E_i - E_K)^3$ dependence for dipole transition widths where $E_i$ is the isomer energy and $E_K$ is the energy of the mediating level, the curves in Fig. 3

show halflives in good agreement with the measured values. It is doubtful that a K-mixing state could lie much below the isomer $^{177}Hf^{m2}$ without affecting its 51 min lifetime. Thus, the value $E_K$ = 2.7 MeV used to generate the curve passing just below that isomer represents a lower bound on the likely energy of an intermediate state of mixed K. Likewise, $E_K$ = 2.8 MeV provides an upper bound for that energy since larger values produce curves which do not reproduce the lifetimes of the isomers $^{174}Hf^{m}$, $^{175}Hf^{m}$ and $^{176}Hf^{m3}$. The excellent agreement seen between halflives predicted for dipole transitions and those measured provides further evidence for a K-mixing level in $^{178}Hf^{m2}$ lying no more than about 300 keV above the isomer.

The presence of such a K-mixing level could in principle be identified in a ($\gamma$,$\gamma$') reaction study similar to those conducted previously [2,3,6], but might be most easily detected in the proposed experiment shown schematically in Fig. 4a. A beam of protons of energy $E_0$ would be incident on $^{178}Hf^{m2}$ nuclei in a sample located within a 4-$\pi$ granular detector array, or "$\gamma$ ball." This arrangement would provide for inelastic scattering of protons in (p,p'$\gamma$) reactions where the $\gamma$ refers to photons emitted in the decay of the excited nucleus. Many scattering events would merely excite low-lying members of the ground-state or isomeric rotational bands with a low multiplicity, n of accompanying $\gamma$-rays. However, the excitation of a K-mixing state from the isomer would result in a transfer of the isomer to the yrast band with an accompanying large multiplicity ($n \geq 4$) of emitted photons. Thus the important aspect in the observation of a K-mixing level would be the measurement of the spectrum of inelastically scattered protons in coincidence with a high multiplicity of photons detected by the $\gamma$ ball. By selecting only events satisfying this criterion it would be possible to confirm the existence of the K-mixing level in an excitation function like that depicted in Fig. 4b. The location of the mediating level would be clearly marked by a threshold at an energy $E_t = E_0 - E_K$.

This letter makes no attempt to estimate the probability for the actual existence of a K-mixing state. However, systematics strongly suggest that such a level may exist in $^{178}Hf^{m2}$, and at a sufficiently low excitation energy to be of great importance to proposals for the use of this isomer in superelastic particle-beam studies, gamma-ray upconversion and the nuclear analog to the ruby laser. At this point further study is needed for a definitive resolution.

## REFERENCES


1. *National Nuclear Data Center Online Evaluated Nuclear Structure Data File (ENSDF)*, 1994, Brookhaven National Laboratory.

2. Collins, C. B., . Eberhard, C. D., Glesener, J. W., and Anderson, J. A., 1988, *Phys. Rev. C*, **37**, 2267.

3. Collins, C. B., Carroll, J. J., Sinor, T. W., Byrd, M. J., Richmond, D. G., Taylor, K. N., Huber, M., Huxel, N., von Neumann-Cosel, P., Richter, A., Spieler, C., and Ziegler, W., 1990, *Phys. Rev. C*, **42**, 1813.

4. Walker, P. M., Sletten, F., Gjørup, N. L., Bentley, M., A., Borggreen, J., Fabricius, B., Holm, A., Howe, D., Pedersen, J., Roberts, J. W., and Sharpey-Schafer, J. F., 1990, *Phys. Rev. Lett.*, **65**, 416.

5. Collins, C. B., and Carroll, J. J., 1994, *Laser Physics*, (This issue).

6. Carroll, J. J., Byrd, M. J., Richmond, D. G., Sinor, T. W., Taylor, K. N., Hodge, W. L., Paiss, Y., Eberhard, C. D., Anderson, J. A., Collins, C. B., Scarbrough, E. C., Antich, P. P., Agee, F. J., Davis, D., Huttlin, G. A., Kerris, K. G., Litz, M. S., and Whittaker, D. A., 1991, *Phys. Rev. C*, **43**, 1238.

7. Oganessian, Yu. Ts., Karamian, S. A., Gangrski, Y. P., Gorski, B., Markov, B. N., Szeglowski, Z., Briançon, Ch., Constantinescu, O., Hussonnois, M., Pinard, J., Kulessa, R., Wollersheim, H. J., de Boer, J., Graw, G., Huber, G., and Muradian, H. V., 1992, in *Proc. Int. Conf. "Nuclear Physics in Our Times."*

8. Oganessian, Yu. Ts., Karamian, S. A., Gangrski, Y. P., Gorski, B., Markov, B. N., Szeglowski, Z., Briançon, Ch., Ledu, D., Meunier, R., Hussonnois, M., Constantinescu, O., and Subbotin, M. I., 1992, *J. Phys. G: Nucl. Part. Phys.*, **18**, 393.

9. Bunker, M. E., and Reich, C. W., 1971, *Rev. Mod. Phys.*, **43**, 348.

# TABLE I

Summary of relevant adopted properties [1] for three-, four-, and five-quasiparticle Hf isomers having excitation energies between 2 - 4 MeV and lifetimes longer than 1 $\mu$s. Parentheses indicate suggested values.

| Isomer | $J^\pi = K^\pi$ | Number of quasiparticles [1,9] | Excitation Energy [MeV] | Halflife |
|---|---|---|---|---|
| $^{174}Hf^{m}$ | $(14^+)$ | 4 | 3.312 | 3.7 $\mu$s |
| $^{175}Hf^{m}$ | $(^{35}/_{2})$ | 5 | 3.016 | 1.21 $\mu$s |
| $^{176}Hf^{m3}$ | $(14^-)$ | 4 | 2.866 | 401 $\mu$s |
| $^{177}Hf^{m2}$ | $^{37}/_{2}^-$ | 5 | 2.740 | 51.4 min |
| $^{178}Hf^{m2}$ | $16^+$ | 4 | 2.446 | 31 yr |

# CAPTIONS

Figure 1: Summary of systematic studies [5,6] of the excitation and deexcitation of quasiparticle isomers in ($\gamma,\gamma'$) reactions. Measured integrated cross sections are plotted by the left-hand axis and the excitation energies for possible K-mixing levels are plotted by the right-hand axis. The X symbols indicate mediating states excited from the ground state or isomer with bremsstrahlung and the + represents the level through which spontaneous decay of $^{174}Hf^{m}$ occurs [4]. Values of integrated cross section peak mid-shell in the mass island below p = 82.

Figure 2: Expanded view of the data of Fig. 1 for the mass island below p = 82. Also indicated by the circles are the excitation energies of four- and five-quasiparticle Hf isomers lying between 2 - 3 MeV and having halflives longer than 1 $\mu$s. The interval $\Delta E_K$ shows the range of energy within which all possible K-mixing levels are expected to lie.

Figure 3: Plot of halflife as a function of excitation energy for the four- and five-quasiparticle Hf isomers of Fig. 2. The interval $\Delta E_K$ is shown within which all K-mixing levels are expected to lie based on previous measurements. The curves represent halflives calculated based on the assumption of the availability of dipole transitions for the deexcitation of the isomers for different choices for the energy of the mediating state and further bound the possible positions of such a level.

Figure 4: a) Schematic depicting a proposed experiment to confirm the existence of a K-mixing state in $^{178}Hf^{m2}$. Protons of energy $E_0$ would be incident on a sample containing $^{178}Hf^{m2}$ placed within a 4-$\pi$ granular "$\gamma$ ball" detector. The energy of protons scattered in (p,p'$\gamma$) reactions

would be measured by the external detector while the $\gamma$ ball would record photons resulting from decay of the nucleus. b) Excitation function expected from a K-mixing level by detecting scattered protons in coincidence with a high multiplicity of $\gamma$ rays. The threshold at $E_t = E_0 - E_K$ locates the excitation energy of the mediating level.

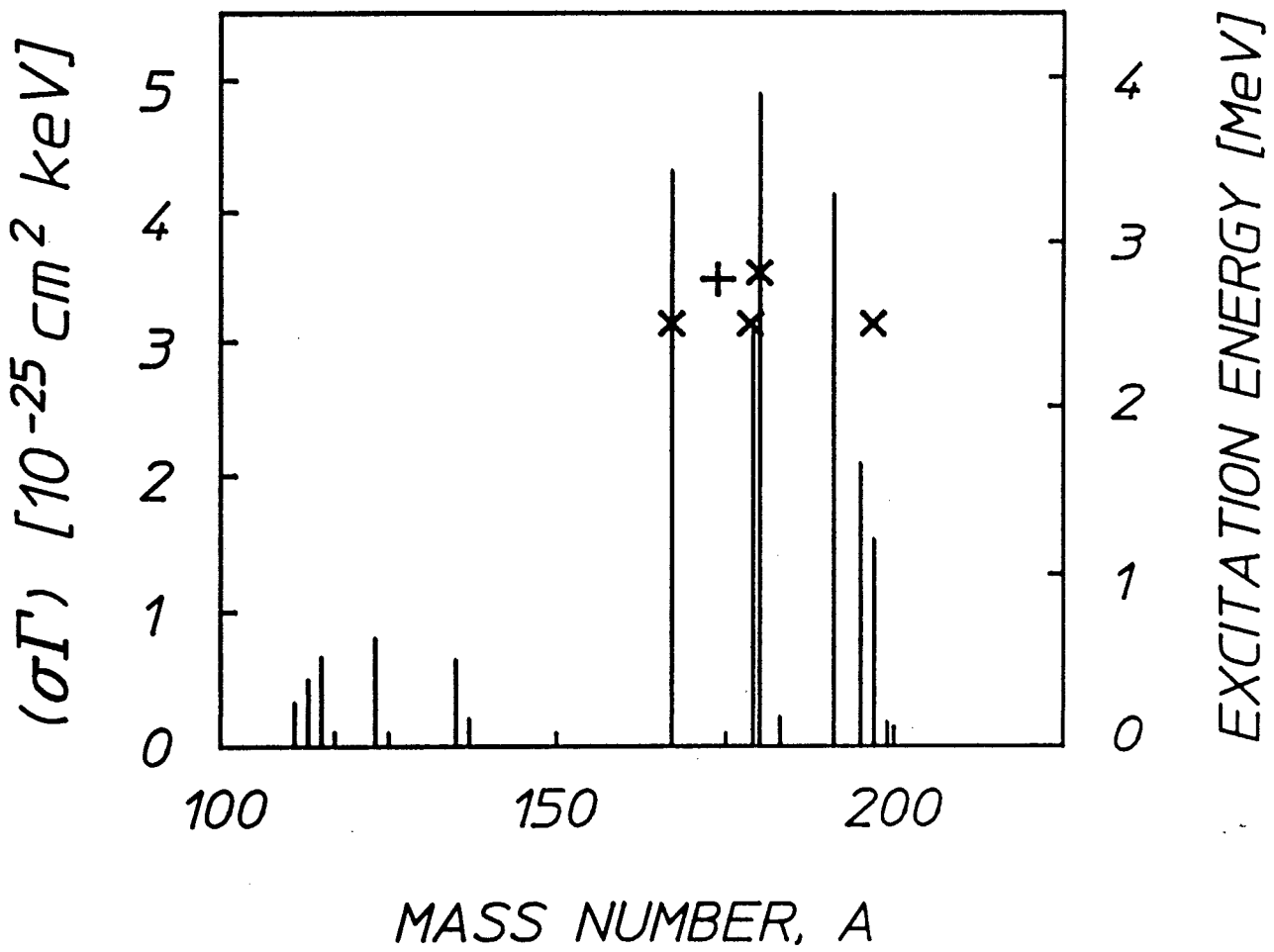
(σΓ) [10-25 cm2 keV]
0
1
2
3
4
5
100
150
200
MASS NUMBER, A
EXCITATION ENERGY [MeV]
0
1
2
3
4

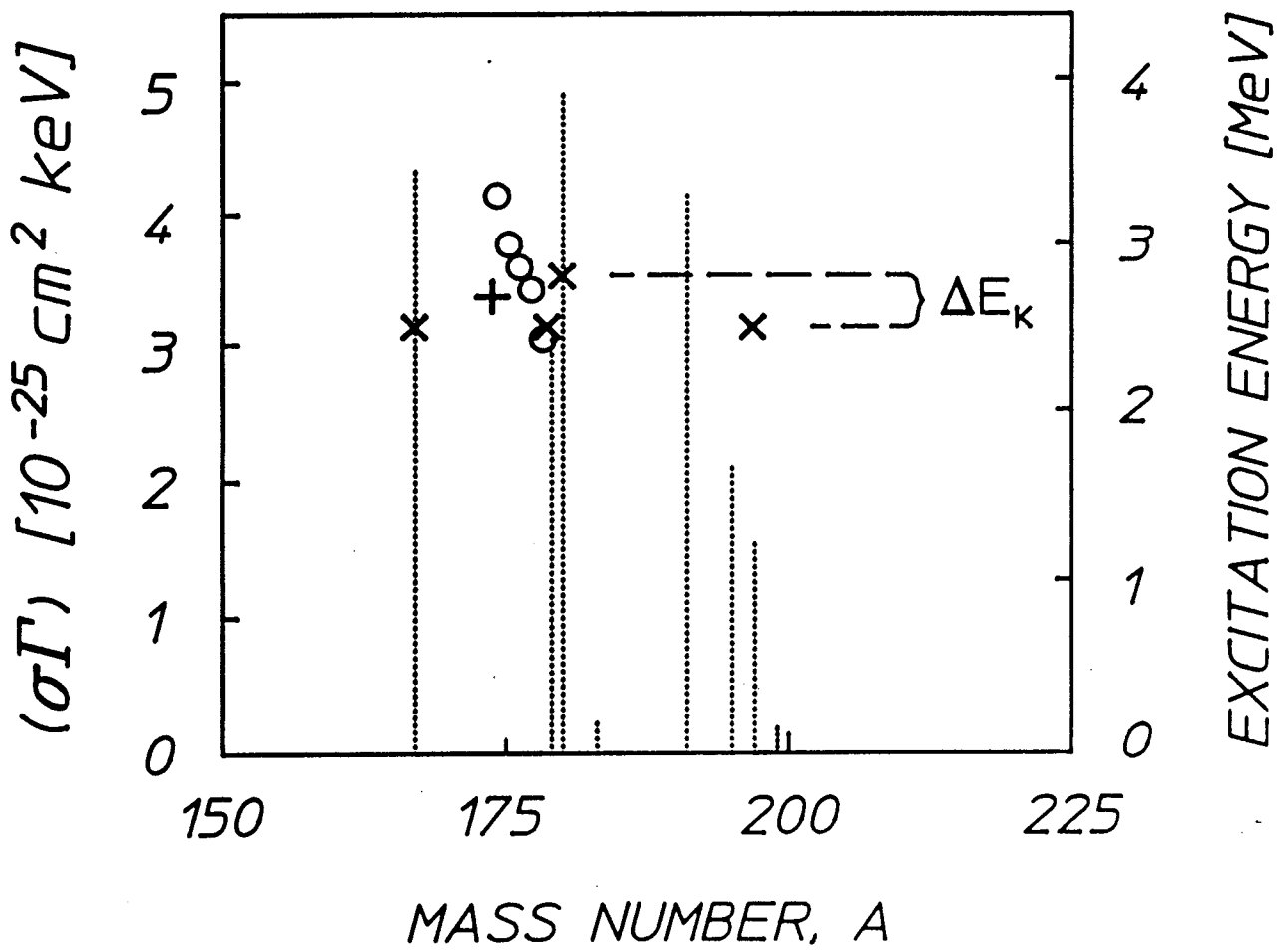
(σΓ) [10⁻²⁵ cm² keV]
EXCITATION ENERGY [MeV]
MASS NUMBER, A
ΔE_K
0
1
2
3
4
5
150
175
200
225

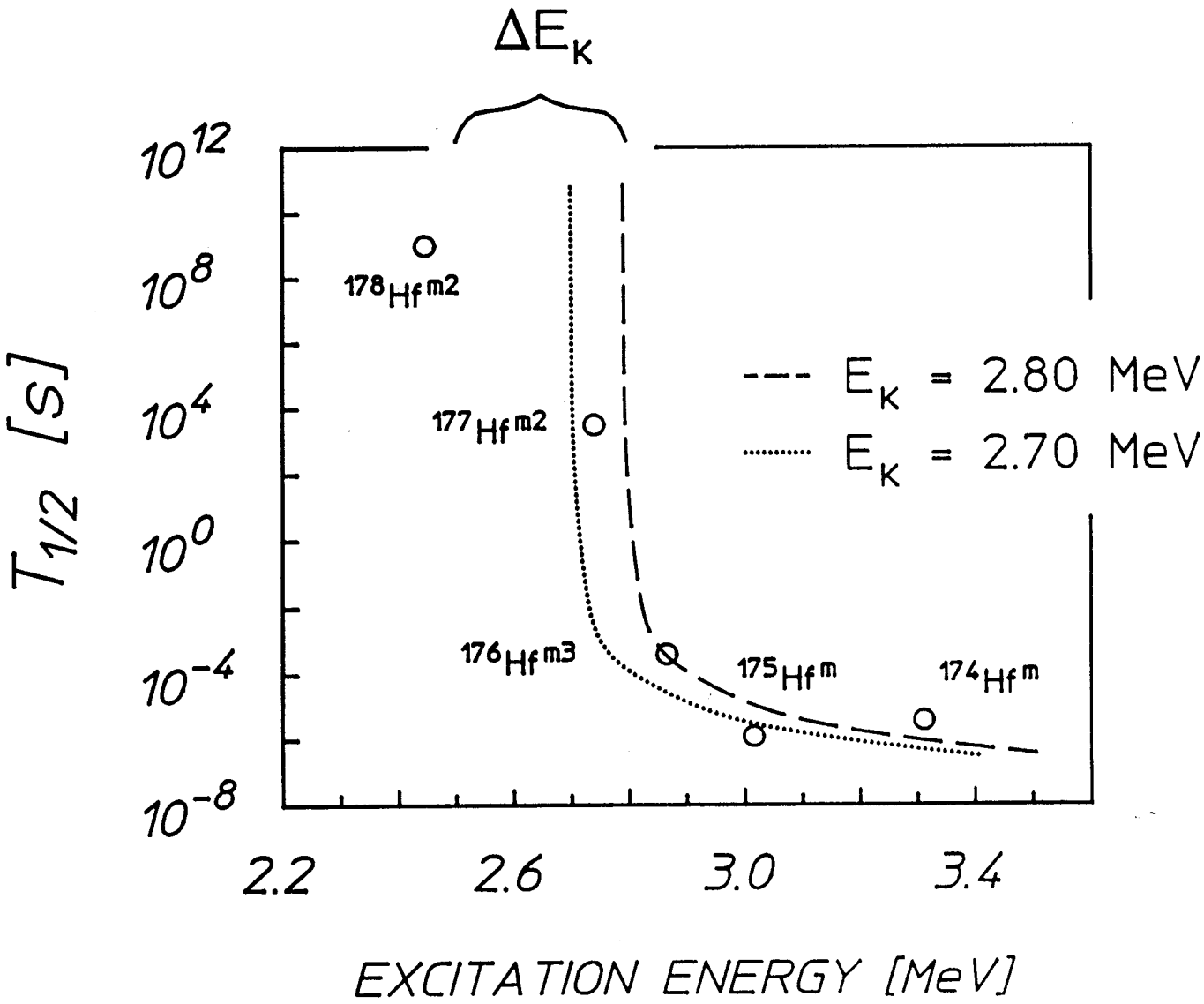
ΔE_K
10^12
10^8
10^4
10^0
10^-4
10^-8
T_1/2 [s]
178Hf m2
177Hf m2
176Hf m3
175Hf m
174Hf m
E_K = 2.80 MeV
E_K = 2.70 MeV
2.2
2.6
3.0
3.4
EXCITATION ENERGY [MeV]

a) EXPERIMENTAL ARRANGEMENT

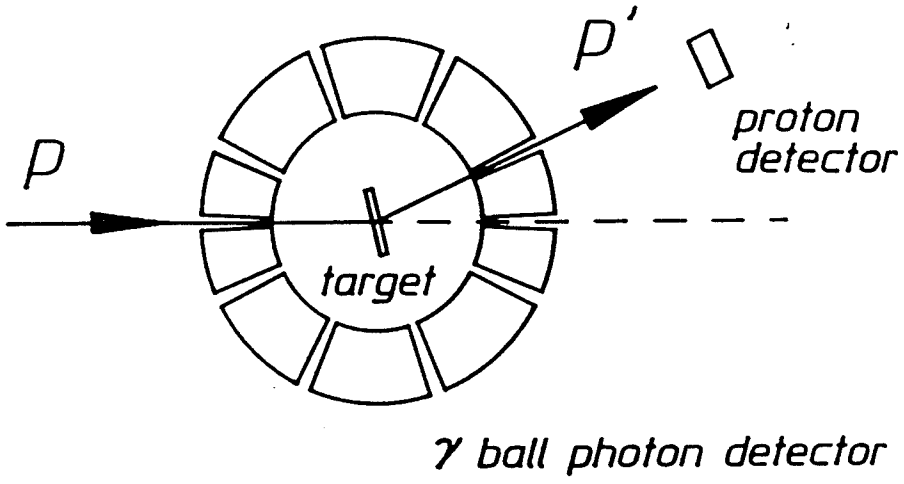


b) EXCITATION FUNCTION

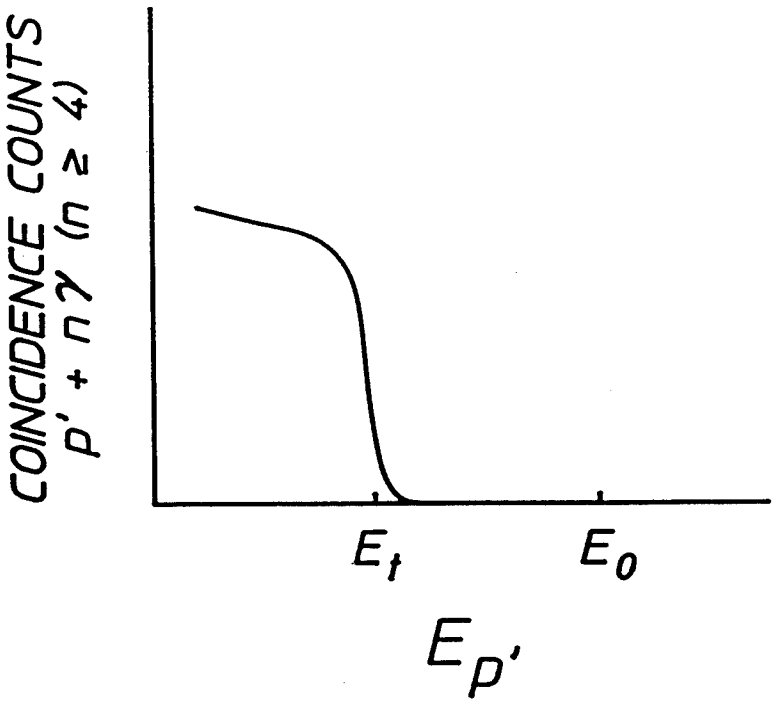

PHYSICAL REVIEW B VOLUME 50, NUMBER 1 1 JULY 1994-I

# Quantum-interference asymmetries in the multiphoton radio-frequency sideband spectra of $^{57}$Fe

S. Olariu* and C. B. Collins
*Center for Quantum Electronics, University of Texas at Dallas, P.O. Box 830688, Richardson, Texas 75083-0688*

T. W. Sinor
*VARO, Inc., Ni-Tec Division, IMO Industries, 3414 Hermann Drive, Garland, Texas 75041*
(Received 20 December 1993)

We determine the intensity of the nuclear multiphoton sidebands to the forbidden components of the 14.4-keV Mössbauer transition in $^{57}$Fe, generated by the application of radio-frequency magnetic fields to ferromagnetic samples, in the presence of static magnetic fields. Further we determine the intensity of the second-order sidebands to the 14.4-keV transition in the case known as the radio-frequency collapse, when the entire hyperfine magnetic field acting on the $^{57}$Fe nuclei follows the oscillations of the applied radio-frequency field. Then we discuss a number of characteristic asymmetries due to quantum interference, appearing in the multiphoton radio-frequency sideband spectra.

## I. INTRODUCTION

We consider in this work a class of nuclear multiphoton processes involving the simultaneous interaction with a nucleus of a $\gamma$-ray photon and of radio-frequency photons from an applied oscillatory magnetic field, the intermediate states being the magnetic sublevels of the nuclear states. The ratio of the intensity of a two-photon transition to the intensity of the single $\gamma$-ray transition between the same nuclear states is of the order of the square of the ratio of the interaction energy of the radio-frequency magnetic field with the nucleus and the frequency of this field.

The first experimental demonstration of a nuclear transition involving simultaneously a $\gamma$-ray photon and a radio-frequency photon is due to West and Matthias in 1978,[1] for the 6.2-keV state of $^{181}$Ta under an applied radio-frequency magnetic field of 23 mT having a frequency of 0.94 MHz. A similar nuclear two-photon process was demonstrated in 1988 by Ikonen *et al.*[2–4] for the 93-keV state of $^{67}$Zn under an applied radio-frequency magnetic field of 13.4 mT at the frequencies 3.1 and 9.3 kHz.

When we consider the possibility to observe such simultaneous $\gamma$ radio-frequency transitions in $^{57}$Fe, we have to take into consideration the fact that the half-life of the 14.4-keV transition in $^{57}$Fe is 98 ns, compared to a 6.8-$\mu$s half-life for the 6.2-keV transition in $^{181}$Ta and a 9.2-$\mu$s half-life for the 93-keV transition in $^{67}$Zn. Moreover, the spins and nuclear magnetic moments of the ground and excited states are, respectively, $\frac{1}{2}$, $0.090\mu_n$ and $\frac{3}{2}$, $-0.155\mu_n$ for $^{57}$Fe, compared to $\frac{7}{2}$, $2.37\mu_n$ and $\frac{9}{2}$, $5.3\mu_n$ for $^{181}$Ta and $\frac{5}{2}$, $0.87\mu_n$ and $\frac{1}{2}$, $0.58\mu_n$ for $^{67}$Zn, where $\mu_n = 5.05\times10^{-27}$ J/T. Thus the energy of interaction of an applied radio-frequency field with a $^{57}$Fe nucleus is considerably smaller than the coupling of the same field to $^{181}$Ta or $^{67}$Zn nuclei. Therefore a two-photon experiment for $^{57}$Fe, without any enhancement mechanism, would require applied magnetic fields with an amplitude of the order of 0.1 T at a frequency of a few MHz, which is difficult to produce.

However, if a $^{57}$Fe nucleus is in a ferromagnetic environment, the direction of the hyperfine magnetic field acting on the nucleus is determined by the direction of the magnetization in the sample, and the orientation of the bulk magnetization can be controlled with the aid of applied static and radio-frequency magnetic fields. This approach has been used by Heiman, Walker, and Pfeiffer[5,6] who observed the spectrum of the $\gamma$ rays scattered by finely powdered metallic iron under the action of an oscillatory magnetic field whose frequency of 26 MHz was equal to the hyperfine splitting of the upper 14.4-keV state of $^{57}$Fe. The incident $\gamma$ rays were themselves resonant to one of the allowed transitions between the magnetic nuclear sublevels, and the arrangement has been referred to by the authors as an excited-state nuclear-magnetic-resonance experiment. As a result of the application of the radio-frequency magnetic field to the iron-powder scatterer, lines appeared in the spectrum of the scattered $\gamma$ radiation at the position of the other known transitions of $^{57}$Fe.

On the theoretical side, the effects of circularly polarized radio-frequency magnetic fields on the Mössbauer spectra of $^{57}$Fe have been analyzed by Gabriel.[7]

Initially, Heiman, Walker, and Pfeiffer tried to use a metallic iron *foil* for the scatterer,[8] but they found that the application of the radio-frequency magnetic field produced in this case additional lines at positions which did not correspond to any known transition in $^{57}$Fe. They have suggested[9] that the observed sidebands, occurring in a foil but with negligible intensity in a powder, result from the acoustic vibrations generated in the foil by the applied radio-frequency magnetic field. Similar observations have been reported by Asti, Albanese, and Bucci.[10,11]

The fact that the hyperfine magnetic field acting on a $^{57}$Fe nucleus in a ferromagnetic environment can be made to oscillate between opposing directions by the application of radio-frequency fields has been demonstrated by

0163-1829/94/50(1)/43(9)/$06.00

the radio-frequency collapse effect discovered by Pfeiffer in 1971.[12,13] He found that, as a result of the application of an oscillatory magnetic field with an amplitude of 1.5 mT and frequencies of 39, 61, and 106 MHz to a 6-$\mu$m-thick Permalloy foil, the six-line hyperfine patter of $^{57}$Fe disappeared and has been replaced by a single central line, accompanied by a number of sidebands displaced on a frequency scale by multiples of the applied frequency.

Pfeiffer attributed the presence of the sidebands in his collapse experiments entirely to the acoustic vibrations generated in the Permalloy foil by the radio-frequency field. However, Olariu, Popescu, and Collins[14] pointed out that the oscillation through large angles of the hyperfine magnetic field acting on the $^{57}$Fe nuclei, produced by the application of the radio-frequency field to the Permalloy sample, results necessarily in the generation of nuclear multiphoton sidebands whose transition intensities are comparable to those observed by Pfeiffer. The fact that the entire hyperfine magnetic field can be made to follow the direction of the applied radio-frequency field and the reduced amplitude of the mechanical vibrations in the Permalloy sample, due to the small magnetostrictive constant of Permalloy, show that it is possible to observe nuclear multiphoton transitions for $^{57}$Fe nuclei in a ferromagnetic environment.

The radio-frequency collapse effect has been further investigated by Kopcewicz *et al.* in ferromagnetic amorphous metals,[15,16] in $FeBO_3$,[17] and in Fe-Ni alloys,[18] with the conclusion that for sufficiently intense radio-frequency fields, of the order of 1.5 mT, the hyperfine magnetic field acting on the $^{57}$Fe nuclei follows the direction of the applied field. The sidebands observed in these experiments have been in general attributed to acoustic modulation.

As a corollary of their studies on the magnetic modulation of the phase of $^{67}$Zn nuclei, Ikonen *et al.*[2] have reiterated the previous prediction[14] that if the hyperfine field acting on a $^{57}$Fe nucleus can be switched between two opposite directions at a rate determined by the frequency of the applied radio-frequency field, this will generate sidebands without any mechanical motion.

The intensities of the nuclear multiphoton sidebands for the six allowed transitions of $^{57}$Fe have been calculated by Olariu[19] for $^{57}$Fe nuclei embedded in thin ferromagnetic films under static and radio-frequency magnetic fields. He remarked that the use of a thin ferromagnetic film having a thickness of a few thousand angstroms, instead of a foil, is likely to minimize the mechanical vibrations and, moreover, would allow the determination with reasonable accuracy of the time evolution of the magnetization of the sample.

The role played by spin waves in the generation of the radio-frequency sidebands has been emphasized by Sinor, Reittinger, and Collins,[20] who showed that it is possible to produce a modulation of the phase of $^{57}$Fe nuclei in paramagnetic media by transporting spin waves of large amplitude from ferromagnetic sources.

The resonance line splitting of hyperfine lines of $^{57}$Fe nuclei in radio-frequency magnetic fields, caused by Rabi oscillations and predicted in a number of papers,[7,19,21] has been recently observed by Vagizov[22] and independently by Tittonen *et al.*[23] Special precautions have been taken in these works to minimize the mechanical vibrations.

It is apparent from this survey of previous works on radio-frequency sidebands that, while the ferromagnetic foil samples can provide the required large radio-frequency fields in the form of oscillatory hyperfine magnetic fields, the observation of the nuclear multiphoton processes is often hindered by the ease with which mechanical vibrations can be induced in ferromagnetic samples through magnetostriction, especially at lower frequencies. The importance of nuclear multiphoton processes becomes apparent when we refer to recent developments in atomic multiphoton processes, where problems such as inversionless amplification[24,25] or electromagnetically induced transparency[26–28] are under active consideration.

The purpose of this work is to bring into evidence a number of characteristic properties of nuclear multiphoton processes involving $\gamma$-ray and radio-frequency photons. Thus, in Sec. II, we determine the intensity of the nuclear multiphoton sidebands to the forbidden components of the 14.4-keV transition of $^{57}$Fe, generated by the application of radio-frequency magnetic fields to ferromagnetic samples in the presence of a static field. In Sec. III we determine the intensity of the second-order sidebands to the 14.4-keV transition of $^{57}$Fe in the case of the radio-frequency collapse when the entire hyperfine magnetic field follows the oscillations of the applied radio-frequency field. In Sec. IV we discuss a number of characteristic asymmetries, due to quantum interference, appearing in the multiphoton radio-frequency sideband spectra.

## II. INTENSITY OF THE FIRST-ORDER SIDEBANDS TO THE FORBIDDEN $e,\frac{3}{2}\rightarrow g,-\frac{1}{2}$ AND $e,-\frac{3}{2}\rightarrow g,\frac{1}{2}$ TRANSITIONS IN $^{57}$Fe

The intensities of the first-order sidebands to the six allowed transitions between the 14.4-keV excited state $e$ and the ground state $g$ of $^{57}$Fe nuclei have been determined in Ref. 19 as a function of the direction and polarization of the $\gamma$ rays for a linear and a circular polarization of the applied radio-frequency magnetic field. The transitions $e,\frac{3}{2}\rightarrow g,-\frac{1}{2}$ and $e,-\frac{3}{2}\rightarrow g,\frac{1}{2}$ are forbidden as single $\gamma$-ray processes, but these forbidden transitions have in general nonvanishing multiphoton sidebands, the intensity of which we shall calculate in this section.

The intensity of the sidebands to the forbidden hyperfine transition of $^{57}$Fe has been reported previously[29] in the particular case of a linearly polarized radio-frequency magnetic field $B_0^h$ and for a direction of propagation of the $\gamma$ rays which was perpendicular to the static and radio-frequency magnetic fields. In the previous paper,[29] it was also pointed out that sidebands to the forbidden hyperfine transition of $^{57}$ can be identified in the Mössbauer spectra of $^{57}$Fe nuclei in Permalloy recently reported by Tittonen *et al.*[23] The presence of the sidebands to the forbidden hyperfine transitions of $^{57}$Fe constitutes an unequivocal proof that nuclear multiphoton processes are indeed taking place in $^{57}$Fe nuclei subject to

radio-frequency magnetic fields, as predicted repeatedly.[2,7,14,19,30]

We shall determine the probability for the transition $e,\frac{3}{2}\rightarrow g,-\frac{1}{2}$ in a $^{57}$Fe nucleus by the emission of a linearly polarized $\gamma$-ray quantum, the orientation of the magnetic $\gamma$-ray field $\mathbf{B}_\gamma$ and of the wave vector $\mathbf{k}_\gamma$ being shown in Fig. 1, under the action of a static hyperfine magnetic field $B_0^h$, oriented along the $z$ axis, and of a radio-frequency magnetic field having the $x$ component $B_{\mathrm{rf},x}\cos(\omega_{\mathrm{rf}}t)$ and the $y$ component $B_{\mathrm{rf},y}\cos(\omega_{\mathrm{rf}}t+\alpha_{\mathrm{rf}})$. The positive direction of the $z$ axis is chosen to coincide with the direction of the static hyperfine magnetic field effectively acting on the $^{57}$Fe nuclei, so that the magnetic sublevels, in order of increasing energy, are $g,\frac{1}{2}$; $g,-\frac{1}{2}$; $e,-\frac{3}{2}$; $e,-\frac{1}{2}$; $e,\frac{1}{2}$; and $e,\frac{3}{2}$.

It can be shown that the transition amplitudes $b_k$ are solutions of the Hamiltonian equations

$$i\hbar\frac{db_k}{dt}=\sum_n F_{kn}(t)b_n \ . \tag{1}$$

The nonvanishing matrix elements are given by

$$F_{g,1/2;g,-1/2}(t)=-\frac{\hbar\omega_g}{2B_0^h}Y(t)^*\exp(-i\omega_g t) \ , \tag{2a}$$

$$F_{e,-3/2;e,-1/2}(t)=\frac{\hbar\omega_e\sqrt{3}}{2B_0^h}Y(t)\exp(-i\omega_e t) \ , \tag{2b}$$

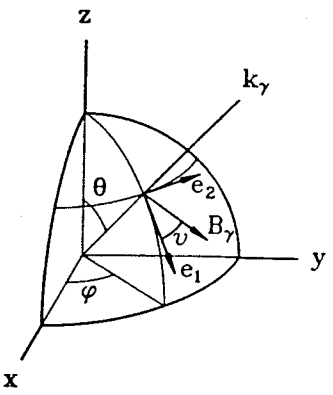


FIG. 1. Orientation of the magnetic field $\mathbf{B}_\gamma$ and of the wave vector $\mathbf{k}_\gamma$ of a quantum of $\gamma$ radiation emitted by a $^{57}$Fe nucleus.

$$F_{e,-1/2;e,1/2}(t)=\frac{\hbar\omega_e}{2B_0^h}Y(t)\exp(-i\omega_e t) \ , \tag{2c}$$

$$F_{e,1/2;e,3/2}(t)=\frac{\hbar\omega_e\sqrt{3}}{2B_0^h}Y(t)\exp(-i\omega_e t) \ , \tag{2d}$$

where

$$Y(t)=B_{\mathrm{rf},x}\cos(\omega_{\mathrm{rf}}t)+iB_{\mathrm{rf},y}\cos(\omega_{\mathrm{rf}}t+\alpha_{\mathrm{rf}}) \ , \tag{3}$$

and by

$$F_{g,-1/2;e,-3/2}(t)=\frac{\sqrt{6}}{2}AB_\gamma\cos(\omega_\gamma t+\phi_\gamma)Z\exp\left[-i\left[\frac{E_e-E_g}{\hbar}-\frac{3\omega_e}{2}-\frac{\omega_g}{2}-\frac{i\Gamma}{2}\right]t\right] , \tag{4a}$$

$$F_{g,-1/2;e,-1/2}(t)=\sqrt{2}AB_\gamma\cos(\omega_\gamma t+\phi_\gamma)\sin\theta\cos\upsilon\exp\left[-i\left[\frac{E_e-E_g}{\hbar}-\frac{\omega_e}{2}-\frac{\omega_g}{2}-\frac{i\Gamma}{2}\right]t\right] , \tag{4b}$$

$$F_{g,-1/2;e,1/2}(t)=-\frac{\sqrt{2}}{2}AB_\gamma\cos(\omega_\gamma t+\phi_\gamma)Z^*\exp\left[-i\left[\frac{E_e-E_g}{\hbar}+\frac{\omega_e}{2}-\frac{\omega_g}{2}-\frac{i\Gamma}{2}\right]t\right] , \tag{4c}$$

$$F_{g,1/2;e,-1/2}(t)=\frac{\sqrt{2}}{2}AB_\gamma\cos(\omega_\gamma t+\phi_\gamma)Z\exp\left[-i\left[\frac{E_e-E_g}{\hbar}-\frac{\omega_e}{2}+\frac{\omega_g}{2}-\frac{i\Gamma}{2}\right]t\right] , \tag{4d}$$

$$F_{g,1/2;e,1/2}(t)=\sqrt{2}AB_\gamma\cos(\omega_\gamma t+\phi_\gamma)\sin\theta\cos\upsilon\exp\left[-i\left[\frac{E_e-E_g}{\hbar}+\frac{\omega_e}{2}+\frac{\omega_g}{2}-\frac{i\Gamma}{2}\right]t\right] , \tag{4e}$$

$$F_{g,1/2;e,3/2}(t)=-\frac{\sqrt{6}}{2}AB_\gamma\cos(\omega_\gamma t+\phi_\gamma)Z^*\exp\left[-i\left[\frac{E_e-E_g}{\hbar}+\frac{3\omega_e}{2}+\frac{\omega_g}{2}-\frac{i\Gamma}{2}\right]t\right] , \tag{4f}$$

where $A$ is a reduced matrix element, and

$$Z=\sin\varphi\sin\upsilon-\cos\varphi\cos\theta\cos\upsilon+i(\cos\varphi\sin\upsilon+\sin\varphi\cos\theta\cos\upsilon) \ . \tag{5}$$

In Eqs. (2) and (4), $\omega_e,\omega_g>0$ represent the separations, on a frequency scale, of the magnetic sublevels of the excited state $e$ and, respectively, of the ground state $g$ due to the static hyperfine $B_0^h$ and $\Gamma=1/\tau$, where the mean life is $\tau=1.4\times10^{-7}$ s for the 14.4-keV level of $^{57}$Fe. $E_e$ and $E_g$ are the energies of the excited and ground states in the absence of any applied magnetic field.

Equation (1) can be solved by a perturbation series, and the second-order contribution, which gives the amplitudes of the first-order sidebands to the $\gamma$-ray transitions, is

$$b^{(2)}_{gm;em_0}=-\frac{1}{\hbar^2}\sum_k\int_0^\infty F_{gm;k}(t)dt\int_0^t F_{k;em_0}(\zeta)d\zeta \ . \tag{6}$$

Substituting in Eq. (6) the expression of the appropriate matrix elements from Eqs. (2)–(5) and neglecting nonresonant terms, we obtain an expression for the intensity of the first-order sidebands for a linear polarization of the radio-frequency field, when $B_{\mathrm{rf},y}=0$, which is given by

$$|\langle g,-\tfrac{1}{2}|e,\tfrac{3}{2}\rangle_{\pm}^{(L)}|^2 = \frac{3|A|^2B_\gamma^2}{32\hbar^2\Gamma^2}(\sin^2\upsilon+\cos^2\theta\cos^2\upsilon) \times\left[\frac{B_{\mathrm{rf},x}}{B_0^h}\right]^2\left[\frac{\omega_e}{\pm\omega_{\mathrm{rf}}+\omega_e}+\frac{\omega_g}{\pm\omega_{\mathrm{rf}}-\omega_g}\right]^2, \tag{7}$$

for

$$\omega_\gamma=\frac{E_e-E_g}{\hbar}+\frac{3\omega_e}{2}-\frac{\omega_e}{2}\pm\omega_{\mathrm{rf}},$$

where the alternate signs should be read along the upper or lower line.

If the radio-frequency field has a right circular polarization, so that $B_{\mathrm{rf},x}=B_{\mathrm{rf},y}=B_{\mathrm{rf}}$ and $\alpha_{rf}=-\pi/2$, the intensity of the sidebands, obtained from Eq. (6), is

$$|\langle g,-\tfrac{1}{2}|e,\tfrac{3}{2}\rangle_{+}^{(\mathrm{CR})}|^2=0, \tag{8a}$$

for

$$\omega_\gamma=\frac{E_e-E_g}{\hbar}+\frac{3\omega_e}{2}-\frac{\omega_g}{2}+\omega_{\mathrm{rf}},$$

$$|\langle g,-\tfrac{1}{2}|e,\tfrac{3}{2}\rangle_{-}^{(\mathrm{CR})}|^2=\frac{3|A|^2}{8\hbar^2\Gamma^2}(\sin^2\upsilon+\cos^2\theta\cos^2\upsilon) \times\left[\frac{B_{\mathrm{rf}}}{B_0^h}\right]^2\left[\frac{\omega_e}{\omega_{\mathrm{rf}}-\omega_e}+\frac{\omega_g}{\omega_{\mathrm{rf}}+\omega_g}\right]^2, \tag{8b}$$

for

$$\omega_\gamma=\frac{E_e-E_g}{\hbar}+\frac{3\omega_e}{2}-\frac{\omega_g}{2}-\omega_{\mathrm{rf}}.$$

If the radio-frequency field has a left circular polarization, so that $B_{\mathrm{rf},x}=B_{\mathrm{rf},y}=B_{\mathrm{rf}}$ and $\alpha_{\mathrm{rf}}=\pi/2$, the intensity of the sidebands, obtained from Eq. (6), is

$$|\langle g,-\tfrac{1}{2}|e,\tfrac{3}{2}\rangle_{+}^{(\mathrm{CL})}|^2 = \frac{3|A|^2B_\gamma^2}{8\hbar^2\Gamma^2}(\sin^2\upsilon+\cos^2\theta\cos^2\upsilon) \times\left[\frac{B_{\mathrm{rf}}}{B_0^h}\right]^2\left[\frac{\omega_e}{\omega_{\mathrm{rf}}+\omega_e}+\frac{\omega_g}{\omega_{\mathrm{rf}}-\omega_g}\right]^2, \tag{9a}$$

for

$$\omega_\gamma=\frac{E_e-E_g}{\hbar}+\frac{3\omega_e}{2}-\frac{\omega_g}{2}+\omega_{\mathrm{rf}},$$

$$|\langle g,-\tfrac{1}{2}|e,\tfrac{3}{2}\rangle_{-}^{(\mathrm{CL})}|^2=0, \tag{9b}$$

for

$$\omega_\gamma=\frac{E_e-E_g}{\hbar}+\frac{3\omega_e}{2}-\frac{\omega_g}{2}-\omega_{\mathrm{rf}}.$$

It can be shown that the intensities of the first-order sidebands to the forbidden transition $e,-\frac{3}{2}\rightarrow g,\frac{1}{2}$ are connected to the previous intensities by the relations

$$|\langle g,\tfrac{1}{2}|e,-\tfrac{3}{2}\rangle_{+}^{(2)}|^2=|\langle g,-\tfrac{1}{2}|e,\tfrac{3}{2}\rangle_{-}^{(2)}|^2, \tag{10a}$$

$$|\langle g,\tfrac{1}{2}|e,-\tfrac{3}{2}\rangle_{-}^{(2)}|^2=|\langle g,-\tfrac{1}{2}|e,\tfrac{3}{2}\rangle_{+}^{(2)}|^2, \tag{10b}$$

for all polarizations of the applied radio-frequency field, where the superscript (2) refers to the second-order contribution in the perturbation series.

As was the case with the sidebands of the allowed transitions,[19] the intensity of the sidebands toward higher frequencies of a parent line is in general different from the intensity of the sideband toward lower frequencies of the same parent line. This asymmetry becomes particularly striking in the case of a circular polarization of the radio-frequency field, when not only the parent forbidden line has a zero intensity, but the intensity of one of the sidebands is also equal to zero.

By combining the results of Ref. 19 and the present work, we obtained the intensities of the sidebands toward higher frequencies, labeled by the subscript +, which are shown in Fig. 2 for linear, right circular, and left circular

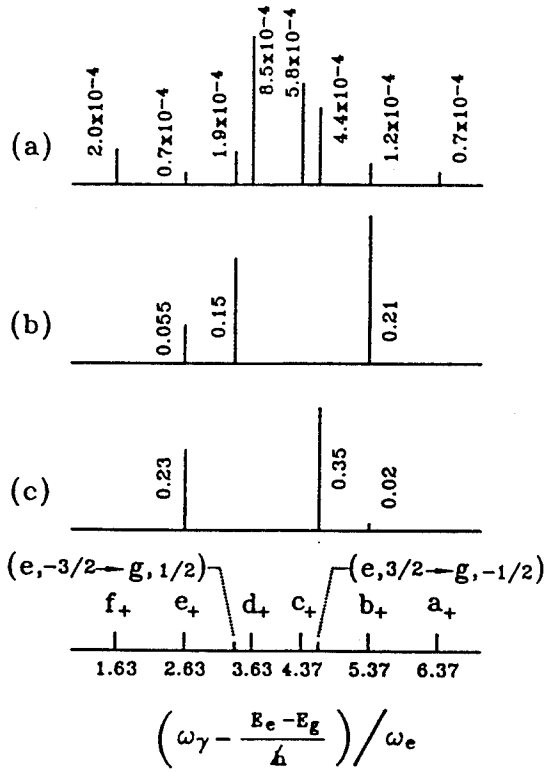


FIG. 2. Intensities of the sidebands toward higher frequencies for the $\gamma$-ray emission spectrum of $^{57}$Fe nuclei under a static magnetic field $B_0^h$ and of an oscillatory magnetic field of frequency $\omega_{\mathrm{rf}}/\omega_e=4$, averaged over the polarization of the $\gamma$ rays for different configurations of the radio-frequency fields. (a) The radio-frequency field is linearly polarized, $B_{\mathrm{rf},x}/B_0^h=\frac{1}{10}$, and the direction of observation is perpendicular to the plane of the applied field, $\theta=\pi/2$, $\varphi=\pi/2$. (b) The radio-frequency field has a right circular polarization, $\alpha_{\mathrm{rf}}=-\pi/2$ and $B_{\mathrm{rf}}/B_0^h=1$. The spectrum is observed along the direction of the static field, $\theta=0$. (c) The radio-frequency field has a left circular polarization, $\alpha_{\mathrm{rf}}=\pi/2$ and $B_{\mathrm{rf}}/B_0^h=1$. The spectrum is observed along the direction of the static field, $\theta=0$.

polarizations of the radio-frequency magnetic field. The intensity of the unperturbed transition $e,\frac{1}{2}\rightarrow g,\frac{1}{2}$, averaged over the polarization of the $\gamma$ rays and observed at the angle $\theta=\pi/2$, was chosen as unity. The remarkable aspect of the pattern in Fig. 2 is the appearance of the supplementary lines which are the sidebands of the forbidden parent transitions. The appearance of these lines in a spectrum is characteristic of the multiphoton generation of the radio-frequency sidebands.

If the $^{57}$Fe nucleus is under the action of a circularly polarized magnetic field but the static field $B_0^h$ is equal to zero, the intensity of the first-order sidebands, at $\omega_\gamma=(E_e-E_g)/\hbar\pm\omega_{\rm rf}$, can be shown to be

$$I_1^{(C)}=\frac{|A|^2B_\gamma^2}{2\hbar^2\Gamma^2}\left[\frac{\mu_eB_{\rm rf}}{J_e\hbar\omega_{\rm rf}}\right]^2[\sin^2\theta\cos^2\upsilon(7+4f+f^2)+(\sin^2\upsilon+\cos^2\theta\cos^2\upsilon)(4+3f+f^2)]\ , \tag{11}$$

where

$$f=-\frac{\mu_gJ_e}{\mu_eJ_g}>0\ .$$

The ratio of the intensity of the first-order sideband to the parent line, at the angle of observation $\theta=0$, is then, for a circular polarization of the radio-frequency field,

$$R_1^{(C)}=\frac{1}{8}\left[\frac{\mu_eB_{\rm rf}}{J_e\hbar\omega_{\rm rf}}\right]^2(4+3f+f^2)\ . \tag{12}$$

The results in Eqs. (11) and (12) differ from the corresponding expressions [Eqs. (32) and (33)] of Ref. 19 by the contribution of the sidebands to the forbidden lines, evaluated in this section.

## III. INTENSITY OF THE SECOND-ORDER SIDEBANDS IN THE CASE OF RADIO-FREQUENCY COLLAPSE FOR $^{57}$Fe

While the second-order perturbation calculations are in general sufficient to describe the generation of radio-frequency sidebands at frequencies of the order of 100 MHz or higher, the third-order contribution to the perturbation series is needed to describe the second-order sidebands which become observable at lower frequencies. In this section we shall determine the intensity of the second-order sidebands for the case of the radio-frequency collapse, when the hyperfine magnetic field acting on the $^{57}$Fe nuclei follows the oscillations of the applied radio-frequency field, so that the static hyperfine field is $B_0^h=0$.

The third-order contribution to the transition amplitude is given by

$$b^{(3)}_{gm;em_0}=\frac{i}{\hbar^3}\sum_k\int_0^\infty F_{gm;l}(t)dt\int_0^t F_{l;k}(\eta)d\eta\int_0^\eta \times\int_0^\eta F_{k;em_0}(\zeta)d\zeta\ . \tag{13}$$

We shall assume, as in the previous section, that the applied radio-frequency field is in the $x,y$ plane and shall evaluate the right-hand side of Eq. (13) for $\gamma$ rays emitted perpendicularly to the $x,y$ plane, so that we shall consider that $\theta=0$, $\varphi=0$.

The nonvanishing matrix elements for the present problem are

$$F_{g,1/2;g,-1/2}(t)=-\frac{\mu_g}{2J_g}Y^*(t)\ , \tag{14a}$$

$$F_{e,-3/2;e,-1/2}(t)=-\frac{\mu_e\sqrt{3}}{2J_e}Y(t)\ , \tag{14b}$$

$$F_{e,-1/2;e,1/2}(t)=-\frac{\mu_e}{J_e}Y(t)\ , \tag{14c}$$

$$F_{e,1/2;e,3/2}(t)=-\frac{\mu_e\sqrt{3}}{2J_e}Y(t)\ , \tag{14d}$$

where $Y(t)$ is the function defined in Eq. (3), and

$$F_{g,-1/2;e,-3/2}(t)=-\frac{\sqrt{6}}{4}AB_\gamma e^{i\phi_\gamma-i\upsilon}e^{i(\omega_\gamma-\omega_0+i\Gamma/2)t}\ , \tag{15a}$$

$$F_{g,-1/2;e,1/2}(t)=\frac{\sqrt{2}}{4}AB_\gamma e^{i\phi_\gamma+i\upsilon}e^{i(\omega_\gamma-\omega_0+i\Gamma/2)t}\ , \tag{15b}$$

$$F_{g,-1/2;e,1/2}(t)=-\frac{\sqrt{2}}{4}AB_\gamma e^{i\phi_\gamma-i\upsilon}e^{i(\omega_\gamma-\omega_0+i\Gamma/2)t}\ , \tag{15c}$$

$$F_{g,-1/2;e,3/2}(t)=\frac{\sqrt{6}}{4}AB_\gamma e^{i\phi_\gamma+i\upsilon}e^{i(\omega_\gamma-\omega_0+i\Gamma/2)t}\ , \tag{15d}$$

where $\omega_0=(E_e-E_g)/\hbar$. Since according to Eqs. (14) and (15) the matrix elements are nonvanishing only for $\Delta m=\pm1$, there is a nonvanishing third-order contribution to the amplitude $b^{(3)}_{gm;em}$ for the 14.4-keV transition only when $|m-m_0|=1$, so that the transitions to be considered are $e,\frac{3}{2}\rightarrow g,\frac{1}{2}$; $e,\frac{1}{2}\rightarrow g,-\frac{1}{2}$; $e,-\frac{1}{2}\rightarrow g,\frac{1}{2}$; and $e,-\frac{3}{2}\rightarrow g,-\frac{1}{2}$. From the symmetry of the matrix elements in Eqs. (14) and (15), it results that it is sufficient to evaluate $b^{(3)}_{g,1/2;e,3/2}$ and $b_{g,-1/2;e,1/2}$ at $\omega_\gamma=\omega_0\pm2\omega_{\rm rf}$. There are four channels contributing to $b^{(3)}_{g,1/2;e,3/2}$, and there are six channels contributing to $b^{(3)}_{g,-1/2;e,1/2}$. Thus we obtain, for the intensity of the second-order sidebands, at $\omega_\gamma=\omega_0\pm2\omega_{\rm rf}$, averaged over the polarization $\upsilon$ of the $\gamma$ rays,

$$I_2=\frac{1}{256}\frac{|A|^2B_\gamma^2}{\hbar^2\Gamma^2}\left[\frac{\mu_e}{J_e\hbar\omega_{\rm rf}}\right]^2[B_1B_1^*B_2B_2^*(19+30f+20f^2+6f^3+f^4)+2[(B_1B_1^*)^2+(B_2B_2^*)^2](3+3f+f^2)]\,, \tag{16}$$

where

$$B_1=B_{{\rm rf},x}+iB_{{\rm rf},y}e^{i\alpha_{\rm rf}}\,, \tag{17a}$$

$$B_2=B_{{\rm rf},x}+iB_{{\rm rf},y}e^{-i\alpha_{\rm rf}}\,. \tag{17b}$$

For a linear polarization of the radio-frequency field, when $B_{{\rm rf},y}=0$, the ratio of the second-order sideband, averaged over $\gamma$-ray polarization, to the unperturbed parent intensity is, for $\omega_\gamma=\omega_0\pm2\omega_{\rm rf}$,

$$R_2^{(L)}=\frac{1}{1024}\left[\frac{\mu_eB_{{\rm rf},x}}{J_e\hbar\omega_{\rm rf}}\right]^4(31+42f+24f^2+6f^3+f^4)\,, \tag{18}$$

where $f=-\mu_gJ_e/\mu_eJ_g$. This expression is equivalent to the result reported previously in Eq. (17) of Ref. 14.

If the radio-frequency field acting on the nucleus can be described as a superposition of two independent orthogonal modes, so that $B_{{\rm rf},x}=B_{{\rm rf},y}=B_{\rm rf}$ and the relative phase $\alpha_{\rm rf}$ is at random, then the ratio of the intensity of the second-order sideband, averaged over $\gamma$-ray polarization, to the parent intensity, is

$$R_2^{(x,y)}=\frac{1}{256}\left[\frac{\mu_eB_{\rm rf}}{J_e\hbar\omega_{\rm rf}}\right]^4(31+42f+24f^2+6f^3+f^4)\,. \tag{19}$$

If the radio-frequency field is circularly polarized, so that $B_{{\rm rf},x}=B_{{\rm rf},y}+B_{\rm rf}$ and $|\alpha_{\rm rf}|=\pi/2$, the ratio of the intensity of the second-order sideband, averaged over the polarization of the $\gamma$ rays, to the unperturbed parent intensity, is

$$R_2^{(C)}=\frac{1}{32}\left[\frac{\mu_eB_{\rm rf}}{J_e\hbar\omega_{\rm rf}}\right]^4(3+3f+f^2)\,. \tag{20}$$

If as a result of the application of an oscillatory magnetic field of frequency $\omega_{\rm rf}$ the hyperfine field assumes alternatively two opposite values $\pm B_s$, the Fourier component of this hyperfine field at the frequency $\omega_{\rm rf}$ will have the enhanced amplitude $(4/\pi)B_s$. The amplitude of the component of the aforementioned hyperfine field at the frequency $2\omega_{\rm rf}$ is equal to zero, but the amplitude of the component at the frequency $3\omega_{\rm rf}$ will be $4B_s/3\pi$ and can produce, at low frequencies, a sizable sideband. These considerations lose their applicability if the passages between the opposing values of the hyperfine field are rounded off.

Combining the results of Ref. 14 and the results of the present work, we have represented in Fig. 3 the emission $\gamma$-ray spectrum with sidebands in the case of radio-frequency collapse for $^{57}$Fe nuclei in a Permalloy sample for a linear polarization of the applied oscillatory magnetic field at several frequencies, assuming that the amplitude of the oscillating hyperfine field is equal to its static value. Moreover, in Fig. 4 we have represented the emission $\gamma$-ray spectrum with sidebands at a fixed frequency for several configurations of the applied radio-frequency field. The intensities in parts (a) and (b) of Fig. 4 are calculated according to the Bessel-function formula of Ref. 14, and the intensities in part (c) and (d) are calculated according to the perturbation expressions of Ref. 14 and the present work. It is apparent from Figs. 3 and 4 that if the hyperfine field follows the applied radio frequency, as it is supposed to be the case for the radio-frequency collapse spectra, the generation of nuclear multiphoton sidebands can be very intense.

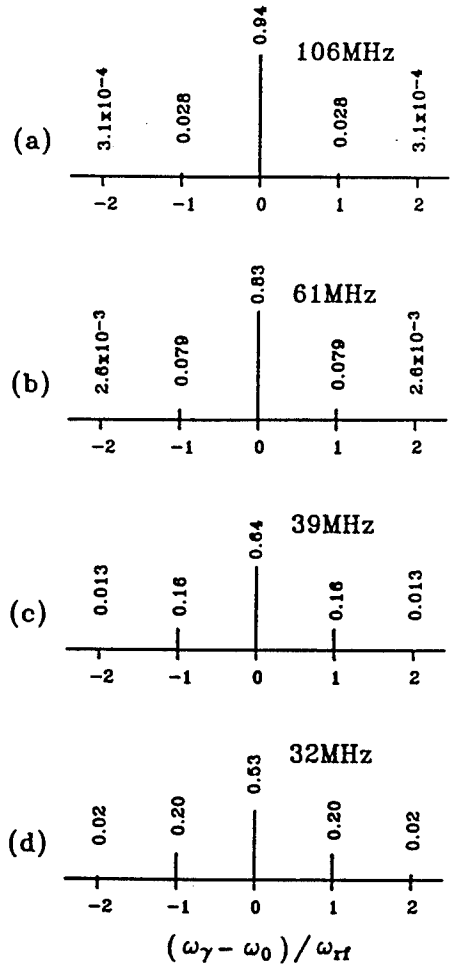


FIG. 3. $\gamma$-ray emission spectrum with sidebands in the case of radio-frequency collapse for $^{57}$Fe nuclei in a Permalloy sample for a linear polarization of the applied magnetic field for several frequencies $\omega_{\rm rf}$ of the oscillatory field. It is assumed that the amplitude of the oscillating hyperfine field is equal to the static hyperfine field. The direction of observation is perpendicular to a plane containing the oscillatory field. These intensities are given by $R^{(N)}=\frac{1}{8}J_N^2[(\omega_g-\omega_e)/2\omega_{\rm rf}]+\frac{1}{2}J_N^2[(\omega_g+\omega_e)/2\omega_{\rm rf}]+\frac{3}{8}J_N^2[(\omega_g+3\omega_e)/2\omega_{\rm rf}]$, where $J_N$ is the Bessel function of order $N$.

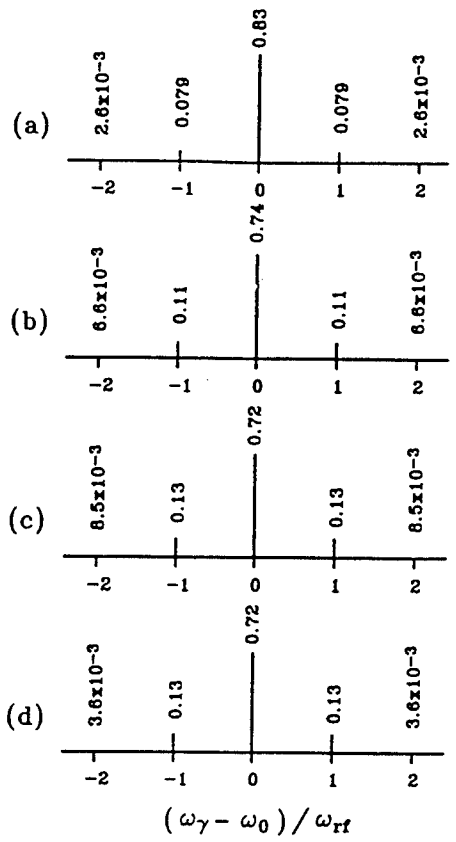


FIG. 4. $\gamma$-ray emission spectrum with sidebands in the case of radio-frequency collapse for $^{57}$Fe nuclei in a Permalloy sample for different configurations of the applied radio-frequency field at the frequency $\omega_{rf}=61$ MHz. (a) The hyperfine oscillatory field is polarized linearly, and its amplitude is equal to the static hyperfine field $B_s$. (b) The hyperfine field is polarized linearly, and its amplitude is $4B_s/\pi$. (c) The hyperfine field is a superposition of two orthogonal components of amplitude $B_s$, uncorrelated in phase. (d) The hyperfine field is polarized circularly, and the rotating amplitude is equal to $B_s$. In all cases the direction of observation is perpendicular to a plane containing the oscillatory field.

## IV. QUANTUM INTERFERENCE EFFECTS IN THE RADIO-FREQUENCY MULTIPHOTON SPECTRA OF $^{57}$Fe

While the intensity of the acoustic sidebands of a given order is a decreasing function of frequency, the intensity of the multiphoton sidebands of a given order, in the presence of static magnetic fields, can *increase* in certain frequency ranges. The increase with frequency of the intensity of the multiphoton transition can arise from the fact that some of the transition amplitudes have resonances when the applied frequency becomes equal to the separation in frequency units between the magnetic sublevels of the ground or excited states, i.e., when a real intermediate state in the nucleus coincides with the position of the virtual multiphoton level.

This pattern is encountered, for example, in the first-order sideband toward lower frequencies of the transition $e,\frac{1}{2}\rightarrow g,\frac{1}{2}$ in the presence of a static magnetic field $B_0^h$ and of a linearly polarized radio-frequency magnetic field. If the emitted $\gamma$ rays are observed along a direction perpendicular to the plane of the applied fields, $\theta=\pi/2$, $\varphi=\pi/2$, then the ratio of the first-order sideband intensity $I_{b,-}^{(L)}$ to the intensity of the unperturbed parent transition $I_b$, both averaged over the $\gamma$-ray polarization becomes[19]

$$\frac{I_{b,-}^{(L)}}{I_b}=\left[\frac{B_{\mathrm{rf},x}}{B_0^h}\right]^2\left[\frac{3}{8}\frac{\omega_e}{\omega_e+\omega_{\mathrm{rf}}}+\frac{1}{4}\frac{\omega_e}{\omega_e-\omega_{\mathrm{rf}}}-\frac{1}{8}\frac{\omega_g}{\omega_g-\omega_{\mathrm{rf}}}\right]^2. \quad (21)$$

The resonances of the relative sideband intensity $I_{b,-}^{(L)}/I_b$, occurring at $\omega_{rf}=\omega_e$ and $\omega_{rf}=\omega_g$, are shown in Fig. 5 for $^{57}$Fe nuclei in iron.

Another circumstance which can lead to an increase with frequency of the intensity of the sidebands is the cancellation for certain frequencies of the partial amplitudes contributing to the total transition amplitude. This pattern is encountered, for example, in the first-order sidebands toward lower frequencies of the transition $e,\frac{1}{2}\rightarrow g,\frac{1}{2}$ in the presence of a static magnetic field $B_0^h$ and of a left circularly polarized radio-frequency field of rotating amplitude $B_{rf}$. The ratio of the first-order sideband intensity $I_{b,-}^{(CL)}$ to the intensity $I_a$ of the unperturbed transition $e,\frac{3}{2}\rightarrow g,\frac{1}{2}$ is[19]

$$\frac{I_{b,-}^{(CL)}}{I_a}=\frac{1}{12}\left[\frac{B_{\mathrm{rf}}}{B_0^h}\right]^2\left[\frac{3\omega_e}{\omega_{\mathrm{rf}}+\omega_e}-\frac{\omega_g}{\omega_g-\omega_{\mathrm{rf}}}\right]^2, \quad (22)$$

for all $\gamma$-ray polarizations and directions of observation. The zero in the relative sideband intensity $I_{b,-}^{(CL)}/I_a$, occurring at $\omega_{rf}=2\omega_e\omega_g/(3\omega_e+\omega_g)$, can be seen in Fig. 6 for $^{57}$Fe nuclei in an iron environment, when the zero occurs at $\omega_{rf}=19.1$ MHz, assuming that $B_{rf}$ is small compared to $B_0^h$.

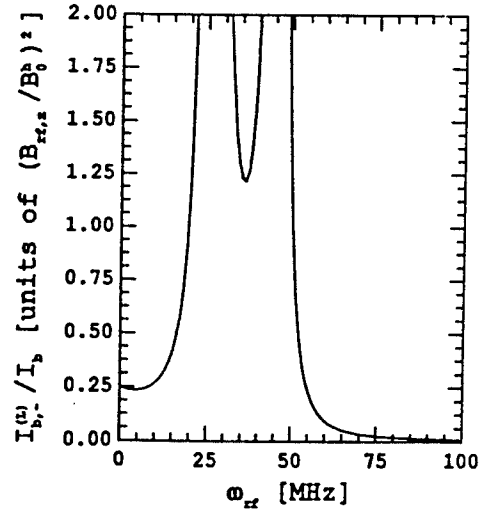


FIG. 5. Relative first-order sideband intensity $I_{b,-}^{(L)}/I_b$ for a static magnetic field $B_0^h$ and a linearly polarized magnetic field of amplitude $B_{\mathrm{rf},x}$ for $^{57}$Fe nuclei in iron. The relative intensity $I_{b,-}^{(L)}/I_b$ has resonances at $\omega_{rf}=\omega_e$, $\omega_{rf}=\omega_g$. The direction of observation is perpendicular to the plane of the applied field. The $\gamma$-ray intensities are averaged over the polarization.

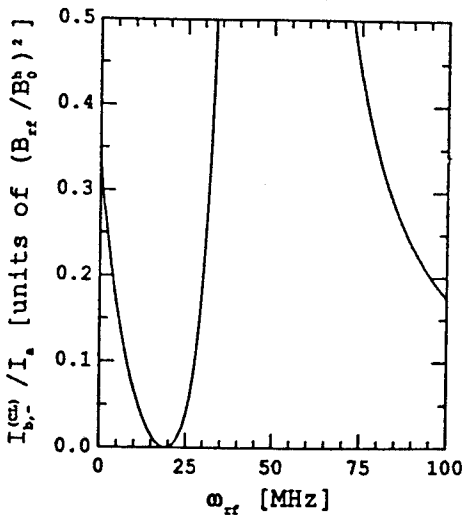


FIG. 6. Relative first-order sideband intensity $I_{b,-}^{(CL)}/I_a$ for a static magnetic field $B_0^h$ and a left circularly polarized radio-frequency field $B_{rf}$ for $^{57}$Fe nuclei in iron. The relative intensity $I_{b,-}^{(CL)}/I_a$ has a zero when $\omega_{rf}=2\omega_e\omega_g/(3\omega_e+\omega_b)$ or $\omega_{rf}=19.1$ MHz. $B_{rf}$ is assumed to be small compared to $B_0^h$.

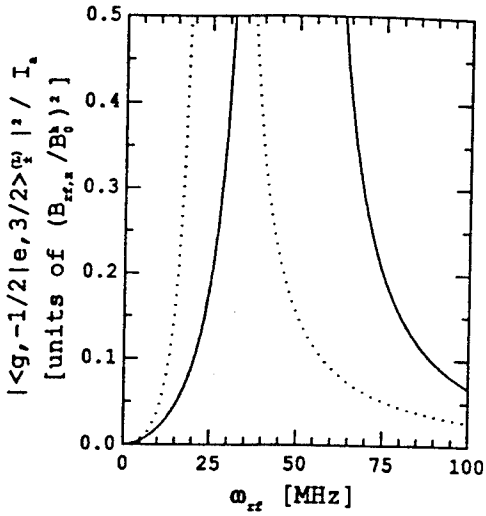


FIG. 7. Relative first-order sideband intensities $|\langle g,-\frac{1}{2}|e,\frac{3}{2}\rangle_+^{(L)}|^2/I_a$ (solid line) and $|\langle g,-\frac{1}{2}|e,\frac{3}{2}\rangle_-^{(L)}|^2/I_a$ (dotted line) for a static magnetic field $B_0^h$ and a linearly polarized radio-frequency field $B_{rf,x}$ for $^{57}$Fe nuclei in iron. The intensities of these sidebands are equal to zero for $\omega_{rf}=0$.

An interesting example of the cancellation of amplitudes is encountered for the first-order sidebands of the forbidden $\gamma$-ray transition $e,\frac{3}{2}\rightarrow g,\frac{1}{2}$. In this case the cancellation of amplitudes occurs at $\omega_{rf}=0$, so that the intensity of the first-order sidebands at $\omega_{rf}=0$ is, according to Eqs. (7)–(9), equal to zero for all polarizations of the applied radio-frequency field, while on the other hand the generation of acoustic sidebands is supposed to increase in intensity at lower frequencies. For example, the ratio of the first-order sideband intensity $|\langle g,-\frac{1}{2}|e,\frac{3}{2}\rangle_\pm^{(L)}|^2$ to the intensity $I_a$ of the unperturbed transition $e,\frac{3}{2}\rightarrow g,\frac{1}{2}$, in the presence of a static magnetic field $B_0^h$ and for a linear polarization of the ratio-frequency field, is, according to Eq. (7),

$$\frac{|\langle g,-\frac{1}{2}|e,\frac{3}{2}\rangle_\pm^{(L)}|^2}{I_a} = \frac{1}{16}\left[\frac{B_{rf,x}}{B_0^h}\right]^2\left[\frac{\omega_e}{\pm\omega_{rf}+\omega_e}+\frac{\omega_g}{\pm\omega_{rf}-\omega_g}\right]^2, \quad (23)$$

for all $\gamma$-ray polarization and directions of observation. The intensity of these sidebands are represented in Fig. 7 for $^{57}$Fe nuclei in iron.

## V. CONCLUSIONS

In this paper we have demonstrated a number of asymmetries characteristic of the nuclear multiphoton generation of radio-frequency sidebands to $\gamma$-ray transitions in $^{57}$Fe nuclei. We have pointed out that there are sidebands of observable intensity to the forbidden 14.4-keV $\gamma$-ray transitions $e,\frac{3}{2}\rightarrow g,-\frac{1}{2}$ and $e,-\frac{3}{2}\rightarrow g,\frac{1}{2}$, and have calculated the intensities of the first-order sidebands for a linear and a circular polarization of the applied radio-frequency field. Then we have determined the intensity of the second-order sidebands in the case of the radio-frequency collapse and have evaluated the sideband intensities for a number of configurations of the applied magnetic field. Finally, we have remarked that, unlike the decreasing patterns of the intensity of the acoustic sidebands, the intensity of the nuclear multiphoton sidebands can increase with frequency over certain frequency ranges, this being a consequence of the resonances extant in the multiphoton transition amplitudes and also of the cancellation for certain frequencies of the interfering amplitudes.

*Permanent address: Str. Fizicienilor nr 2, bloc M6, apt. 5, 76900 Bucharest/Magurele, Romania.

[1]P. J. West and E. Matthias, Z. Phys. A **288**, 369 (1978).
[2]E. Ikonen, P. Helistõ, J. Hietaniemi, and T. Katila, Phys. Rev. Lett. **60**, 643 (1988).
[3]E. Ikonen, J. Hietaniemi, and T. Katila, Phys. Rev. B **38**, 6380 (1988).
[4]E. Ikonen, J. Hietaniemi, T. Katila, J. Lindén, and I. Tittonen, Hyperfine Interac. **47**, 139 (1989).
[5]N. D. Heiman, J. C. Walker, and L. Pfeiffer, Phys. Rev. **184**, 281 (1969).
[6]N. D. Heiman, J. C. Walker, and L. Pfeiffer, in *Mössbauer Effect Methodology*, edited by I. J. Gruverman (Plenum, New York, 1971), Vol. 6, p. 123.
[7]H. Gabriel, Phys. Rev. **184**, 359 (1969).
[8]Heiman, Walker, and Pfeiffer, in Ref. 6, p. 133.

[9]N. D. Heiman, L. Pfeiffer, and J. C. Walker, Phys. Rev. Lett. **21**, 93 (1968).
[10]G. Asti, G. Albanese, and C. Bucci, Nuovo Cimento B **57**, 531 (1968).
[11]G. Asti, G. Albanese, and C. Bucci, Phys. Rev. **184**, 260 (1969).
[12]L. Pfeiffer, J. Appl. Phys. **42**, 1725 (1971).
[13]L. Pfeiffer, in *Mössbauer Effect Methodology,* edited by I. J. Gruverman (Plenum, New York, 1971), Vol. 7, p. 263.
[14]S. Olariu, I. I. Popescu, and C. B. Collins, Phys. Rev. C **23**, 1007 (1981).
[15]M. Kopcewicz, H. G. Wagner, and U. Gonser, J. Magn. Magn. Mater. **40**, 139 (1983).
[16]M. Kopcewicz, H. G. Wagner, and U. Gonser, J. Magn. Magn. Mater. **51**, 225 (1985).
[17]M. Kopcewicz, H. Engelmann, S. Stenger, G. V. Smirnov, U. Gonser, and H.-G. Wagner, Appl. Phys. A **44**, 131 (1987).
[18]M. Kopcewicz, M. El Zayat, and U. Gonser, Hyperfine Interact. **42**, 1123 (1988).
[19]S. Olariu, Phys. Rev. B **37**, 7698 (1988).
[20]T. W. Sinor, P. W. Reittinger, and C. B. Collins, Phys. Rev. Lett. **62**, 2547 (1989).
[21]M. N. Hack and M. Hamermesh, Nuovo Cimento **19**, 546 (1961).
[22]F. G. Vagizov, Hyperfine Interact. **61**, 1359 (1990).
[23]I. Tittonen, M. Lippmaa, E. Ikonen, J. Linden, and T. Katila, Phys. Rev. Lett. **69**, 2815 (1992).
[24]S. E. Harris, Phys. Rev. Lett. **62**, 1033 (1989).
[25]O. Kocharovskaya, P. Mandel, and Y. V. Radeonychev, Phys. Rev. A **45**, 1997 (1992).
[26]M. O. Scully, Phys. Rev. Lett. **67**, 1855 (1991).
[27]J. E. Field, K. H. Hahn, and S. E. Harris, Phys. Rev. Lett. **67**, 3062 (1991).
[28]S. E. Harris, Phys. Rev. Lett. **70**, 552 (1993).
[29]S. Olariu, T. W. Sinor, and C. B. Collins, Phys. Rev. B **50**, 616 (1994).
[30]A. V. Mitin, Zh. Eksp. Teor. Fiz. **52**, 1596 (1967) [Sov. Phys. JETP **25**, 1062 (1967)].

# PROGRESS IN THE PUMPING OF A GAMMA-RAY LASER

C. B. Collins and J. J. Carroll
The University of Texas at Dallas, Center for Quantum Electronics
P. O. Box 830688, Richardson, Texas 75083-0688

A gamma-ray laser would provide stimulated emission at the shortest possible wavelengths (< 1 Å) from transitions between excited nuclear states. Even if the output beam was poorly collimated, simply the ability to release the large amounts of energy stored in nuclei without a nuclear reaction could have important consequences. Nuclear transitions hold unique advantages that promise the integration of pump energy over ns to μs times, rather than ps as is the case with x-ray lasers. First suggested in 1961, the interdisciplinary nature of the problem frustrated early efforts and by 1980 it was concluded that a gamma-ray laser was impossible using the traditional approach. Since 1982 research has been revitalized by the introduction of new ideas which may make such a device possible. Among those, the concept of "optical" pumping, in its most straightforward form as a nuclear analog to the ruby laser, has provided the most sustained and positive results. Now experimentally measured data show that a gamma-ray laser is feasible if some isotope has its properties sufficiently close to the ideal. Breakthroughs in optical pumping of nuclei will be discussed here along with systematics for the first-ranked candidate. With this material it may be possible to realize the triggered release of MeV/nucleus as induced gamma radiation, and perhaps a gamma-ray laser.

## INTRODUCTION

The original proposal for a gamma-ray laser was made in 1961 [1] although it went largely unnoticed at the time. In 1963 the first cycle of research on this topic developed a strong momentum as a result of independent early publications from the US and Russia. In that cycle attention was primarily concentrated on suddenly assembling a critical density of prepumped nuclei to reach the threshold for stimulated emission and on pumping *in situ* with intense particle fluxes. By 1980 it was generally accepted that such "traditional" approaches were essentially hopeless and an encyclopedic review [2] concluded the impossibility of a gamma-ray laser based upon all techniques for pumping known at that time. However, the precursors of a new interdisciplinary concept were just appearing [3-6]. Based upon nuclear analogs of quantum electronics, the "optical" approach developed rapidly, launching a renaissance in the field. By 1982 the basic theory [7] of upconversion at the nuclear level was in place. Either multiphoton processes (coherent pumping) or multiple electromagnetic transitions (incoherent pumping) would be used to release the energy stored in nuclear isomers. This would avoid many of the difficulties encountered with the traditional schemes.

One blueprint for an optically-pumped gamma-ray laser now appears in the textbooks [8] and in 1986 substantial effort was initiated toward the demonstration of its feasibility. Generally, there are three separate problems to be solved: pumping a nuclear population to a laser level, coupling the output coherently to the radiation field, and managing the thermal load to the host material. The greatest effort by the main line of research has been made towards the first and third aspects. Host preservation has been largely solved by developments in creating thin Diamond films into which Mössbauer isotopes can be implanted [9]. However, the major breakthroughs have been realized in optically pumping nuclei. That work will be reviewed here and has provided the most sustained and positive results, including the experimental demonstration that the energy stored in populations of nuclear isomers can be pumped by x rays into freely-radiating levels. Also, the transition strengths for optically pumping isomers are concentrated into a few levels that provide bandwidth funneling with "giant" integrated cross sections. Those results significantly increase the feasibility of a gamma-ray laser by showing how to induce gamma emission with the potential for upconversion [10]. Excellent concepts have been introduced for the development of coherent output from the levels being pumped, together with other concepts which may significantly reduce threshold requirements, and are discussed elsewhere.

At first it would seem that the prospects for all ultrashort-wavelength lasers would be vitiated by the same fundamental factor [2] that inhibits the production of large output powers from x-ray lasers. The $\nu^3$ dependence of transition probabilities so limits the storage of pump energies in atoms and molecules that even at soft x-ray energies, a threshold population must be excited in exceeding short times. However, nuclear electromagnetic transitions offer three unique advantages:

1) The constant linking $\nu^3$ with lifetime is more favorable by orders-of-magnitude because of the accessibility of a variety of transition moments, and magnetic dipole and electric quadrupole transitions are common. Pumping can integrate a population in an upper laser level to larger values over longer times.

2) Nuclear metastables (isomers) store keV - MeV for lifetimes up to years. Pumping a gamma-ray laser would not require that all the energy be input *in situ*. Metastables can also be concentrated to solid densities.

3) Nuclear transitions need not experience thermal broadening and natural linewidths are routinely obtained with the Mössbauer effect. Unbroadened stimulated emission cross sections are large and values for 1 Å transitions typically exceed that of Nd in YAG.

In the optical pumping approach, a gamma-ray laser isotope implanted into a thin, low-Z medium would resonantly absorb useful pump power over short distances to produce high concentrations of nuclei excited into a lasing level. Wasted wavelengths would only be degraded to heat in much larger volumes. This avoids severe thermal damage to the host that would destroy the Mössbauer effect as with particle pumping. In the blueprint of 1982 [7], the nuclear analog of the ruby laser embodied the simplest concepts for a gamma-ray laser, although the prospects for upconversion using isomers as storage levels is even more attractive. Not surprisingly, the greatest rate of achievement in the last decade in the pumping of high-energy density media has been realized in this direction. For the ruby laser, the identification of a bandwidth funnel was the critical element. A broad absorption band was linked through efficient cascading to the narrow laser level. The blueprint called for a nuclear analog of this structure, unknown in 1982 but now confirmed experimentally.

## PUMP MODEL AND VALIDATION

The scheme for pumping a nuclear lasing level, perhaps by triggering the release of the energy stored in an isomeric state, is shown in Fig. 1. The initial level may be the ground state or an isomer from which population is transferred by absorption by a broad pump band, or "gateway" state. A branch of the normal decay from the gateway leads to the upper laser level, accompanied by prompt gamma emission

Optical pumping using x rays as in Fig. 1 has been known in nuclear physics for over 50 years [11]. However, relatively few results were published until the last decade, primarily due to practical difficulties calibrating intense x-ray sources. Recent developments in technology have provided improved calibration procedures, both experimental [12] and computational [13], and investigations using bremsstrahlung now approach the precision long enjoyed with particle beams [14]. The excitation process shown in Fig. 1 is classified as an inelastic scattering, or $(\gamma,\gamma')$ reaction in the literature of nuclear physics. The notation is $X(\gamma,\gamma')X^*$ where X is the target nucleus and $X^*$ is the same nucleus in its final state.

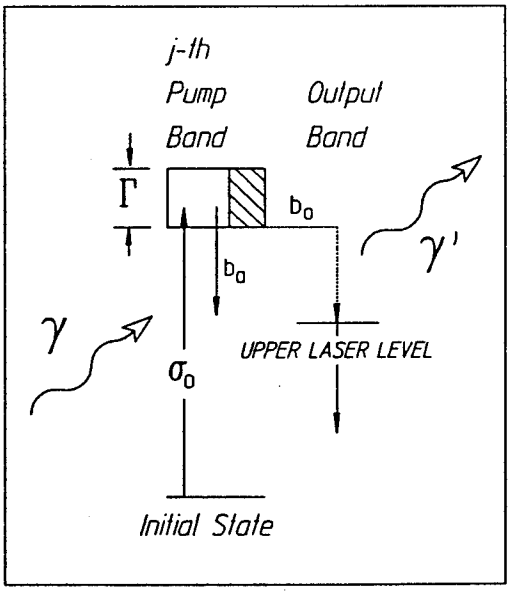


Figure 1: Schematic representing a bandwidth funnel for population of a laser level through a gateway state with natural width, Γ. The incident photon γ is absorbed with a cross section $\sigma_0$ from the initial level. The cascade from gateway to laser level is shown by the dotted line with promptly emitted photons being the γ'. Only one gateway is shown but there could be more.

For a sample that is optically thin at the pump wavelength, the number of nuclei pumped by a $(\gamma,\gamma')$ reaction into a given final is straightforward [7,15]. Bremsstrahlung provides a continuum of x rays, so the irradiation of $N_i$ target nuclei in the initial state results in a time-integrated yield of final-state nuclei, $N_f$ according to

$$N_f = N_i \Phi_0 \int_0^{E_0} \sigma(E)\, F(E,E_0)\, dE \quad , \qquad (1)$$

where the reaction is described by the energy-dependent cross section, $\sigma(E)$. The x-ray continuum is characterized by its endpoint, $E_0$ and the time-integrated spectral intensity, written as a product of the total flux, $\Phi_0$ and the distribution of intensities, $F(E,E_0)$. The distribution is normalized to give unity when integrated over the full spectrum of energies. At incident photon energies below the threshold for neutron evaporation at about 6 - 8 MeV, $(\gamma,\gamma')$ reactions predominantly excite discrete levels through resonant absorption; for the population or depopulation of isomers, the absorbing level of interest is a gateway like that shown in Fig. 1. Only one gateway appears there, but there could be more with each mediating level, identified by the index j, being excited at a different energy, $E_j$. Each gateway branches to some extent into the same fluorescent final state, f. The x-ray continuum is structureless on

the scale over which σ(E) varies for the j-th gateway, even when the level width would be considered broad for a nuclear state. Thus, the final-state yield is given by

$$A_f(E_0) \equiv \frac{N_f}{N_i \Phi_0} = \sum_j (\sigma\Gamma)_{fj} F(E_j, E_0) \quad , \tag{2}$$

where the activation, $A_f(E_0)$ has been introduced. This quantity gives the fractional yield of the final state per unit photon flux, so values of $A_f(E_0)$ may appear small in magnitude even for an efficient pumping reaction since the vast majority of photons are outside the absorption bandwidth. The summation in Eq. (2) includes all gateways with $E_j \le E_0$. The figure of merit for photo-pumping reactions excited with continua is the quantity $(\sigma\Gamma)_{fj}$, the cross section of the j-th gateway integrated over its Lorentzian lineshape. Whether the initial level is an isomer or the ground state, the integrated cross section therefore reflects the efficacy for the transfer of population to a fluorescence level, and therefore available to an output transition. Thus, it is the nuclear equivalent of the fluorescence efficiency so important in the early development of atomic and molecular lasers. The magnitude of integrated cross section for a fully allowed single-particle transition in nuclei is typically 1 - 10 uu., where uu. = $10^{-29}$ cm$^2$ keV = 0.1 eV b. It is straightforward to show that in terms of more fundamental parameters,

$$(\sigma\Gamma)_{fj} = (\pi\sigma_0 b_a b_o \Gamma / 2)_{fj} \quad , \tag{3}$$

where $b_a$ and $b_o$ are the branching ratios for decay from the j-th gateway of natural width Γ back into the initial state or by cascade to the output level, respectively. The quantity $\sigma_0$ is the Breit-Wigner cross section [11] for the absorption transition and is proportional to the squared wavelength of the incident photon having energy $E_j$.

The model of Eqs. (1) - (3) was confirmed in extensive experiments performed using six different accelerators. These included two nuclear simulators, DNA/PITHON and DNA/Aurora, two medical linacs and two research linacs, the injector to the superconducting Darmstadt linear accelerator (S-DALINAC) and the Texas X at the Center for Quantum Electronics. Standard techniques of gamma spectroscopy were used to determine the yield of isomers produced in irradiations of gram-sized samples containing the few calibration isomers whose gateway structures were well-known from the literature. Bremsstrahlung spectra were calculated with the EGS4 electron/photon transport code, common for medical applications, and the spectra were verified by in-line dosimetry. The results of those experiments [16-20] were in excellent agreement with the predictions of Eqs. (1) - (3) using literature values for gateway energies and integrated cross sections. A typical example is given in Fig. 2 which shows a composite excitation function [10] obtained for the calibration isomer $^{87}Sr^m$. It is important to note that at an endpoint of 4 MeV, the yield of the $^{87}Sr^m$ isomer was enhanced 16 orders-of-magnitude by bandwidth funneling over that which could have been produced by direct excitation of the metastable level from the ground state.

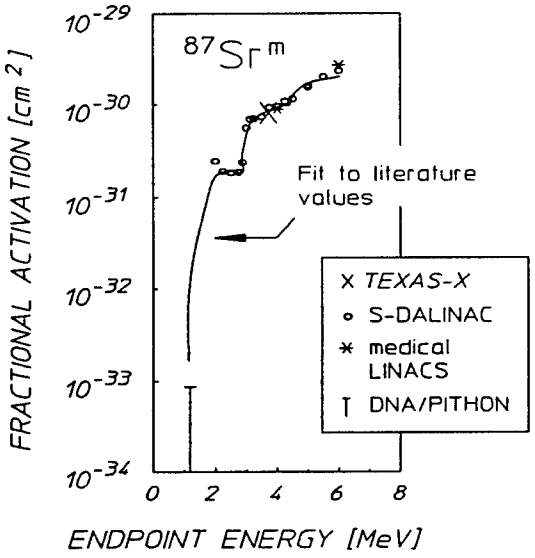


Figure 2: Excitation function showing measured fractional activation, $A_f$ for the reaction $^{87}Sr(\gamma,\gamma')^{87}Sr^m$ as a function of bremsstrahlung endpoint, $E_0$. The solid curve plots values computed from Eq. (3) using gateway parameters found in the literature and calculated photon spectra.

## PUMPING BREAKTHROUGHS

Of the 1886 distinguishable nuclear isotopes, 29 first-class candidate nuclides were identified in 1986 by a search of the nuclear data base, but an exact ranking could not be determined due to the paucity of nuclear fluorescence data. The most attractive candidates for a gamma-ray laser have long-lived isomers that store large amounts of energy for convenient times. Also, it is desirable that they possess freely-radiating transitions whose energies are consistent with large recoil-free-fractions, and whose lifetimes are comparable to the typical output durations of pulsed-power devices which could be used for pumping. A critical issue is that the pump step must utilize the smallest possible trigger photon. Thus, isotopes providing the greatest

potential for storage of energy input *ex situ* are the most attractive. The majority of such candidates are deformed nuclei for which the quantum, K must be introduced in addition to the total angular momentum, J. This new quantum is the projection of J on the nuclear body axis and rotation of the spheroidal shape about a perpendicular axis gives rise to a band structure resembling that of a diatomic molecule. For deformed nuclei, electromagnetic transitions are governed by selection rules for the change of both J and K according to $|\Delta J| \leq M$ and $|\Delta K| \leq M$, where M is the multipolarity of the radiation. The longest-lived isomeric levels arise because they lie in bands whose K differs greatly from those containing freely-radiating states to which their decay would otherwise be allowed by energetics and the J selection rule. "K isomers" are therefore ideal as storage levels for upconversion schemes since most of the energy is already in the nucleus.

The longest-lived K isomer is possessed by the nuclide $^{180}$Ta, but this was nevertheless ranked among the poorest candidates. It stores only 75 keV/nucleus and requires $\Delta K = 8$ for transitions to freely-radiating levels in the ground-state band [21]. A bandwidth funnel would have to span a comparable $\Delta K$ and so theoretical estimates of the integrated cross section for the pumping were expected to be as small as $10^{-15}$ uu. Still, this isotope exists naturally in 100 % inversion since its isomer has a lifetime in excess of $10^{12}$ years while its ground state has a halflife against transmutation of only 8.1 hours. A macroscopic sample was readily available so $^{180}$Ta$^m$ was the first candidate tested. In an experiment conducted [22] in 1987, an enriched sample containing 1.2 mg of $^{180}$Ta$^m$ was irradiated with bremsstrahlung from a 6-MeV medical linac and a large fluorescence yield was observed following the exposure. For the first time this demonstrated experimentally that the energy stored in an isomer could be dumped to freely-radiating states by a trigger photon. Simply the observation of any fluorescence from a milligram-sized target showed an unexpected efficiency for the process because grams of material were needed for the calibration isotopes. In fact, the fluorescence yield was so large that measurements were subsequently performed [20] with samples containing the isotope $^{180}$Ta in its natural abundance of 0.012 %. Analysis of the data indicated that the partial width, $b_a b_o \Gamma$ for dumping the $^{180}$Ta$^m$ population was nearly 0.5 eV, with a corresponding integrated cross section of 42,000 uu. This reflects a windfall of $10^4$ over a typical single-particle transition and $10^{19}$ compared to the theoretical pessimism.

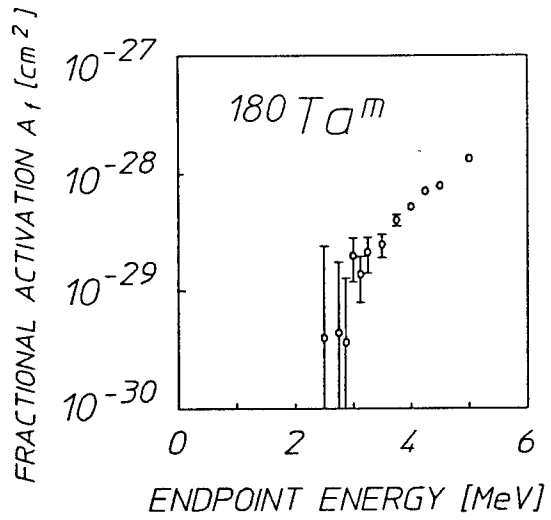


Figure 3: Excitation function showing fractional activation, $A_f$ for the reaction $^{180}$Ta$^m(\gamma,\gamma')^{180}$Ta as a function of bremsstrahlung endpoint, $E_0$. These data demonstrate the dumping of an isomeric population to freely-radiating states with trigger x rays.

The experiment [22] of 1987 could not determine the number, excitation energies and integrated cross sections of individual gateways since the endpoint of the medical linac was fixed. To investigate this, further experiments [20] were performed with the variable-energy S-DALINAC. The measured excitation function showing the ground-state yield produced by dumping the $^{180}$Ta isomer is shown in Fig. 3. As was seen for the calibration isomer $^{87}$Sr$^m$, sharp increases in $A_f(E_0)$ indicated the energies of the gateways, with the lowest, and most important, at $2.8 \pm 0.1$ MeV above the isomer. An iterative fit to the data was combined with computed photon spectra to determine an integrated cross section of 12,000 uu. for the bandwidth funnel through that gateway. This exceptional value led to the gateway's classification as a "giant" pumping resonance in comparison to usual $(\gamma,\gamma')$ reactions. The demonstration that populations of nuclear isomers can be dumped by x rays with such large integrated cross sections stands as the first major breakthrough in the optical pumping of gamma-ray laser media.

A survey of 19 isotopes [23] conducted over a fairly coarse mesh of bremsstrahlung endpoints confirmed the existence of giant pumping resonances for the photoexcitation of isomers in the region of masses near A = 180. A summary of the results is shown in Fig. 4. Excitation functions measured [24] using the S-DALINAC determined the gateway energies for several isomers in the mass region containing $^{180}$Ta and those $E_j$ are also shown in the figure. Another study showed [25] that the giant pumping resonances reappeared at lower masses near 120. It is the close correlation of gateway strengths and locations for nuclei with dissimilar single-particle structures that identified the giant pumping resonances as a property of the nuclear core. In fact, the strengths of giant pumping resonances were shown experimentally to be correlated [24] with the ground-state deformation. The systematics for optically pumping nuclear states were further investigated for the excitation of laser-like levels with lifetimes on the order of tens of μs. The data analysis [26] for four nuclides tested indicated that the integrated cross sections were comparable in magnitude to those previously found for the population of long-lived isomers. Whatever the mechanism, the experimental fact remains that bandwidth funneling that connects isomers to freely-

radiating levels can be almost commonly found throughout the mass-180 region. The partial widths for the transfer of population are enormous, 0.5 eV, even when the change of angular momentum projection must be as great as $\Delta K = 8$. This is the nuclear analog of the giant resonance for pumping ruby at the atomic level.

Due to the exceedingly favorable appearance of giant pumping resonances, the possibility of the results containing spurious contributions from reactions other than $(\gamma,\gamma')$ events was carefully considered. For example, experiments [10,27] were conducted using standard activation techniques to determine the flux of thermal, epithermal and fast neutrons which could have produced additional isomeric yields through $(n,\gamma)$ or $(n,n')$ reactions. In most accelerator environments, those fluxes were found to be below the level of detectability and even when measurable fluxes were present, their magnitudes were sufficient to produce less than 0.01 % typically and 6 % in the worst case of the measured isomeric yield.

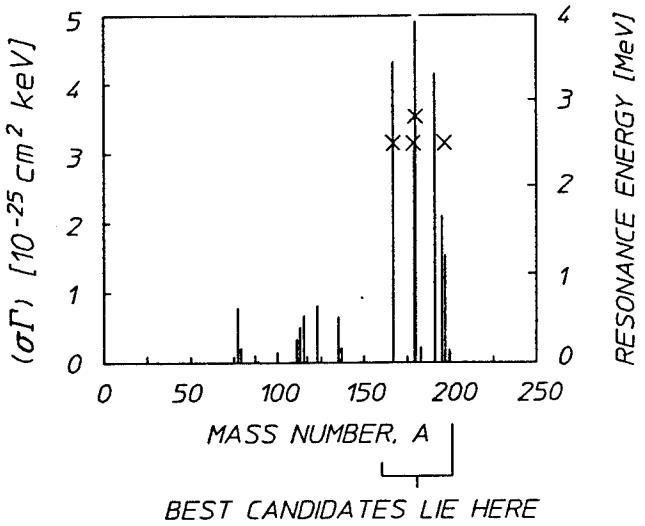


Figure 4: Systematics for excitation energies and integrated cross sections of gateway states providing bandwidth funneling for optical pumping of nuclear isomers. The groupings correspond to mass islands between magic numbers for neutrons and protons. Generally, the best candidates lie in the mass-180 island, also where the largest values of $(\sigma\Gamma)_j$ are found.

The surprisingly large integrated cross sections for getaways in the mass-180 region indicate an ease in pumping and dumping isomers through large $\Delta K$ that is difficult to interpret in terms of a single-particle model. Evidence of levels capable of strong "K breaking" or "K mixing" have also been recently observed for other nuclei [28]. Most striking are the measurements [29] of a level at 2.65 MeV which provides $\Delta K = 14$ in the spontaneous decay of the 3.312-MeV, 3.7-μs isomer of $^{174}$Hf. That K-mixing state is remarkably close to the gateway at $2.8 \pm 0.1$ MeV discovered for the dumping of $^{180}$Ta$^m$. A full understanding of this pervasive behavior is not yet available, but there are suggestive speculations. Calculations [30] have confirmed that some nuclides develop multiple minima in nuclear potential as a function of core deformation. Second minima can contain fission isomers for higher masses, but for lighter nuclei the Coulomb barrier prevents fission. Shape isomers result when states bound within a second well cannot easily decay to freely-radiating states of significantly different nuclear shape within the primary well. If instead of a second minimum a plateau occurs in the potential energy, shape isomers could not occur. However, within a narrow band of energies excited states would not correspond to a fixed core deformation. For such levels K would not be a good quantum number and unhindered, low-multipolarity transitions could connect them to states with widely differing K values. It has also been suggested [29] that tunneling through the potential barrier between minima may provide the observed violation of the usual K selection rule.

## CANDIDATE RANKING

An exact ranking of the 29 candidate isomers for a gamma-ray laser depends upon a complex weighting of nuclear parameters, many of which are poorly known. However, the potential importance of several nuclides is magnified by some very pragmatic considerations. From the perspective of shelf life and availability, $^{180}$Ta$^m$ is far superior. It is a naturally occurring material and can be prepared simply by separating natural Ta by atomic mass. Samples of milligram weight exist and one such specimen was used in the breakthrough experiment that proved x rays can dump the energy stored in isomeric populations. In contrast, the entire world inventory of the isomer $^{178}$Hf$^{m2}$ was reported in 1992 to be about $10^{15}$ nuclei [31] although recently this amount has been increased to about $5 \times 10^{16}$. However, from the perspective of triggering energetics $^{180}$Ta$^m$ is poor. Although the energy storage is still impressively high, 2.8 MeV is needed to excite the K-breaking gateway. For $^{178}$Hf$^{m2}$ the energy of the isomer at 2.45 MeV is the highest known that still lies below the likely gateway energy between 2.5 - 3.0 MeV [32]. The isomer $^{174}$Hf$^m$ is even higher at 3.312 MeV, but that level spontaneously decays [29] through a K-mixing state at 2.685 MeV so its halflife is only 3.7 μs. Ideally, for ease of triggering an isomer would store as much energy as possible without exceeding that of the K-breaking level for that nuclide. As long as the transition energy needed for triggering is positive, the isomer cannot dump spontaneously as happens with $^{174}$Hf$^m$. The lifetime of the initial population will then be long and problems of storage will be minimized. Guided to $^{178}$Hf$^{m2}$ by energetics, a reasonable next concern from the pragmatic viewpoint is for the duration of the trigger pulse.

Even in the best scenarios the requirement for the energy in a trigger pulse is large. The problem is compounded if the fluorescence lifetime of the level into which the isomeric population is to be dumped is too short. Large pulsed-power devices typically deliver their outputs over durations of ns to μs, so it would be desirable to utilize a laser candidate with strong fluorescence lines of comparable lifetimes. In this case as well, the $^{178}Hf^{m2}$ is favorable since it has transitions with lifetimes of both tens of ns and tens of μs. Thus, the first priority candidate for a gamma-ray laser is the 31-year isomer of $^{178}Hf$, superior to the next possibilities by orders-of-magnitude. The energy-level diagram [18] for $^{178}Hf$ is shown in Fig. 5 with prominent fluorescent transitions indicated. The fundamental question is whether the giant pumping resonance will be found at the level shown in the figure that is predicted by systematics. In case of a weak success in K-breaking, pumping would preferentially populate the band to the right of the figure. This would lead to fluorescence at 437 keV with 35% efficiency from the bandhead having a 68-μs lifetime. Detection of that fluorescence is well within current experimental capabilities [26].

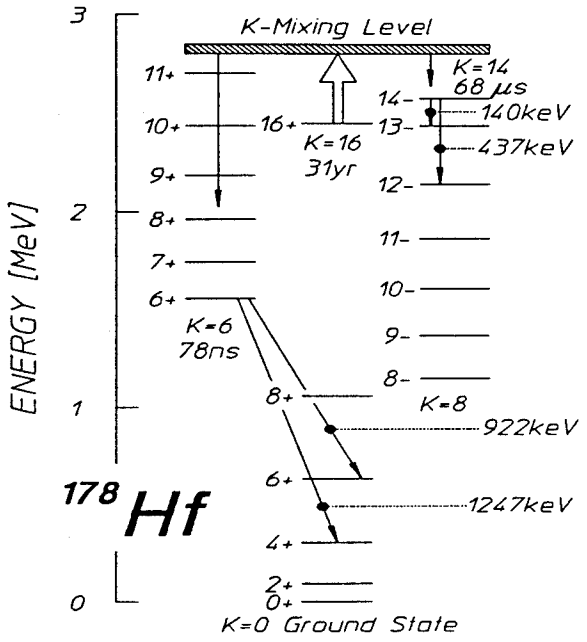


Figure 5: Energy level diagram of the nuclide $^{178}Hf$. The 31-year isomer stores 2.45 MeV/nucleus and forms the K = 16 bandhead. Natural decay of the isomer proceeds to the K = 8, requiring ΔK = 8, and then to the ground-state band. This cannot excite either the higher-lying K = 14 bandhead or members of the K = 6 band on the left-hand side. A K-mixing gateway level inferred from systematics is shown near 2.8 MeV and could populate laser-like states within those bands.

In the event of a strong success in which K-breaking is complete, the left-side band would be preferentially populated, leading to fluorescence at 922 keV with 65% efficiency and 1247 keV with 30% efficiency from the bandhead having a 78-ns lifetime. Demonstrations of the dumping reaction would then require the use of an accelerator with shorter pulses such as those provided by typical e-beam, pulsed-power devices. The great advantage would be that bremsstrahlung with 0.7 - 0.8 MeV endpoints could pump the left-side band, giving gamma fluorescence at 1.25 MeV. The upconverted signal could then be detected in a straightforward manner with suitable electronic discrimination.

The potential of $^{178}Hf^{m2}$ as the first-ranked candidate for the triggered release of MeV/nucleus into the radiation field, perhaps coherently as a gamma-ray laser, rests on the existence and properties of a K-mixing gateway which provides bandwidth funneling to freely-radiating states. Since the 31-year metastable of $^{178}Hf$ is an example of a multi-quasiparticle, high-spin isomer, it is instructive to examine systematics of similar levels in other hafnium isotopes. A full discussion can be found in Ref. [32].

Figure 6 shows an expanded view of the data of Fig. 4 for the mass island immediately below P = 82. Measured excitation energies of apparent K-mixing levels [20,24,29] mediating those reactions are plotted as X and + symbols by the right-hand ordinate and fall between 2.5 - 2.8 MeV, defining an interval $\Delta E_K$ within which such levels may be reasonably expected. The circles give the energies of the four- and five-quasiparticle isomers $^{174}Hf^{m}$, $^{175}Hf^{m}$, $^{176}Hf^{m3}$, $^{177}Hf^{m2}$ and $^{178}Hf^{m2}$, which tend to lower values with increasing mass numbers. The important detail in Fig. 6 is the position of those isomers relative to the possible excitation energies of K-mixing levels. At present no direct observations of $(\gamma,\gamma')$ reactions are available for those isotopes and thus the discussion is based on $\Delta E_K$ which bounds the likely energies of mediating states.

For $^{174}Hf^{m}$ and $^{175}Hf^{m}$ the isomers lie well above the upper bound of $\Delta E_K$ and it can be reasonably expected from Fig. 6 that those states would be relatively short-lived due to the availability of K-mixing states which could mediate spontaneous decay. As mentioned before this is indeed the case for $^{174}Hf^{m}$ with a halflife of 3.7 μs. Similarly, $^{175}Hf^{m}$ has a 1.21-μs halflife. In the case of $^{176}Hf^{m3}$, the isomer lies at 2.866 MeV, slightly above the upper bound of $\Delta E_K$. Thus, it could be expected to have a short lifetime somewhat lengthened by a small transition energy to a K-mixing level. This is supported by a measured halflife of 401 μs. The isomer $^{177}Hf^{m2}$ lies just below the upper bound of $\Delta E_K$, possibly at a lower energy than any mediating state. In that event a long lifetime would be suggested since spontaneous decay could not occur, but this could also be the result if a K-mixing level were located little below the isomer, providing an yrast trap. The measured halflife of 51 min agrees well with either possibility. Of the most importance, the isomer $^{178}Hf^{m2}$ appears to lie below the likely position of a mediating state. This points to a long lifetime and indeed the measured value is 31 years. Clearly the known halflives [21] of these multi-

quasiparticle Hf isomers agree well with the conclusion that K-mixing levels are prevalent in the mass-180 region and lie between 2.5 - 2.8 MeV.

The strong dependence of isomer lifetime on the possible excitation energy of a mediating state is shown directly in Fig. 7. Again, $\Delta E_K$ indicates the interval within which all measured values for possible K-mixing levels lie. This interval can be further constrained by comparing the data to lifetimes derived from single-particle widths [33]. Since low-multipolarities would be indicated for transitions between the isomers and states of mixed K, dipole radiation is considered here. Derived using the typical $1/(E_i - E_K)^3$ dependence for dipole transition widths where $E_i$ is the isomer energy and $E_K$ is the energy of the mediating level, the curves in Fig. 7 show halflives in good agreement with the measured values. It is doubtful that a K-mixing state could lie much below the isomer $^{177}Hf^{m2}$ without affecting its 51-min lifetime. Thus, the value $E_K$ = 2.7 MeV used to generate the curve passing just below that isomer represents a lower bound on the likely energy of an intermediate state of mixed K. Likewise, $E_K$ = 2.8 MeV provides an upper bound for that energy since larger values produce curves which do not reproduce the lifetimes of the isomers $^{174}Hf^{m}$, $^{175}Hf^{m}$ and $^{176}Hf^{m3}$. The excellent agreement seen between halflives predicted for dipole transitions and those measured provides further evidence for a K-mixing level in $^{178}Hf^{m2}$ lying no more than about 300 keV above the isomer, and perhaps much lower.

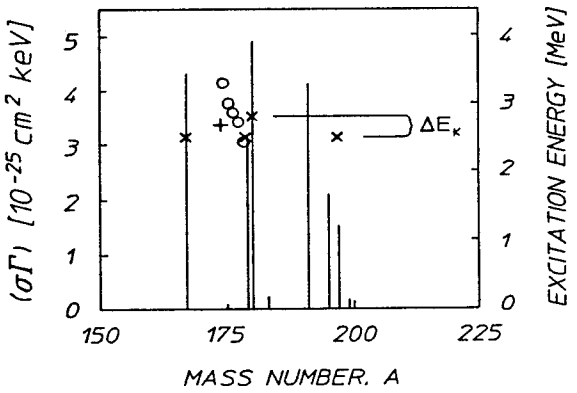


Figure 6: Expanded view of Fig. 4 for the mass island below P = 82. Circles indicate the excitation energies of four- and five-quasiparticle Hf isomers lying between 2 - 3 MeV with halflives $T_{1/2} > 1$ μs. The interval $\Delta E_K$ shows the range within which K-mixing levels are expected to lie.

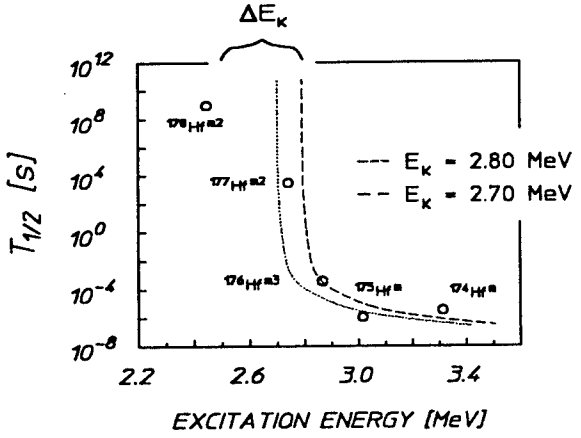


Figure 7: Halflife as a function of excitation energy for the four- and five-quasiparticle Hf isomers of Fig. 6. The curves represent calculated dipole-transition halflives for the deexcitation of the isomers for different choices for the gateway energy and further bound the possible positions of such a level.

## SUMMARY

The discovery of giant resonances for pumping and dumping nuclear populations has greatly enhanced the feasibility of an gamma-ray laser. The critical step was the introduction of the concept of optical pumping and experimental results along that line have shown consistent achievements since 1986. Now the principles necessary to solve the problems of pumping and host preservation have been demonstrated experimentally and a ranking has been developed to identify the best candidate for pumping. A recent model [10] using the new data indicates that a nuclear system can be optically pumped to threshold without the need to melt a low-Z host lattice. *At this time there are no a priori obstacles to the realization of a gamma-ray laser.* However, exact pump requirements depend sensitively on the structure of the actual isotope and the feasibility of a gamma-ray laser remains an open question. The goal of the main line of research is now to obtain and test the first-ranked candidate.

## ACKNOWLEDGMENTS

The authors wish to acknowledge the contributions of Prof. Dr. A. Richter and Dr. P. von Neumann-Cosel of the Institut für Kernphysik, Technische Hochschule Darmstadt, Prof. S. A. Karamian and Prof. Yu. Ts. Oganessian of the Flerov Laboratory of Nuclear Reactions, Joint Institute for Nuclear Research, Dubna, and Prof. V. Zoran of the Institute for Nuclear Physics, University of Bucharest, Romania. This work was supported by BMDO/TNI through NRL.

## REFERENCES


1. Rivlin, L. A., *USSR Patent #621265*, Appl. January 10, 1961.
2. G. C. Baldwin, J. C. Solem and V. I. Goldanskii, Rev. Mod. Phys. **53**, 687 (1981).
3. V. S. Letokhov, Sov. J. Quant. Electron. **3**, 360 (1974).
4. B. Arad, S. Eleizer and Y. Paiss, Phys. Lett. **74A**, 395 (1979).
5. S. Olariu, I. Popescu and C. B. Collins, Phys. Rev. C **23**, 50 (1981).
6. C. B. Collins, in *Proceedings of the International Conference on Lasers '80*, ed. C. B. Collins (STS Press, McLean, VA, 1981) p. 524.
7. C. B. Collins, F. W. Lee, D. M. Shemwell, B. D. DePaola, S. Olariu and I. Popescu, J. Appl. Phys. **53**, 4645 (1982).
8. C. B. Collins, in *CRC Handbook of Laser Science and Technology, Supplement 1: Lasers*, ed. by M. J. Weber (CRC Press, Boca Raton, Fl., 1991) p. 561.
9. T. W. Sinor, J. D. Standifird, F. Davanloo, K. N. Taylor, C. Hong, J. J. Carroll and C. B. Collins, Appl. Phys. Lett. 64, 1221 (1994).
10. C. B. Collins and J. J. Carroll, Int. J. Laser Phys. (in press for 1995).
11. See for example B. Pontecorvo and A. Lazard, C. R. Acad. Sci. **208**, 99 (1939).
12. J. J. Carroll, D. G. Richmond, T. W. Sinor, K. N. Taylor, C. Hong, J. D. Standifird and C. B. Collins, Rev. Sci. Instrum. **64**, 2298 (1993).
13. *The EGS4 Code System*, W. R. Nelson, H. Hirayama and D. W. O. Rogers, Stanford Linear Accelerator Center Report No. SLAC 265, 1985 (unpublished).
14. P. von Neumann-Cosel, A. Richter, C. Spieler, W. Ziegler, J. J. Carroll, T. W. Sinor, D. G. Richmond, K. N. Taylor, C. B. Collins and K. Heyde, Phys. Lett. B **266**, 9 (1991).
15. F. R. Metzger, Prog. Nucl. Phys. **7**, 54 (1959).
16. J. A. Anderson and C. B. Collins, Rev. Sci. Instrum. **58**, 2157 (1987).
17. J. A. Anderson and C. B. Collins, Rev. Sci. Instrum. **59**, 313 (1988).
18. C. B. Collins, J. A. Anderson, Y. Paiss, C.D. Eberhard, R. J. Peterson and W. L. Hodge, Phys. Rev. C **38**, 1852 (1988).
19. J. A. Anderson, M. J. Byrd and C. B. Collins, Phys. Rev. C **38**, 2833 (1988).
20. C. B. Collins, J. J. Carroll, T. W. Sinor, M. J. Byrd, D. G. Richmond, K. N. Taylor, M. Huber, N. Huxel, P. von Neumann-Cosel, A. Richter, C. Spieler and W. Ziegler, Phys. Rev. C **42**, R1813 (1988).
21. National Nuclear Data Center On-line Evaluated Nuclear Structure Data File, Brookhaven National Laboratory, 1994.
22. C. B. Collins, C. D. Eberhard, J. W. Glesener and J. A. Anderson, Phys. Rev. C **37**, 2267 (1988).
23. J. J. Carroll, M. J. Byrd, D. G. Richmond, T. W. Sinor, K. N. Taylor, W. L. Hodge, Y. Paiss, C. D. Eberhard, J. A. Anderson, C. B. Collins, E. C. Scarbrough, P. P. Antich, F. J. Agee, D. Davis, G. A. Huttlin, K. G. Kerris, M. S. Litz and D. A. Whittaker, Phys. Rev. C **43**, 1238 (1991).
24. C. B. Collins, J. J. Carroll, K. N. Taylor, D. G. Richmond, T. W. Sinor, M. Huber, P. von Neumann-Cosel, A. Richter and W. Ziegler, Phys. Rev. C **46**, 952 (1992).
25. J. J. Carroll, T. W. Sinor, D. G. Richmond, K. N. Taylor, C. B. Collins, M. Huber, N. Huxel, P. von Neumann-Cosel, A. Richter, C. Spieler and W. Ziegler, Phys. Rev. C **43**, 1238 (1991).
26. C. Hong, K. N. Taylor, J. J. Carroll and C. B. Collins, Rev. Sci. Instrum. (pending).
27. J. A. Anderson, C. D. Eberhard, J. J. Carroll, M. J. Byrd and C. B. Collins, in *Center for Quantum Electronics Annual Report FY-1988*, 1988 (unpublished) p. 147.
28. B. Crowell, P. Chowdhury, S. J. Freeman, C. J. Lister, M. P. Carpenter, R. G. Henry, R. V. F. Janssens, T. L. Khoo, T. Lauritsen, Y. Liang, F. Soramel and I. G. Bearden, Phys. Rev. Lett. **72**, 1164 (1994); P. M. Walker, G. D. Dracoulix, A. P. Byrne, T. Kibèdi and A. E. Stuchbery, Phys. Rev. C **49**, 1718 (1994).
29. G. Sletten, N. L. Gjørup, S. Juutinen, A. Maj, J. Nyberg, P. M. Walker, D. M. Cullen, P. Fallon, A. N. James, J. F. Sharpey-Schafer, M. A. Bentley, A. M. Bruce and B. J. Varley, Nucl. Phys. **A520**, 325 (1990);P. M. Walker, F. Sletten, N. L. Gjørup, M. A. Bentley, J. Borggreen, B. Fabricius, A. Holm, D. Howe, J. Pedersen, J. W. Roberts and J. F. Sharpey-Schafer, Phys. Rev. Lett. 65, 416 (1990).
30. M. Girod, J. P. Delaroche, D. Gogny and J. F. Berger, Phys. Rev. Lett. **65**, 416 (1990).
31. Yu. Ts. Oganessian, S. A. Karamian, Y. P. Gangrski, B. Gorski, B. N. Markov, Z. Szeglowski, Ch. Briançon, D. Ledu, R. Meunier, M. Hussonnois, O. Constantinescu and M. I. Subbotin, J. Phys. G: Nucl. Part. Phys. **18**, 393 (1992).
32. C. B. Collins, J. J. Carroll, Yu. Ts. Oganessian and S. A. Karamian, Int. J. Laser Phy. (in press for 1995).
33. *Theoretical Nuclear Physics, Volume I: Nuclear Structure*, A. deShalit and H. Feshbach (Wiley, New York, 1990) p. 702.